



5-2018

Decentralized and Fault-Tolerant Control of Power Systems with High Levels of Renewables

Mohammad Ehsan Raoufat

University of Tennessee, mraoufat@vols.utk.edu

Recommended Citation

Raoufat, Mohammad Ehsan, "Decentralized and Fault-Tolerant Control of Power Systems with High Levels of Renewables." PhD diss., University of Tennessee, 2018.
https://trace.tennessee.edu/utk_graddiss/4936

This Dissertation is brought to you for free and open access by the Graduate School at Trace: Tennessee Research and Creative Exchange. It has been accepted for inclusion in Doctoral Dissertations by an authorized administrator of Trace: Tennessee Research and Creative Exchange. For more information, please contact trace@utk.edu.

To the Graduate Council:

I am submitting herewith a dissertation written by Mohammad Ehsan Raoufat entitled "Decentralized and Fault-Tolerant Control of Power Systems with High Levels of Renewables." I have examined the final electronic copy of this dissertation for form and content and recommend that it be accepted in partial fulfillment of the requirements for the degree of Doctor of Philosophy, with a major in Electrical Engineering.

Seddik M. Djouadi, Kevin I. Tomsovic, Major Professor

We have read this dissertation and recommend its acceptance:

Yilu Liu, Xiaopeng Zhao

Accepted for the Council:

Dixie L. Thompson

Vice Provost and Dean of the Graduate School

(Original signatures are on file with official student records.)

Decentralized and Fault-Tolerant Control of Power Systems with High Levels of Renewables

A Dissertation Presented for the
Doctor of Philosophy
Degree
The University of Tennessee, Knoxville

Mohammad Ehsan Raoufat

May 2018

© by Mohammad Ehsan Raoufat, 2018
All Rights Reserved.

*To my parents, Susan Afagh and M. Hossein Raoufat
and my beloved, Nastaran Basiri*

*whose love, support, and encouragement
over the years have made the writing of
this dissertation possible.*

Acknowledgments

I wish to express my deepest gratitude to my academic co-advisors, Prof. Seddik Djouadi and Prof. Kevin Tomsovic for their support, guidance and invaluable comments during my study. The trust, support and "the freedom to create" that they have provided throughout my Ph.D. is very much appreciated, I simply cannot imagine better advisers.

Next, I would like to thank my other committee members, Prof. Yilu Liu, Prof. Jow H. Chow and Prof. Xiaopeng Zhao who have constantly given me valuable inputs on my research projects. I am also thankful to all the students, staff and professors in the CURENT Engineering Research Center. Especially, I would like to thank my friends and colleagues Yichen Zhang, Jin Dong and Ouassim Bara with whom I have worked on several research projects. They have always believed in me and inspired me to dream beyond my limitations.

Finally, I would like to express my appreciation and love to my family, especially my beloved, Nastaran Basiri, for their unconditional love, encouragement, and support which made it possible for me to complete my Ph.D. This research was supported by U.S. National Science Foundation (NSF) and Department of Energy (DOE) through CURENT Engineering Research Center. I sincerely acknowledge the financial support extended to this project by the sponsors.

Abstract

Inter-area oscillations have been identified as a major problem faced by most power systems and stability of these oscillations are of vital concern due to the potential for equipment damage and resulting restrictions on available transmission capacity. In recent years, wide-area measurement systems (WAMSs) have been deployed that allow inter-area modes to be observed and identified.

Power grids consist of interconnections of many subsystems which may interact with their neighbors and include several sensors and actuator arrays. Modern grids are spatially distributed and centralized strategies are computationally expensive and might be impractical in terms of hardware limitations such as communication speed. Hence, decentralized control strategies are more desirable.

Recently, the use of HVDC links, FACTS devices and renewable sources for damping of inter-area oscillations have been discussed in the literature. However, very few such systems have been deployed in practice partly due to the high level of robustness and reliability requirements for any closed loop power system controls. For instance, weather dependent sources such as distributed winds have the ability to provide services only within a narrow range and might not always be available due to weather, maintenance or communication failures.

Given this background, the motivation of this work is to ensure power grid resiliency and improve overall grid reliability. The first consideration is the design of optimal decentralized controllers where decisions are based on a subset of total information. The second consideration is to design controllers that incorporate actuator limitations to guarantee the stability and performance of the system. The third consideration is to build robust controllers to ensure resiliency to different actuator failures and availabilities. The fourth consideration

is to design distributed, fault-tolerant and cooperative controllers to address above issues at the same time. Finally, stability problem of these controllers with intermittent information transmission is investigated.

To validate the feasibility and demonstrate the design principles, a set of comprehensive case studies are conducted based on different power system models including 39-bus New England system and modified Western Electricity Coordinating Council (WECC) system with different operating points, renewable penetration and failures.

Table of Contents

1	Introduction	1
1.1	Problem Description and Previous Works	4
1.2	Motivation and Contributions	6
1.3	Dissertation Outline	9
2	Optimal \mathcal{H}_2 Decentralized Control of Spatially Invariant Systems	10
2.1	Introduction	11
2.2	Discrete Cone Causal Systems	13
2.3	Design of Optimal \mathcal{H}_2 Decentralized Controller	18
2.4	Numerical Results	23
2.5	Summary	27
3	Damping Controllers in the Presence of Saturation	29
3.1	Introduction	30
3.2	Dynamic Model of System with Saturation	31
3.3	Estimation of the DA	34
3.4	Enlarging the DA Using State-Feedback Controller	37
3.5	Enlarging the DA Using Dynamic Output-Feedback Controller	45
3.6	Summary	49
4	Virtual Actuators for Wide-Area Damping Control	50
4.1	Introduction	51
4.2	Power System Dynamic Model	52

4.2.1	Generator Dynamic Model	52
4.2.2	HVDC Dynamic Model	53
4.2.3	SVC Dynamic Model	53
4.3	Multi-Objective Wide-Area Damping Controller Design	54
4.4	Fault-Tolerant Control Design	57
4.5	Numerical Results	61
4.5.1	Case Study I: Kundur Two-Area System	61
4.5.2	Case Study II: New England 39-Bus System	65
4.6	Summary	70
5	Dynamic Control Allocation for Damping of Inter-area Oscillations	71
5.1	Introduction	72
5.2	Multi-Objective Wide-area Damping Controller Design	74
5.3	Modal-based Control Allocation	74
5.4	Dynamic Model of the WECC Test System	78
5.4.1	Generator Dynamic Model	78
5.4.2	DFIG-based Wind Farm Model	82
5.5	Numerical Results	83
5.5.1	Modal Analysis	83
5.5.2	Model Reduction and Design of WADC	84
5.5.3	Design of Modal-Based Control Allocation	85
5.5.4	Discussion	86
5.6	Summary	93
6	Sparse Control Allocation for Wide Area Coordinated Damping	94
6.1	Introduction	95
6.2	Modal-based Sparse Control Allocation	96
6.3	Dynamic Model of the WECC Test System	101
6.4	Numerical Results	102
6.4.1	Linear Analysis and Design of WADC	102
6.4.2	Design of Modal-Based Control Allocation	102

6.4.3	Nonlinear Simulations	103
6.5	Summary	106
7	Stability of Wide Area Controls with Intermittent Information Transmis-	108
	sion	
7.1	Introduction	109
7.2	Preliminaries on Time Scale Theory	111
7.3	Wide Area Control with Intermittent Information	112
7.3.1	State Feedback Problem Formulation	113
7.3.2	Stability Criteria	115
7.3.3	Extension to Dynamic Output-feedback	116
7.4	Numerical Results	119
7.4.1	Case Study I: SMIB Power System	119
7.4.2	Case Study II: Kundur's Two-Area System	123
7.5	Summary	126
8	Conclusion	127
	Bibliography	130
	Appendix	146
A	Controller Parameters	147
A.1	Controller parameters of case study I:	147
A.2	Controller parameters of case study II:	148
Vita		149

List of Tables

2.1	Comparison of Optimal Norm for Different Temporal Orders of the Distributed Controller.	26
3.1	CCT and Coefficient Comparison for SMIB System with Different Controllers.	44
4.1	Critical Modes of Two-Area System	62
4.2	Modes of New England Ten-Machine 39-Bus System	67
5.1	DFIG Wind Farms Outputs in the WECC Test System.	83
5.2	Modal Analysis of the WECC Test System with 20% Wind Penetration.	84
5.3	Damping Ratio of Mode 3 with Respect to Different Controllers and Fault Combinations.	92
6.1	Low-Frequency Modes of the Modified WECC System, Base Case with no Controllers.	102
6.2	Damping Ratio of the Critical Mode for Different Actuator Fault Combinations.	106
7.1	Communication Failure Duration for Stable SMIB System.	123
7.2	Critical Modes of Two-Area System	124
7.3	Communication Failure Duration for Kundur's two-area system	125

List of Figures

1.1	A typical example of inter-area oscillation.	2
2.1	Support of the spatio-temporal impulse response of a centralized (left) and a cone causal (right) system.	14
2.2	Support of a finite approximation of a cone causal system using equation (2.4) in the right and equation (2.5) in the left.	14
2.3	General control configuration.	17
2.4	Positive feedback block diagram realization of K	23
3.1	A single-machine infinite-bus power system.	31
3.2	Boundary of null controllable region ($\partial\mathcal{C}$) and estimated DA for LQR controller (D_{LQR}) in the presence of saturation.	38
3.3	Boundary of estimated DA and trajectory of nonlinear SMIB system with LQR controller and critical fault duration of $CCT = 0.081s$	39
3.4	Boundary of null controllable region ($\partial\mathcal{C}$), estimated DA for LQR controller (D_{LQR}) and enlarged DA (D_{Enl}) in the presence of actuator saturation.	41
3.5	Comparison of estimated DA and trajectory of nonlinear SMIB system with LQR controller and critical fault duration of $CCT = 0.109s$	42
3.6	Comparison of transient responses for the system with fault duration of $t_f = 0.1s$	43
3.7	Comparison of supplementary control signals for system with fault duration of $t_f = 0.1s$	43

3.8	Comparison of transient responses for the system with fault duration of $t_f = 0.1s$, employing LQR, optimized state-feedback and optimized output-feedback controllers.	48
3.9	Comparison of supplementary control signals for the system with fault duration of $t_f = 0.1s$, employing LQR, optimized state-feedback and optimized output-feedback controllers.	48
4.1	Pole-placement in LMI regions.	55
4.2	Control reconfiguration block diagram (Fault-hiding approach).	57
4.3	Two-area power system with WADC and virtual actuators.	60
4.4	Frequency response of full-order and reduced-order system with respect to inputs and output measurement signals.	61
4.5	Dynamic response of two-area power system to tripping and re-closing one of the tie-lines.	63
4.6	Dynamic response of two-area system to tripping and re-closing one of the tie-lines with WADC signal redirected to G_2	64
4.7	Dynamic response of two-area system to tripping and re-closing one of the tie-lines with WADC signal redirected to SVC.	64
4.8	Dynamic response of two-area system to tripping and re-closing one of the tie-lines with WADC signal redirected to HVDC.	65
4.9	New England 10-machine 39-bus system with WADC and virtual actuators.	66
4.10	Frequency response of full-order and reduced-order system with respect to inputs and output measurement signals.	66
4.11	Dynamic responses of New England system to three-phase fault at bus 1.	67
4.12	Dynamic responses of New England system to three-phase fault at bus 1 when VA redirected WADC signal to G_6	68
4.13	Dynamic responses of New England system to three-phase fault at bus 1 when VA redirected WADC signal to SVC.	69
4.14	Dynamic responses of New England system to three-phase fault at bus 1 when VA redirected WADC signal to HVDC.	69

5.1	Control block diagram of the feedback loop with Supervisory MB-CA embedded.	75
5.2	Single-line diagram of the modified 192-bus WECC system with DFIG wind farms.	80
5.3	Schematic of the high-gain AVR system with supplementary input u	81
5.4	Schematic of DFIG reactive power control loop with supplementary input u .	81
5.5	Normalized controllability measure associated with inter-area mode 3 for all possible actuators.	81
5.6	Normalized observability measure associated with modes 1-4.	82
5.7	Frequency response of the full-order and reduced order models of the WECC system from supplementary inputs.	85
5.8	Dynamic response of the system to three-phase fault at bus #14.	87
5.9	Power flow on the tie-line connecting the areas 2 and 4 after a three-phase fault at bus #14.	87
5.10	Dynamic response of the system to three-phase fault at bus #14 when MB-CA redirects the WADC signal to healthy actuators.	89
5.11	Power flow on the tie-line connecting areas 2 and 4 to a three-phase fault at bus #14 when MB-CA redirects WADC signal to healthy actuators.	89
5.12	Supplementary signals (MB-CA outputs) in Case A.	90
5.13	Supplementary signals (MB-CA outputs) in Case B.	90
5.14	Supplementary signals (MB-CA outputs) in Case C.	90
5.15	Effects of actuator faults on feasible virtual control region for inter-area mode 3.	91
5.16	Histogram showing the number of iterations required by the optimization algorithm in Case B from $t = 1$ s to $t = 6$ s.	92
6.1	One-line diagram of a WECC power system with Type 4 wind farms.	100
6.2	Single-generator representation of aggregated wind farm model.	101
6.3	Hankel singular values of the modified WECC system.	103
6.4	Responses of the WECC system to three-phase fault at bus #139 in case A.	104
6.5	Responses of the WECC system to three-phase fault at bus #139 in case B.	104

6.6	Responses of the WECC system to three-phase fault at bus #139 in case C.	105
6.7	Supplementary control signal u for different actuators in response to three-phase fault at bus #139 in case A.	107
6.8	Supplementary control signal u for different actuators in response to three-phase fault at bus #139 in case B.	107
7.1	A networked control system with components that are remotely operated over a communication network.	110
7.2	Sample of control signal with intermittent communication transmissions using hold strategy (top sub-figure) and zero strategy (bottom sub-figure).	113
7.3	Block digram of communication failure in control signal.	118
7.4	Block digram of communication failure in measurement signal.	119
7.5	A single-machine infinite-bus power system.	120
7.6	Speed deviation of SMIB power system in case of ideal communication network.	121
7.7	Stability criteria for SMIB power system.	121
7.8	Speed deviation of closed loop and open loop SMIB power system in case of ideal and non-ideal ($\tau = 0.1$ and $\mu = 0.23$) communication network.	122
7.9	A two-area Kundur power system.	123
7.10	Speed deviation of two-area Kundur power system in case of ideal communication network.	124
7.11	Stability criteria for two-area Kundur power system.	125
7.12	Speed deviation of closed loop and open loop two-area Kundur power system in case of ideal and non-ideal ($\tau = 0.2$ and $\mu = 0.39$) communication network.	125

Nomenclature

δ	Generator angle
ω	Generator rotor speed
ω_r	Generator normalized speed;
ω_s	Generator synchronous speed;
B_L	SVC equivalent admittance
D	Generator damping coefficient
D_t	Turbine damping
E'_d	Generator d -axis transient voltage
E'_q	Generator q -axis transient voltage
E_{fd}	Exciter field voltage
G	Open-loop transfer function
H	Generator inertia constant
i	Discrete space variable
I_d	d -axis armature current
I_q	q -axis armature current
K	Controller transfer function

K_A	AVR excitation gain
K_D	Damping coefficient
K_p	PSS stabilizer gain
K_S	Synchronizing coefficient
K_s	SVC controller gain
P_s^{HVDC}	HVDC link supplementary control input
P_{dc}	HVDC link modified ordered power
P_{ref}	HVDC link reference power
Q	Youla parameter transfer function
R	Turbine-governor droop
t	Discrete time variable
T'_{d0}	Generator d -axis transient time constant
T'_{q0}	Generator q -axis transient time constant
T_A	AVR excitation time constant
T_M	Generator mechanical torque
T_{1g}, \dots, T_{3g}	Turbine-governor time constants
T_{1p}, \dots, T_{5p}	PSS time constants
T_{1s}, \dots, T_{5s}	SVC time constants
T_{dc}	HVDC link time constant
T_{Mref}	Reference mechanical torque
V	Bus voltage value

V_s^{EXC}	Supplementary control input of the excitation
V_s^{SVC}	SVC supplementary control input
V_d	d -axis voltage
V_q	q -axis voltage
V_s	Supplementary control input
V_∞	Infinite bus voltage
V_p	PSS output signal
V_{ref}	AVR reference voltage value
V_t	Generator terminal voltage
W	Weighting function
X'_d	Generator d -axis transient reactance
X'_q	Generator q -axis transient reactance
X_d	Generator d -axis reactance
X_l, X_t	Line and transformer reactance
X_q	Generator q -axis reactance
X_{1g}, X_{2g}	Turbine-governor state variables
X_{1p}, \dots, X_{3p}	PSS state variables
X_{1s}, X_{2s}	SVC state variables
z	two-sided spatial variable

Chapter 1

Introduction

Power system is one of the most impressive engineering feats of the modern era due to its vast geographical area, enormous dimension, and very high-reliability requirements. The competitive market structure with penalty payments for interruptions has challenged power system operators to maintain the grid free from major interruptions [1]. However, when the network covers large areas it increases the risk of external disturbances and the possibility of dynamic interferences. Further, with increasing levels of distributed energy resources (DERs) including winds and photovoltaic (PV) generation, modern grids are more vulnerable to system-wide disturbances [2]. These system-wide disturbances require more sophisticated control and measurement systems to avoid system collapse as local responses that are delivered based on the local observations are not sufficient anymore.

This will bring new challenges as coping with instability problems now require more sophisticated wide-area measurement and control systems (WAMCS). Generally, power systems consist of interconnections of spatially distributed subsystems which may interact with their neighbors and include several sensors/actuators. Hence, centralized control systems (all subsystems are connected to the same controller) are computationally expensive, might be impractical in terms of hardware limitations such as communication speed and decentralized control strategies are more desirable. Information structure has a direct impact on the scalability and tractability of computing these optimal decentralized controllers [3]. As a result, extensive research is required to provide insight into decentralized, efficient and reliable design of the future wide-area controllers.

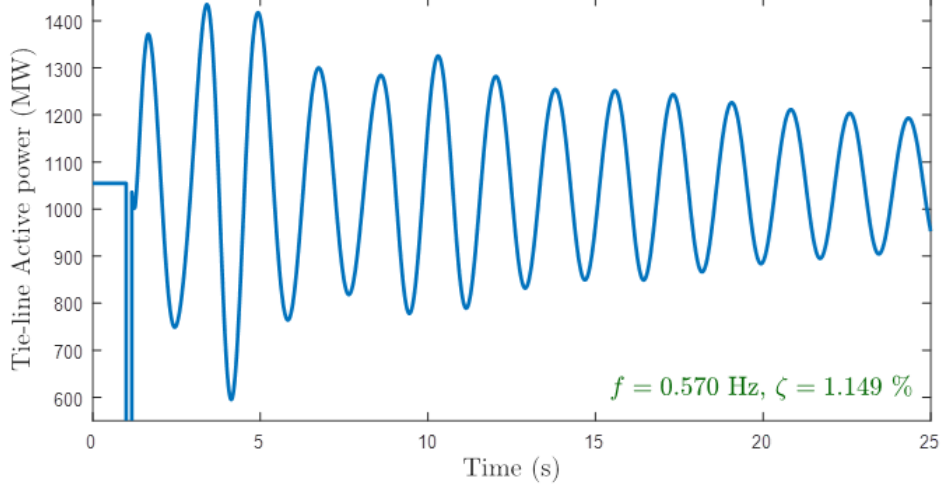


Figure 1.1: A typical example of inter-area oscillation.

One of the major concern faced by modern power systems is small-signal instability, which refers to the ability of the system to remain in synchronism after being subjected to a small disturbance [4]. Generally, the root cause of small-signal instability is insufficient damping of low-frequency electromechanical oscillations and the following two distinct modes of oscillation are of main concern [5]:

- *Inter-area modes* are associated with swinging of many generators in one part of the system against machines in other parts. The characteristic frequency of inter-area modes of oscillation is generally in the range of 0.1 to 1.0 Hz and are usually caused by heavy power transfers across weak tie-lines
- *Local modes* are associated with one generator swinging against the rest of the system. This type of oscillation is localized to one station or a small part of the system and has higher oscillation frequency compare to the inter-area modes. These local modes are usually induced by the interaction between the mechanical and electrical modes of a turbine-generator system.

The time frame of interest in small-signal stability studies is of the order of 10 to 30 seconds following a disturbance. Stability of inter-area oscillations is of vital concern due to the potential for equipment damage and resulting restrictions on available transmission capacity between on the tie-lines between different areas. A typical example of the variation

in tie-line active power flow is shown in Fig. 1.1. Over the past years, many incidents of system blackout resulting from these oscillations have been reported and the followings are some of these inter-area modes observation [6].

- In 1960's with the interconnection of Ontario Hydro, Hydro-Qubec and Detroit Edison systems, oscillations were experienced
- In 1969, oscillations were observed in the Finland-Sweden and Norway-Denmark interconnected system.
- In 1971 - 1972, more than 70 incidents of unstable inter-area oscillations occurred in the Mid-Continent Area Power Pool system.
- In 1975, unstable oscillations of 0.6 Hz were encountered on the interconnected power system of New South Wales and Victoria.
- In 1982 - 1983, the State Energy Commission of Western Australia identified low damped inter-area oscillations with a frequency range of 0.2 to 0.3 Hz.
- In 1996, the Pacific AC Inter-tie in WECC experienced unstable low-frequency inter-area oscillations following the outage of four 400 kV lines.

Typically, local modes of oscillation can be damped by using power system stabilizers (PSSs) but PSSs are less effective for inter-area modes. In recent years, wide-area measurement systems (WAMSs) have been deployed that allow inter-area modes to be easily observed and identified [7]. As a result, low-frequency oscillations can be observed globally and then appropriately designed wide-area controllers can be deployed. These systems should be

- Distributed or decentralized, modular and adaptive
- Make efficient use of actuator limits and capabilities
- Robust to sensor, communication, and actuator loss

This dissertation studies decentralized, fault-tolerant and coordinated wide area control of future power grids. The work in this dissertation is inspired by the following facts in modern power grids. Firstly, power grids consist of interconnections of many subsystems distributed over a vast geographical area and centralized controllers are impractical or uneconomical. Secondly, new generation sources connected to the grid through inverters, such as, distributed wind generations have limited capabilities and it is critical to consider their actuator constraints. Finally, changes in scheduling of generators may mean that some actuators are unavailable. The use of renewable sources to contribute to power system stability may also be limited by the fact that they are not always available. The goal of this dissertation is to develop new control theories and apply them to improve the power system reliability.

1.1 Problem Description and Previous Works

In practice, most complex systems consist of interconnections of many subsystems. Each subsystem may interact with its neighbors and include several sensors and actuator arrays. Examples of such interconnected systems include control of smart grids [8], coordination of large-scale electric vehicle charging [9] and flight formation [10]. In some cases, lumped approximations of PDEs can also be used for modeling and control of identical interconnected systems such as distributed heating/sensing [3] and large vehicle platoons [11]. For these spatially distributed systems, centralized strategies (all subsystems are connected to the same controller) are computationally expensive and might be impractical. Hence, decentralized control problems have received a considerable attention in recent years. These problems arise when a system consists of several decision makers (DMs) in which their actions are based on decentralized information structure [12]. The term decentralized used in this work as a general term where decisions are based on a subset of total information available about the system.

Decentralized control problems were first studied by Radner as a team decision problem [13]. Major difficulties that arise in these problems are from the information patterns. Early work by Witsenhausen [14] demonstrated the computational difficulties associated with team

decision making even in a simple two-player process. This counterexample demonstrates that nonlinear control strategies outperform all linear laws in that decentralized decision making problem. Another possibility is that decentralized control problem caused by delayed information sharing pattern (e.g. network delay), which limits the information sharing between different controllers. In [15], it has been shown that for a unit-delay information sharing pattern, the optimal controller is linear. However, decentralized control problems with multi-step delayed information sharing patterns generally do not have this property.

A major concern faced by modern power systems is small-signal instability, which refers to the ability of the system to remain in synchronism after being subjected to a small disturbance [4]. The key is to have sufficient damping that oscillations die out within a short amount of time after the disturbance, say, within 10 seconds. If damping becomes too low, the associated power swings may cause generators to fall out of synchronism or trigger protection. In recent years, wide-area measurement systems (WAMS) have been deployed that allow inter-area modes to be easily observed and identified [7]. In WAMS, phasor measurement units (PMUs) are being used to collect synchronized measurements from the power grid. As a result, the problem of lack of global observation for local controllers can be addressed and improvement in the damping of inter-area oscillations can be achieved by using remote feedback signals and specially designed WADCs.

There exists a large body of work in the control literature on stability analysis of systems with input constraints [16, 17, 18, 19]. However, the effects of saturation have not been taken into account in previous works for analyzing and designing damping controllers for power system components, including traditional synchronous generators [20, 21, 22, 23], modern FACTS devices [24, 25], energy storage systems [26] and renewable resources [27]. These efforts generally do not consider the nonlinear effects of hard saturation limits on control signals. Note that this is different from the traditional magnetic saturation of generators but instead reflects the practical limitations of equipment ratings and can be expressed using hard saturation limits restricting the amplitude of the controller output.

In order to transmit remote feedback signals to a WADC and then to the actuators, highly reliable communications and computations are required. Time delay and communication failures or cyber-attacks can easily degrade the performance of the aforementioned controllers

[28, 25]. The network may experience constant or time varying delays [29], packet dropout [30] or packet disordering [31]. Hence, the communication network introduces uncertainty in the operation of the closed-loop system. Moreover, changes in scheduling of generators may mean that some actuators are unavailable. The use of renewable sources to contribute to power system stability may also be limited by the fact that they are not always available. For example, on calm days wind turbines may not be generating electric power if there is insufficient wind to drive the turbines. Hence, the availability of these weather dependent renewable resources could cause significant reliability issues. In contrast with a large wind farm in a concentrated location, deployment of multiple small-scale wind farms will require special techniques for actuator coordination as none could be used individually to achieve adequate damping. Moreover, the availability of these weather dependent renewable resources could pose design challenges for the reliability of critical controllers.

1.2 Motivation and Contributions

Given the background, the motivation of this dissertation is to improve the reliability and resiliency of power systems. The primary sub-tasks of this research with motivations and contribution can be described below.

1. *Design optimal decentralized controllers where decisions are based on the subset of total information available about the system.* Generally, decentralized controllers are the only feasible solution for large-scale power systems as centralized control architectures are impractical or hard to implement. However, the information structure has a direct impact on the scalability and tractability of computing optimal decentralized controllers and most researchers have to resort to suboptimal methods. As a result, we have formulated the problem of optimal H_2 decentralized control for specially invariant systems and transformed the problem to an infinite number of model matching with a specific structure that can be solved efficiently. In addition, we have derived the closed-form expression (explicit formula) of the decentralized controllers for the first time and presented a constructive procedure to obtain the state-space representation. In particular, it is shown that the optimal decentralized controller is given by a specific

positive feedback scheme. A numerical example is given and compared with previous works which illustrate the effectiveness of our proposed method.

2. *Design controllers that incorporates actuator limitations to guarantee the stability and performance of the system.* Most of the new generation resources have limited capability and can contribute to grid stability within a narrow range depending on operating conditions. However, it is critical to consider the effects of actuator constraints, these have not been taken into account in previous work. To guarantee the stability, we have estimated the domain of attraction (DA) of a single-machine infinite-bus (SMIB) power system with saturation nonlinearity and compared with the exact description of the null controllable region. Then, we have designed both state-feedback and dynamic output-feedback controllers to enlarge the DA. Simulation results on a detailed nonlinear model of a synchronous generator indicate that the DA enlarges with our proposed controller. Our results also indicate that Critical Clearing Time (CCT) and damping of the system with saturation can be improved using our proposed method.
3. *Design robust controllers to ensure resiliency to different actuator failures and actuator availability.* Wide-area controllers are becoming more common in modern power grids. However, still very few such systems have been deployed in practice at least partly due to the robustness that is required for any closed loop power system controls. Increasing interconnections and power demands in modern power systems lead to greater vulnerability to faults and components failures. Hence, we have presented a new fault-tolerant WADC such that nominal controller remains operational after faults in the actuators. We have addressed this problem by inserting virtual actuators (VAs) between the faulty plant and nominal controller to re-route the control signals to other healthy actuators and recover the performance of fault-free system without the need to retune the controller. Our proposed approach is applied to Kundur's two-area system and the 39-bus New England system and numerical results show the effectiveness of the proposed method subjected to different failures.

4. *Design cooperative controllers, ensuring resiliency and considering actuator limitations with high levels of renewables.* To address the above tasks simultaneously, we have developed a new design method for fault-tolerant wide-area controllers using modal-based control allocation (MB-CA), which manage actuator availability and coordinates a set of actuators based on effects on the modal system, desired control actions and actuator constraints. We have developed an optimization algorithm to solve the problem in real-time and presented a visualization of the average feasible virtual control regions in modal coordinates. This approach has also been further developed to sparse MB-CA where supervisory controller only communicates with necessary actuators to achieve the desired performance. The proposed approaches are applied to a modified Western Electricity Coordinating Council (WECC) system with high levels of renewables to verify the feasibility on a complex power system.

5. *Stability of wide area controls with intermittent information transmission* Due to the interruption in communication links between remote measurements and damping controller or from the damping controller to the damping actuators, the closed loop system might become unstable. To estimate instability, we have formulated the problem as discrete-continuous time models and the stability conditions are derived using time scale theory. This method allows us to handle discrete and continuous models as two pieces of the same framework, such that the system switches between a continuous time subsystem (when the communication occurs) and a discrete-time system (when the communication fails). The contribution is in quantifying the maximum time of interruption in order to guarantee exponential stability. The findings are useful in specifying the minimum requirements for communication infrastructure and the time to activate remedial action schemes.

1.3 Dissertation Outline

This dissertation mainly deals with decentralized, fault-tolerant and coordinated control to improving the resiliency of modern grids in the presence of high penetration of renewable.

A brief introduction that describes the previous works, motivations and contributions have been presented in **Chapter 1**. The remainder of this dissertation is organized as follows:

Chapter 2 presents explicit solution for decentralized control of a class of spatially invariant systems. In addition, we provide a constructive procedure to obtain the state-space representation of the decentralized controller.

Chapter 3 presents the analysis and a method to design damping controllers considering the effects of saturation limits. As shown in this Chapter, nonlinear effects of saturation should be considered to guarantee the stability and satisfactory performance.

In **Chapter 4**, a new approach is presented to design fault-tolerant wide-area damping controllers. Our approach is based on the concept of virtual actuators to benefit from redundancy in the actuator's equipped with supplementary control.

Next in **Chapter 5**, a modal-based control allocation approach has been presented. This approach coordinates a set of actuators to contribute to damping of inter-area oscillations based on their effects on the modal system, desired control actions and actuator constraints.

In **Chapter 6**, the previous method has been further developed to sparse modal-based control allocation where supervisory controller only communicates with necessary actuators to achieve the desired performance.

Future, stability of wide area controls with intermittent information transmission has been studied in **Chapter 7** to estimate instability in modern power grids with non-ideal communication links.

Finally, the conclusion with a summary of work and directions for future research are provided in **Chapter 8**.

Chapter 2

Optimal \mathcal{H}_2 Decentralized Control of Spatially Invariant Systems

This chapter presents an explicit solution to decentralized control of a class of spatially invariant systems. The problem of optimal \mathcal{H}_2 decentralized control for cone causal systems is formulated. Using Parseval's identity, the optimal \mathcal{H}_2 decentralized control problem is transformed into an infinite number of model matching problems with a specific structure that can be solved efficiently. In addition, the closed-form expression (explicit formula) of the decentralized controller is derived for the first time. In particular, it is shown that the optimal decentralized controller is given by a specific positive feedback scheme. A constructive procedure to obtain the state-space representation of the decentralized controller. A numerical example is given and compared with previous works which illustrate the effectiveness of the proposed method. Part of the results in this chapter will be appear in [\[32\]](#).

2.1 Introduction

Decentralized control problems, different from classical centralized ones, have received a considerable attention in recent years. These problems arise when a system consists of several decision makers (DMs) in which their actions are based on decentralized information structure [12]. The term decentralized used in this chapter as a general term where decisions are based on a subset of total information available about the system. The information structure has a direct impact on the scalability and tractability of computing optimal decentralized controllers [33]. Over the past few years, different decentralized information structure has been analyzed and the theory of such systems has been studied in detail [12, 33, 34, 35].

In this research, we study the decentralized control of spatially invariant systems that are made up of infinite numbers of identical subsystems and are functions of both temporal and spatial variables. Spatial invariance means the distributed system is symmetric in the spatial structure and the dynamics do not vary as we shift along with spatial coordinates. In [3], a framework for spatially invariant systems with distributed sensing and actuation has been proposed and optimal control problems such as LQR, \mathcal{H}_2 and \mathcal{H}_∞ has been studied in a centralized fashion. In [36], the authors claimed that for spatially invariant systems, dependence of the optimal controller on information decays exponentially in space and the controller have some degree of decentralization.

Decentralized control problems can also be reformulated in a model matching framework using the Youla parametrization. For general systems, this nonlinear mapping from the controller to the Youla parameter removes the convexity of constraint sets (e.g. decentralized structure) [37]. However, a large class of systems called quadratic invariance have been introduced in [38], under which the constraint set is invariant under above transformation. Different constraint classes such as distributed control with delay, decentralized control and sparsity constraints have been considered in literature and a vectorization technique has been used for computation. However, no explicit solution has been provided and due to high computation requirements and numerical issues, vectorization approach is limited to systems with a small number of states [39].

Distributed controller design problem for classes of spatially invariant systems with limited communications can also be cast as a convex problem using Youla parametrization. This class includes spatially invariant systems with additional cone causal property where information propagates with a time delay equal to their spatial distance [40]. A more general class for cone causality, termed as funnel causality where the propagation speeds in the controller are at least as fast than the plant was introduced in [41]. It is important to note that decentralized control with structures such as cone or funnel causality yields a convex problem. However, these problems are in general infinite dimensional and finding the explicit solution or developing an efficient procedure for solving these problems are still open, and are the subject of intense research.

In the previous work reported in [42], the optimal centralized control problem for this type of spatially invariant systems have successfully been posed as a distance minimization in a general L_∞ space, from a vector function to a subspace with a mixed L_∞ and \mathcal{H}_∞ space structure. In [43], Banach space duality structure of the problem in terms of tensor product spaces have been formulated. It has been shown that the dual and pre-dual spaces together with the annihilator and pre-annihilator subspaces can be realized as specific tensor spaces and subspaces, respectively. In [44] and [45], the optimal centralized and decentralized \mathcal{H}_2 control problem is formulated using an orthogonal projection from a tensor Hilbert space of L_2 and \mathcal{H}_2 onto a particular subspace. It is important to note that these projections can be solved numerically to only compute the optimal cost function. However, further extensions are needed to solve the problem explicitly and calculate the transfer function or state-space characterization of the optimal decentralized controller.

Motivated by the concern outlined above, in this research, the optimal \mathcal{H}_2 decentralized control problem for a class of spatially invariant system is considered. By building on our previous results, we derived the decentralized problem for cone causal systems. Using Parseval's identity, the optimal \mathcal{H}_2 decentralized control problem is transformed to infinite number of model matching problem with a specific structure that can be solved efficiently. In addition, the closed-form expression (explicit formula) of the optimal decentralized controller is derived in which the optimal control was previously unknown. A constructive procedure to obtain the state-space representation of the decentralized controller is also provided.

A numerical example is given and compared with previous works which demonstrate the effectiveness of the proposed method.

This chapter is organized as follows. In Section 2.2, mathematical preliminaries and state-space representation of discrete cone causal systems are presented. In Section 2.3, we demonstrate that the optimal decentralized controller can be designed based on an infinite number of model matching problems which can be solved efficiently. This is followed in Section 2.4 by an example illustrating the validity of the results. Finally, some concluding remarks are drawn in Section 2.5.

2.2 Discrete Cone Causal Systems

The framework considered in this research for discrete cone casual systems was first introduced in [40]. The spatially invariant system G with inputs $u(i, t)$ and outputs $y(i, t)$ has the following form

$$\begin{aligned} y(i, t) &= \sum_{j=-\infty}^{\infty} \sum_{\tau=-\infty}^{\infty} \hat{g}(i-j, t-\tau) u(j, \tau) \\ \hat{g}(i, t) &= 0, \quad \forall t < 0 \quad (\text{due to temporal causality}) \end{aligned} \quad (2.1)$$

where i is discrete space, t is discrete time, and $\hat{g}(i, t)$ represents the spatio-temporal impulse response of G and has temporal causality. Using the λ -transform $g(i, \lambda) = \sum_{t=0}^{\infty} \hat{g}(i, t) \lambda^t$, the spatio-temporal transfer function G is given by

$$G(z, \lambda) := \sum_{i=-\infty}^{\infty} g(i, \lambda) z^i \quad (2.2)$$

where z denotes the two-sided spatial transform variable, λ denotes the one-sided temporal transform variable and input-output relation is as follow

$$Y(z, \lambda) = G(z, \lambda) U(z, \lambda) \quad (2.3)$$

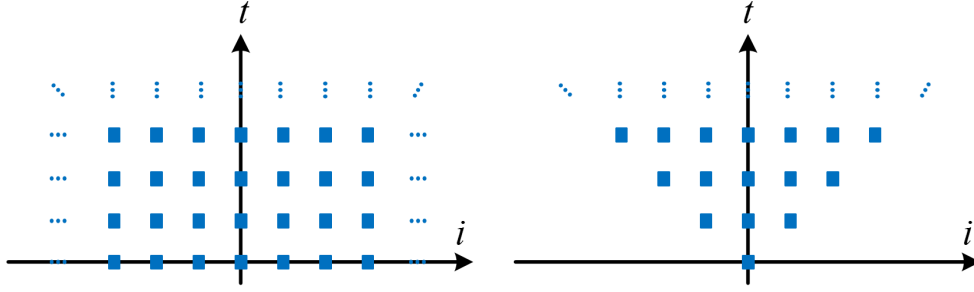


Figure 2.1: Support of the spatio-temporal impulse response of a centralized (left) and a cone causal (right) system.

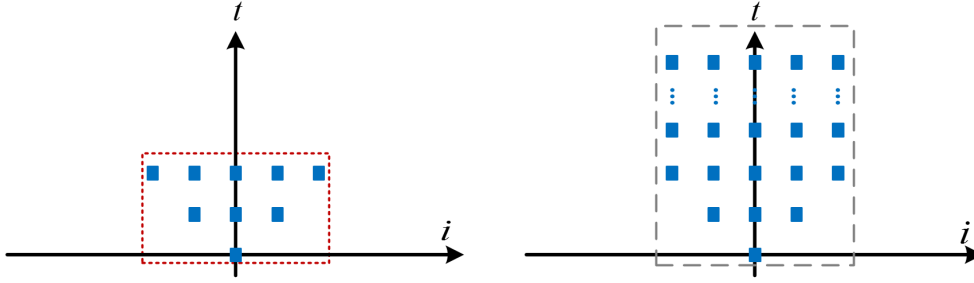


Figure 2.2: Support of a finite approximation of a cone causal system using equation (2.4) in the right and equation (2.5) in the left.

where $Y(z, \lambda)$ is the transform of $y(i, t)$ and $U(z, \lambda)$ is the transform of $u(i, t)$.

Particular structure of interest is the case where the spatio-temporal impulse response of the system $\hat{g}(i, t)$ has the cone causal structure as shown in Fig. 2.1.

Definition 2.1. A discrete linear system $y = Gu$ is called cone causal if it has the following form [40]

$$\begin{aligned} G(z, \lambda) &= \sum_{i=-\infty}^{\infty} g_i(\lambda) z^i \\ g_i(\lambda) &= \lambda^{|i|} \tilde{g}_i(\lambda) \end{aligned} \tag{2.4}$$

where the transfer function $\tilde{g}_i(\lambda)$ corresponds to temporally causal systems.

The interpretation of this property is that the input u_k to the k th system g_k affects the output y_m of the m th system g_m , which is $|k - m|$ spatial location away with a delay of

$|k - m|$ time steps [40]. This type of cone causal systems can also be written in the following form

$$\begin{aligned} G(z, \lambda) &= \sum_{k=0}^{\infty} g_k(z) \lambda^k \\ g_k(z) &= \sum_{n=-k}^k g_{n,k} z^n \end{aligned} \quad (2.5)$$

For an infinite number of terms, the above two systems are equivalent. However, we usually use a finite number of terms in the calculations, thus the first definition is more general as shown in Fig. 2.2 for one example.

In general, the transfer function $G(z, \lambda)$ can be seen as a multiplication operator on $\mathcal{L}_2(\mathbf{T}, \bar{\mathcal{D}})$ where \mathbf{T} is the unit circle and $\bar{\mathcal{D}}(\mathcal{D})$ is the closed (open) unit disc of the complex domain \mathbb{C} . Assume that $G(z, \lambda)$ is stable, then we have [44]

$$\begin{aligned} G(z, \lambda) : \mathcal{L}_2(\mathbf{T}, \bar{\mathcal{D}}) &\longrightarrow \mathcal{L}_2(\mathbf{T}, \bar{\mathcal{D}}) \\ u &\longrightarrow Gu = G(e^{i\theta}, \lambda)u(e^{i\theta}, \lambda) \end{aligned} \quad (2.6)$$

where $0 \leq \theta < 2\pi$, and $|\lambda| \leq 1$.

From H^p -theory [46] asserts that if $f \in \mathcal{H}_2$, then $f(e^{jw}) \in L_2$, that is, H_2 may be viewed as a closed subspace of L_2 . Letting \mathcal{H}_2^\perp be the orthogonal complement in L_2 , then we have

$$L_2 = \mathcal{H}_2 \oplus \mathcal{H}_2^\perp, \quad (2.7)$$

which means that every $f \in L_2$ can be written uniquely as

$$f = f_1 + f_2, \quad (2.8)$$

with $f_1 \in H_2$ and $f_2 \in \mathcal{H}_2^\perp$. The ℓ_2 -norm of the original system can be defined as

$$\|G\|_2 = \left(\sum_{i=-\infty}^{\infty} \sum_{t=0}^{\infty} |\hat{g}(t, i)|^2 \right)^{\frac{1}{2}} \quad (2.9)$$

and the \mathcal{H}_2 -norm of its transform $G(z, \lambda)$ is given by

$$\|G\|_{\mathcal{H}_2} = \frac{1}{2\pi} \left[\int_{\theta \in [0, 2\pi]} \int_{w \in [0, 2\pi]} |G(e^{i\theta}, e^{iw})|^2 dw d\theta \right]^{\frac{1}{2}} \quad (2.10)$$

where the isometry $\|G\|_2 = \|G\|_{\mathcal{H}_2}$ holds. Before solving the optimal \mathcal{H}_2 decentralized control problem for cone causal systems, it is also important to review the basics of state-space representation of this class of systems.

Definition 2.2. *Consider the system G with state-space representation*

$$G = \left[\begin{array}{c|c} A(z) & B \\ \hline C(z) & D \end{array} \right] = D + \lambda C(z)(I - \lambda A(z))^{-1} B \quad (2.11)$$

The set of ℓ -causal system refers to the system where B and D are independent of z and matrices $A(z)$ and $C(z)$ are of the following forms [47]

$$A(z) = A_{-1}z^{-1} + A_0 + A_1z^1 \quad (2.12)$$

$$C(z) = C_{-1}z^{-1} + C_0 + C_1z^1 \quad (2.13)$$

where A_n and C_n are independent of z and the dimension of the matrix A denotes the temporal order of the system.

The set of ℓ -causal systems is equal to the set of cone causal systems. Note that this set is closed under addition, composition, and inversion of systems [47]. Thus, it is closed under feedback and linear fractional (Youla) transformations. For complex systems, the state space representation of the controller can be obtained by realizing each element of the transfer function by performing basic sum, product, and inverse operations. Suppose that G_1 and G_2 are two subsystems with the following state-space representation

$$G_1 = \left[\begin{array}{c|c} A_1(z) & B_1 \\ \hline C_1(z) & D_1 \end{array} \right], \quad G_2 = \left[\begin{array}{c|c} A_2(z) & B_2 \\ \hline C_2(z) & D_2 \end{array} \right] \quad (2.14)$$

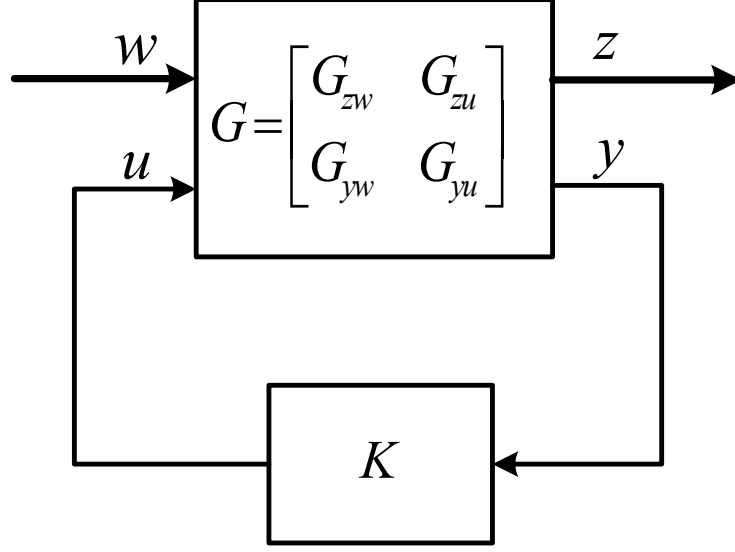


Figure 2.3: General control configuration.

The following operations are useful to build the state-space model of the transfer function [\[48\]](#)

$$G_1^{-1} = \left[\begin{array}{c|c} A_1(z) - B_1 D_1^{-1} C_1(z) & -B_1 D_1^{-1} \\ \hline D_1^{-1} C_1(z) & D_1^{-1} \end{array} \right] \quad (2.15)$$

$$G_1 + G_2 = \left[\begin{array}{cc|c} A_1(z) & 0 & B_1 \\ 0 & A_2(z) & B_2 \\ \hline C_1(z) & C_2(z) & D_1 + D_2 \end{array} \right] \quad (2.16)$$

$$G_1 G_2 = \left[\begin{array}{cc|c} A_1(z) & B_1 C_2(z) & B_1 D_2 \\ 0 & A_2(z) & B_2 \\ \hline C_1(z) & D_1 C_2(z) & D_1 D_2 \end{array} \right] \quad (2.17)$$

In the next section, the decentralized problem is verbalized in detail and an explicit solution is presented.

2.3 Design of Optimal \mathcal{H}_2 Decentralized Controller

Our goal in this research is to design the optimal \mathcal{H}_2 decentralized controllers for general disturbance attenuation problem as shown Fig. 2.3. The open loop system is denoted by G , the controller by K , the performance outputs by z , the measurements by y , the input control signals by u and the external disturbances by w . The closed loop disturbance response from w to z is given by

$$T_{zw} = G_{zw} + G_{zu}K(I - G_{yu}K)^{-1}G_{yw} \quad (2.18)$$

where the stable spatio-temporal controller K (internally) stabilizes and minimizes the \mathcal{H}_2 norm of the disturbance transfer function T_{zw} . The particular structure of interest is when the spatio-temporal transfer function G_{yu} yields the following cone causal form (as defined in Section 2.2):

$$\begin{aligned} G_{yu}(z, \lambda) &= \sum_{i=-\infty}^{\infty} g_i(\lambda)z^i \\ g_i(\lambda) &= \lambda^{|i|}\tilde{g}_i(\lambda) \end{aligned} \quad (2.19)$$

The optimal decentralized controllers K have the same structure as G_{yu} [40, 49], that is,

$$\begin{aligned} K(z, \lambda) &= \sum_{i=-\infty}^{\infty} k_i(\lambda)z^i \\ k_i(\lambda) &= \lambda^{|i|}\tilde{k}_i(\lambda) \end{aligned} \quad (2.20)$$

which means that the measurements of the j th location will be available at the i th system after $|j - i|$ time steps delay.

The following proposition asserts that the decentralized constraints on the controller K can be enforced on the Youla parameter Q using similar convex constraints.

Proposition 2.3. *For open loop stable systems, all stabilizing controllers K with the structure (2.20) are given by [40, 49]*

$$K = -Q(I - G_{yu}Q)^{-1} \quad (2.21)$$

with Q given by

$$\begin{aligned} Q(z, \lambda) &= \sum_{i=-\infty}^{\infty} q_i(\lambda) z^i \\ q_i(\lambda) &= \lambda^{|i|} \tilde{q}_i(\lambda) \end{aligned} \quad (2.22)$$

where $\tilde{q}_i(\lambda)$ is stable.

Using the Youla parameterization, the disturbance transfer function can be recast as $T_{zw} = T_1 - T_2Q$. The decentralized \mathcal{H}_2 optimal control problem can then be written as

$$\begin{aligned} J &:= \inf_{K_{\text{stabilizing}} \text{ s.t. (2.20) hold}} \|T_{zw}\|_{\mathcal{H}_2} \\ &= \inf_{Q \text{ stable s.t. (2.22) hold}} \|T_1 - T_2Q\|_{\mathcal{H}_2} \end{aligned} \quad (2.23)$$

The inner-outer factorization of T_2 defined as

$$T_2(e^{j\theta}, \lambda) = T_{2in}(e^{j\theta}, \lambda) T_{2out}(e^{j\theta}, \lambda) \quad (2.24)$$

where inner function T_{2in} is isometry and outer function T_{2out} is causally invertible. Therefore, (2.23) reduces to

$$J = \inf_{Q \text{ stable s.t. (2.22) hold}} \|T_{2in}^* T_1 - T_{2out} Q\|_{L_2} \quad (2.25)$$

Since $\{z^i\}_{i=-\infty}^{\infty}$ is an orthogonal basis of L_2 , $T_{2in}^* T_1$ can be written as:

$$T_{2in}^*(z, \lambda) T_1(z, \lambda) = \sum_{i=-\infty}^{\infty} \tilde{T}_i(\lambda) z^i \quad (2.26)$$

where $\tilde{T}_i(\lambda) \in L^2$. The outer function T_{2out} also admits the same cone structure

$$\begin{aligned} T_{2out}(z, \lambda) &= \sum_{i=-\infty}^{\infty} v_i(\lambda) z^i \\ v_i(\lambda) &= \lambda^{|i|} \tilde{v}_i(\lambda) \end{aligned} \tag{2.27}$$

and $\tilde{v}_i(\lambda)$ is stable. Therefore, $T_{2out}Q$ have the following structure

$$T_{2out}(z, \lambda)Q(z, \lambda) = \sum_{i=-\infty}^{\infty} \eta_i(\lambda) z^i \tag{2.28}$$

where $\eta_i(\lambda)$ can be written as

$$\begin{aligned} \eta_i(\lambda) &= \sum_{j=-\infty}^{\infty} \lambda^{|j|} \tilde{q}_j(\lambda) \lambda^{|i-j|} \tilde{v}_{i-j}(\lambda) \\ &= \sum_{j=-\infty}^{\infty} \lambda^{|j|+|i-j|} \tilde{q}_j(\lambda) \tilde{v}_{i-j}(\lambda) \end{aligned} \tag{2.29}$$

From triangle inequality, we have

$$|j| + |i-j| \geq |j+i-j| = |i| \tag{2.30}$$

As a result, for any $\eta_i(\lambda)$, there is always a stable term of $\lambda^{|i|}$ that can be factorized in the sum. It is important to note that $\lambda^{|i|}$ has the same index as $\eta_i(\lambda)$. Moreover, $\tilde{q}_j(\lambda)$ and $\tilde{v}_{i-j}(\lambda)$ are both stable. Therefore, we can write

$$\begin{aligned} \eta_i(\lambda) &= \lambda^{|i|} \sum_{j=-\infty}^{\infty} \lambda^{|j|+|i-j|-|i|} \tilde{q}_j(\lambda) \tilde{v}_{i-j}(\lambda) \\ &= \lambda^{|i|} \tilde{\eta}_i(\lambda) \end{aligned} \tag{2.31}$$

where $\tilde{\eta}_i(\lambda)$ is stable. Substituting (2.26) and (2.28) into the decentralized optimization (2.25) yields

$$\begin{aligned} J^2 &= \inf_{\eta_i(\lambda) \text{ is cone stable}} \left\| \sum_{i=-\infty}^{\infty} \tilde{T}_i(\lambda) z^i - \sum_{i=-\infty}^{\infty} \eta_i(\lambda) z^i \right\|_{L_2}^2 \\ &= \inf_{\tilde{\eta}_i(\lambda) \text{ is stable}} \left\| \sum_{i=-\infty}^{\infty} \tilde{T}_i(\lambda) z^i - \sum_{i=-\infty}^{\infty} \lambda^{|i|} \tilde{\eta}_i(\lambda) z^i \right\|_{L_2}^2 \end{aligned} \quad (2.32)$$

Using the Parseval's identity

$$J^2 = \inf_{\tilde{\eta}_i(\lambda) \text{ is stable}} \sum_{i=-\infty}^{\infty} \left\| \tilde{T}_i(\lambda) - \lambda^{|i|} \tilde{\eta}_i(\lambda) \right\|_{L_2}^2 \quad (2.33)$$

where the following equation gives the optimal (minimal) \mathcal{H}_2 decentralized cost (J_{opt}) for this class of spatially invariant systems

$$J_{opt}^2 = \sum_{i=-\infty}^{\infty} \left\| \frac{\tilde{T}_i(\lambda)}{\lambda^{|i|}} \right\|_{\mathcal{H}_2^\perp}^2 \quad (2.34)$$

The minimum in (2.33) is achieved by choosing $\tilde{\eta}_i(\lambda)$ satisfying

$$\tilde{\eta}_i(\lambda) = \Pi \left[\frac{\tilde{T}_i(\lambda)}{\lambda^{|i|}} \right] \quad (2.35)$$

where $i \in (-\infty, \infty)$ and Π is the orthogonal projection from L_2 into \mathcal{H}_2 . The optimal decentralized Youla parameter is then given by

$$Q = \frac{\sum_{i=-\infty}^{\infty} \lambda^{|i|} \tilde{\eta}_i(\lambda) z^i}{T_{2out}(z, \lambda)} \quad (2.36)$$

From (2.21), the explicit optimal \mathcal{H}_2 decentralized controller $K(z, \lambda)$ is given in the following closed form

$$K = -\frac{\sum_{i=-\infty}^{\infty} \lambda^{|i|} \tilde{\eta}_i(\lambda) z^i}{T_{2out}(z, \lambda)} \left[I - G_{yu}(z, \lambda) \frac{\sum_{i=-\infty}^{\infty} \lambda^{|i|} \tilde{\eta}_i(\lambda) z^i}{T_{2out}(z, \lambda)} \right]^{-1} \quad (2.37)$$

To realize the controller $K(z, \lambda)$, the most straightforward way is to first realize each element of the transfer functions $\sum \lambda^{|i|} \tilde{\eta}_i(\lambda) z^i$, T_{2out} and G_{yu} individually. Each realization can be obtained by sum or product of several simply realizable transfer function. Finally, the optimal H_2 decentralized control law K in (2.37) can be combined using basic operations (2.15)-(2.17) and can be realized by a positive feedback interconnection as follows

$$G_1(z, \lambda) := \sum_{i=-\infty}^{\infty} \lambda^{|i|} \tilde{\eta}_i(\lambda) z^i = \left[\begin{array}{c|c} A_1(z) & B_1 \\ \hline C_1(z) & D_1 \end{array} \right] \quad (2.38)$$

$$G_2(z, \lambda) := T_{2out}(z, \lambda) = \left[\begin{array}{c|c} A_2(z) & B_2 \\ \hline C_2(z) & D_2 \end{array} \right] \quad (2.39)$$

$$G_{yu}(z, \lambda) = \left[\begin{array}{c|c} A(z) & B \\ \hline C(z) & D \end{array} \right] \quad (2.40)$$

and we have

$$G_2(z, \lambda)^{-1} = \left[\begin{array}{c|c} \frac{A_2(z) - B_2 D_2^{-1} C_2(z)}{D_2^{-1} C_2(z)} & \frac{-B_2 D_2^{-1}}{D_2^{-1}} \\ \hline \end{array} \right] \quad (2.41)$$

$$\frac{G_1(z, \lambda)}{G_2(z, \lambda)} = \left[\begin{array}{cc|c} A_1(z) & B_1 D_2^{-1} C_2(z) & B_1 D_2^{-1} \\ 0 & \frac{A_2(z) - B_2 D_2^{-1} C_2(z)}{D_1 D_2^{-1} C_2(z)} & \frac{-B_2 D_2^{-1}}{D_1 D_2^{-1}} \\ \hline C_1(z) & \underbrace{D_1 D_2^{-1} C_2(z)}_{C_3} & \underbrace{D_1 D_2^{-1}}_{D_3} \end{array} \right] \quad (2.42)$$

From Fig. 2.4, it follows that a state space realization of K is given by

$$K(z, \lambda) = \left[\begin{array}{c|c} A_k(z) & B_k \\ \hline C_k(z) & D_k \end{array} \right] \quad (2.43)$$

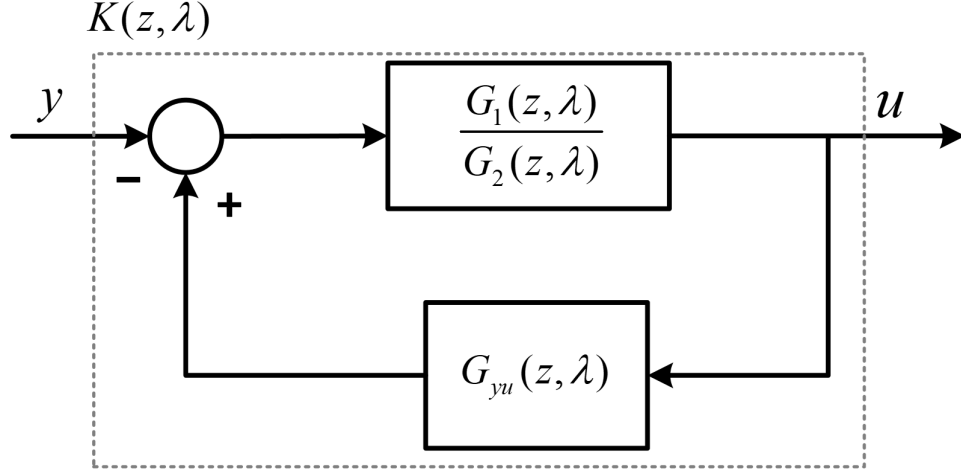


Figure 2.4: Positive feedback block diagram realization of K .

where A_k , B_k , C_k and D_k are defined in as follows

$$A_k(z) = \begin{bmatrix} A_3(z) + B_3 D(I - D_3 D)^{-1} C_3(z) & B_3(I - D D_3)^{-1} C(z) \\ B(I - D_3 D)^{-1} C_3(z) & A(z) + B D_3(I - D D_3)^{-1} C(z) \end{bmatrix} \quad (2.44)$$

$$B_k = \begin{bmatrix} -B_3(I - D D_3)^{-1} \\ -B D_3(I - D D_3)^{-1} \end{bmatrix} \quad (2.45)$$

$$C_k(z) = \begin{bmatrix} (I - D D_3)^{-1} C_3(z) & (I - D D_3)^{-1} D_3 C(z) \end{bmatrix} \quad (2.46)$$

$$D_k = -D_3(I - D_3 D)^{-1} \quad (2.47)$$

2.4 Numerical Results

In this section, the above framework is applied to design an optimal H_2 decentralized controller and represent the state-space description of the controller. For comparison purposes, we followed the discrete time example given in [40] obtained by discretizing a specific partial differential equation. The goal is to compute the optimal H_2 disturbance attenuation for the system with transfer function $G(z, \lambda)$ and the weighting function $W(z, \lambda)$

as follows

$$G(z, \lambda) = \frac{\tau \lambda}{1 - (\gamma/2)(z^{-1} + 2\alpha + z)\lambda} \quad (2.48)$$

$$W(z, \lambda) = \frac{\lambda}{1 - (c/2)(z^{-1} + 2a + z)\lambda} \quad (2.49)$$

The weighting function has similar structure as the plant $G(z, \lambda)$. Assume that $\tau = 1$, $\gamma = 1/3$, $\alpha = 1$, $c = 1/4$ and $a = 1$. The problem can then be formulated as follows

$$J = \inf_{Q \text{ stable s.t. (2.22)}} \|T_{zw}\|_{\mathcal{H}_2} \quad (2.50)$$

where

$$\|T_{zw}\|_{\mathcal{H}_2} = \|(1 - GQ)W\|_{\mathcal{H}_2} = \|T_1 - T_2Q\|_{\mathcal{H}_2} \quad (2.51)$$

The transfer function $T_1(z, \lambda)$ and $T_2(z, \lambda)$ are as follows

$$T_1(z, \lambda) = \frac{\lambda}{1 - r(z)\lambda} \quad (2.52)$$

$$T_2(z, \lambda) = \frac{\tau \lambda^2}{(1 - \rho(z)\lambda)(1 - r(z)\lambda)} \quad (2.53)$$

and

$$\rho(z) = z/6 + 1/3 + z^{-1}/6 \quad (2.54)$$

$$r(z) = z/8 + 1/4 + z^{-1}/8 \quad (2.55)$$

The following inner-outer factorization is computed as

$$T_{2in}(z, \lambda) = \lambda^2 \quad (2.56)$$

$$T_{2out}(z, \lambda) = \frac{\tau}{(1 - \rho(z)\lambda)(1 - r(z)\lambda)} \quad (2.57)$$

where T_{2in} is an isometry and T_{2out} is causally invertible with respect to the temporal variable. It can be seen that

$$\begin{aligned} T_{2in}^*(z, \lambda)T_1(z, \lambda) &= \frac{\lambda^{-1}}{1 - r(z)\lambda} = \lambda^{-1} + r(z) \\ &+ \lambda r^2(z) + \lambda^2 r^3(z) + \dots \end{aligned} \quad (2.58)$$

Using (2.26) and (2.58), $\tilde{T}_i(\lambda)$ can be approximated as

$$\begin{aligned} \tilde{T}_0(\lambda) &= \lambda^{-1} + \frac{1}{4} + \frac{3}{32}\lambda^1 + \frac{5}{128}\lambda^2 + \dots \\ \tilde{T}_{\pm 1}(\lambda) &= \frac{1}{8} + \frac{1}{16}\lambda + \frac{15}{512}\lambda^2 + \frac{7}{512}\lambda^3 + \dots \\ \tilde{T}_{\pm 2}(\lambda) &= \frac{1}{64}\lambda + \frac{3}{256}\lambda^2 + \frac{7}{1024}\lambda^3 + \frac{15}{4096}\lambda^4 \dots \end{aligned} \quad (2.59)$$

Therefore, $\tilde{\eta}_i$ can be calculated as

$$\begin{aligned} \tilde{\eta}_0(\lambda) &= \frac{1}{4} + \frac{3}{32}\lambda^1 + \frac{5}{128}\lambda^2 + \dots \\ \tilde{\eta}_{\pm 1}(\lambda) &= \frac{1}{16} + \frac{15}{512}\lambda^1 + \frac{7}{512}\lambda^2 + \dots \\ \tilde{\eta}_{\pm 2}(\lambda) &= \frac{3}{256} + \frac{7}{1024}\lambda^1 + \frac{15}{4096}\lambda^2 + \dots \end{aligned} \quad (2.60)$$

Note that the problem is infinite dimensional and we have showed the above calculation for five spatial order. From (2.36), the Youla-parametrization variable Q can then be calculated as follows

$$\begin{aligned} Q(z, \lambda) &= \frac{1}{4} - \frac{1}{96}(z^{+1} + 5 + z^{-1})\lambda - \frac{1}{1536}(2z^{+2} \\ &+ 21z^{+1} + 32 + 21z^{-1} + 2z^{-2})\lambda^2 + \dots \end{aligned} \quad (2.61)$$

In general, the transfer function $\sum \tilde{\eta}_i(\lambda)z^i$ has infinite number of terms. As a result, $Q(z, \lambda)$ is also infinite dimensional. By computing the transfer function $Q(z, \lambda)$ for three terms, the distributed controller $K(z, \lambda)$ can be calculated as shown in (2.62). The state-space description of $K(z, \lambda)$ can also be obtained using the procedure in Section 2.3 as shown in (2.63).

Table 2.1: Comparison of Optimal Norm for Different Temporal Orders of the Distributed Controller.

Temporal Order		$J = T_{zw} _{\mathcal{H}_2}$
$\sum \tilde{\eta}_i(\lambda)z^i$	$Q(z, \lambda)$	
0	2	1.0261
1	3	1.0180
2	4	1.0162
3	5	1.0159
4	6	1.0158
5	7	1.0158
6	8	1.0157
Using Relaxed Controller in [40]		1.0659
Optimal Decentralized Norm [40]		1.0157
Using Centralized Controller [40]		1.0000

Table 2.1 shows the resulting closed-loop performance for the optimal decentralized controller with different approximation order as well as other types of decentralized controllers. It is interesting to note that our method converges very fast to the optimal decentralized norm. In [40], the authors had calculated the solution of the relaxed controller and the optimal decentralized norm numerically. There was no explicit solution on the non-relaxed decentralized controller K (or Youla parameter Q). It can clearly be seen that our proposed method achieves better performance in comparison to a suboptimal controller based on relaxation.

$$\begin{aligned}
K = & \frac{(-2z^3 - 11z^2 - 26z^1 - 34 - 26z^{-1} - 11z^{-2} - 2z^{-3})\lambda^3}{(12z^2 + 42z^1 + 60 + 42z^{-1} + 12z^{-2})\lambda^3 + (-48z^1 - 48 - 48z^{-1})\lambda^2 - 384\lambda + 1536} \\
& + \frac{(20z^2 + 66z^1 + 92 + 66z^{-1} + 20z^{-2})\lambda^2(16z^1 + 80 + 16z^{-1})\lambda - 384}{(12z^2 + 42z^1 + 60 + 42z^{-1} + 12z^{-2})\lambda^3 + (-48z^1 - 48 - 48z^{-1})\lambda^2 - 384\lambda + 1536} \quad (2.62)
\end{aligned}$$

2.5 Summary

In this work, we have developed a method to design the optimal \mathcal{H}_2 decentralized controller for a class of spatially invariant systems. The decentralized controller assumed the same structure as the plant whose impulse response admits a cone structure. Using Parseval's identity, the optimal \mathcal{H}_2 decentralized control problem is transformed into an infinite number of model matching problems with a specific structure that can be solved efficiently. In addition, the closed-form expression (explicit formula) of the decentralized controller is derived for the first time. Moreover, a constructive procedure to obtain the state-space representation of the decentralized controller which is more convenient for implementation. An illustrative numerical example is presented. In a forthcoming paper, the control design of optimal \mathcal{H}_2 decentralized control laws for funnel causal spatially invariant systems will be studied.

$$\begin{aligned}
T_{out}^{-1}(z, \lambda) : A(z) &= \begin{bmatrix} 0 & -0.125 - 0.25 - 0.125z^{-1} \\ 0 & 0 \end{bmatrix}, \quad B = \begin{bmatrix} -1.0 \\ -1.0 \end{bmatrix}, \quad C^T(z) = \begin{bmatrix} 0.167z + 0.333 + 0.167z^{-1} \\ 0.125z + 0.250 + 0.125z^{-1} \end{bmatrix}, \quad D = 1.0 \\
\sum_i \tilde{\eta}_i(\lambda) z^i \approx : A(z) &= 0, \quad B = 1.0, \quad C^T(z) = 0.0625z + 0.0938 + 0.0625z^{-1}, \quad D = 0.25 \\
G(z, \lambda) : A(z) &= 0.167z + 0.333 + 0.167z^{-1}, \quad B = 1.0, \quad C^T(z) = 1.0, \quad D = 0 \\
K(z, \lambda) : A(z) &= \begin{bmatrix} 0 & -0.125z - 0.25 - 0.125z^{-1} & -0.0625z - 0.0938 - 0.0625z^{-1} & 0.25 \\ 0 & 0 & -0.0625z - 0.0938 - 0.0625z^{-1} & 0.25 \\ 0 & 0 & 0 & -1 \\ -0.167z - 0.333 - 0.167z^{-1} & -0.125z - 0.25 - 0.125z^{-1} & -0.0625z - 0.0938 - 0.0625z^{-1} & 0.167z + 0.583 + 0.167z^{-1} \end{bmatrix} \\
B &= \begin{bmatrix} -0.25 \\ -0.25 \\ 1.0 \\ -0.25 \end{bmatrix}, \quad C^T(z) = \begin{bmatrix} -0.167z - 0.333 - 0.167z^{-1} \\ -0.125z - 0.250 - 0.125z^{-1} \\ -0.0625z - 0.0938 - 0.0625z^{-1} \\ 0.25 \end{bmatrix}, \quad D = 0.25
\end{aligned} \tag{2.63}$$

Chapter 3

Damping Controllers in the Presence of Saturation

This chapter presents the analysis and a method to design supplementary damping controllers (SDCs) for synchronous generators considering the effects of saturation limits. Usually, such saturation of control signals are imposed in order to enforce practical limitations such as component ratings. However, to guarantee the stability in the presence of saturation limits, the state trajectories must remain inside the domain of attraction (DA). In this chapter, the domain of attraction of a single-machine infinite-bus (SMIB) power system with saturation nonlinearity is estimated and compared with the exact description of the null controllable region. Then, both state-feedback and dynamic output-feedback controllers are designed to enlarge the DA. Our analysis shows that nonlinear effects of saturation should be considered to guarantee stability and satisfactory performance. Simulation results on a detailed nonlinear model of a synchronous generator indicate that the DA enlarges with the proposed controller. The results also indicate that Critical Clearing Time (CCT) and damping of the system with saturation can be improved by the proposed method. Part of the results in this chapter appeared in [\[50\]](#).

3.1 Introduction

Multiple approaches have been proposed in literature to design SDCs for power system components, including traditional synchronous generators [20, 21, 22, 23], modern FACTS devices [24, 25], energy storage systems [26] and renewable resources [27]. These efforts generally do not consider the nonlinear effects of hard saturation limits on control signals. Moreover, new generation sources connected to the grid through inverters, such as, photovoltaics, have the ability to provide damping signals but only within a narrow range dependent on operating conditions. It is critical to consider these actuator constraints for such components especially distributed generation resources and storage systems [51, 52].

In this chapter, saturation, or a hard limit, is considered for the control signals. Note that this is different from the traditional magnetic saturation of generators but instead reflects the practical limitations of equipment ratings and can be expressed using hard saturation limits restricting the amplitude of the controller output. These limits can be considered in the excitation to prevent undesirable tripping initiated by over-excitation or under-excitation of generators [53]. In case of generator SDCs, saturation limits should be considered in the supplementary control input signal and are usually in the range of ± 0.05 to ± 0.1 per unit which guarantee a modest level of contribution [54]. These limits allow an acceptable control range to provide adequate damping while preventing tripping of the equipment protection. Moreover, this may minimize the negative effects of SDCs on the voltage regulatory response.

There exists a large body of work in the control literature on stability analysis of systems with input constraints [16, 17, 18, 19]. However, the effects of saturation have not been taken into account in previous works for analyzing and designing SDCs [20, 23, 26, 24]. This research also extends the work reported in [55] and [56] in which the nonlinear effects of saturation on stability has not been considered. Saturation can negatively impact the performance of SDC since this restriction can limit the control effort available to damp the oscillation and consequently decreases the damping or leads to instability.

The main goal in this chapter is to propose a new method to design SDCs which results in a larger domain of attraction (DA) in the presence of saturation. In this chapter, the DA of a single-machine infinite-bus (SMIB) power system with saturation nonlinearity is

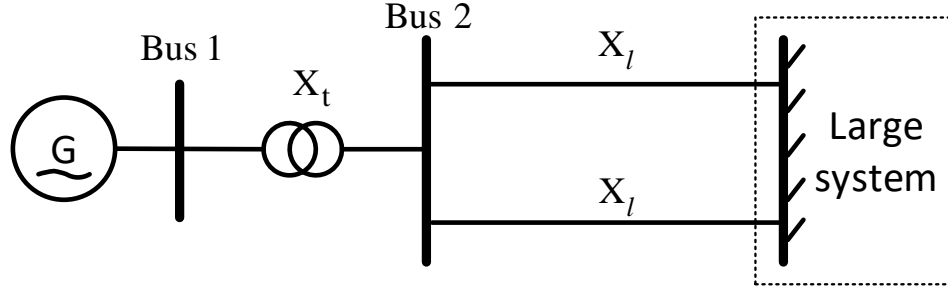


Figure 3.1: A single-machine infinite-bus power system.

estimated to guarantee a safety region of initial conditions (which may be caused by faults) and compared with exact description of the null controllable region. Then, state-feedback and output-feedback controllers are designed to enlarge the guaranteed domain of attraction. In this way, the stability of the SMIB power system is guaranteed and saturation limits are represented in the analysis and design procedure. Our analysis shows that nonlinear effects of saturation should be considered to guarantee the stability and satisfactory performance. Moreover, enlargement of DA effectively enhances the Critical Clearing Time (CCT) and damping of the system with saturation can be improved by the proposed method.

The rest of this chapter is structured as follows: preliminaries on dynamic modeling of the SMIB power system with input saturation nonlinearity are described in Section 3.2. Section 3.3 is devoted to optimal estimation of the DA for a power system with pre-designed state-feedback controller. For comparison purposes, exact description of the null controllable region of the SMIB power system is given in this section. An optimization method to design state-feedback and output-feedback controllers to enlarge the DA is described in section 3.6 and 3.5. The results are compared through detailed nonlinear simulations. Summary of remarks are presented in section 3.6.

3.2 Dynamic Model of System with Saturation

In this study, a SMIB power system model is considered. However, the analysis can be extended to cases of SMIB power system with FACTS devices. As shown in Fig. 3.1, this

system consists of a synchronous generator connected through two transmission lines to an infinite bus that represents an approximation of a large system. A flux-decay model of the synchronous generator equipped with a fast excitation system can be represented by the following set of dynamic equations:

$$\dot{\delta} = \omega_s(\omega_r - 1) \quad (3.1)$$

$$\dot{\omega}_r = \frac{1}{2H} [T_M - (E'_q I_q + (X_q - X'_d) I_d I_q + D\omega_s(\omega_r - 1))] \quad (3.2)$$

$$\dot{E}'_q = -\frac{1}{T'_{d0}} [E'_q + (X_d - X'_d) I_d - E_{fd}] \quad (3.3)$$

$$\dot{E}_{fd} = -\frac{E_{fd}}{T_A} + \frac{K_A}{T_A} [V_{ref} - V_t + \text{sat}(V_s)] \quad (3.4)$$

while satisfying the following algebraic equations:

$$R_e I_q + X_e I_d - V_q + V_\infty \cos(\delta) = 0 \quad (3.5)$$

$$R_e I_d - X_e I_q - V_d + V_\infty \sin(\delta) = 0 \quad (3.6)$$

$$V_t = \sqrt{V_d^2 + V_q^2} \quad (3.7)$$

where R_e and $X_e = X_t + \frac{1}{2}X_l$ are the total external resistance and reactance, respectively. One of the nonlinearities associated with the above model is due to the hard saturation limit considered on the supplementary control input of the exciter. In this work, the hard limit is defined as:

$$\text{sat}(V_s) = \text{sign}(V_s) \min\{m, |V_s|\} \quad (3.8)$$

$$m = V_s^{\max} = -V_s^{\min} \quad (3.9)$$

where the nonlinearity is assumed to be symmetric and $\pm m$ are the saturation limits. To design a SDC and study the effects of saturation, the above nonlinear model can be linearized around the nominal operating point and expressed in the following state-space representation:

$$\dot{x}(t) = Ax(t) + B\text{sat}(V_s) \quad (3.10)$$

where

$$x = \begin{bmatrix} \Delta\delta & \Delta\omega_r & \Delta E'_q & \Delta E'_{fd} \end{bmatrix}^T$$

$$A = \begin{bmatrix} 0 & \omega_s & 0 & 0 \\ -\frac{K_1}{2H} & -\frac{D\omega_s}{2H} & -\frac{K_2}{2H} & 0 \\ -\frac{K_4}{T'_{d0}} & 0 & -\frac{1}{K_3 T'_{d0}} & \frac{1}{T'_{d0}} \\ -\frac{K_A K_5}{T_A} & 0 & -\frac{K_A K_6}{T_A} & -\frac{1}{T_A} \end{bmatrix}, B = \begin{bmatrix} 0 \\ 0 \\ 0 \\ \frac{K_A}{T_A} \end{bmatrix} \quad (3.11)$$

and K_1 – K_6 are the well-known linearization constants summarized as follows [57]:

$$\Delta_e = R_e^2 + (X'_d + X_e)(X_q + X_e) \quad (3.12)$$

$$K_1 = -\frac{1}{\Delta_e} [I_q V_\infty (X'_d - X_q) ((X_q + X_e) \sin(\delta) - R_e \cos(\delta)) \quad (3.13)$$

$$+ V_\infty \{ (X'_d - X_q) I_d - E'_q \} \{ (X'_d + X_e) \cos(\delta) + R_e \sin(\delta) \}] \quad (3.14)$$

$$K_2 = \frac{1}{\Delta_e} [I_q \Delta_e - (I_q (X_q + X_e) + R_e I_d) (X'_d - X_q) + R_e E'_q] \quad (3.15)$$

$$K_3 = \frac{\Delta_e}{\Delta_e + (X_d - X'_d)(X_q + X_e)} \quad (3.16)$$

$$K_4 = \frac{V_\infty}{\Delta_e} (X_d - X'_d) [(X_q + X_e) \sin(\delta) - R_e \cos(\delta)] \quad (3.17)$$

$$K_5 = \frac{1}{\Delta_e V_t} [V_d X_q R_e V_\infty \sin(\delta) + V_d X_q V_\infty (X'_d + X_e) \cos(\delta) \quad (3.18)$$

$$+ V_q X'_d R_e V_\infty \cos(\delta) - V_q X'_d V_\infty (X_q + X_e) \sin(\delta)] \quad (3.19)$$

$$K_6 = \frac{1}{\Delta_e V_t} [V_d R_e X_q - V_d X'_d (X_q + X_e)] + \frac{V_d}{V_t}$$

Although the large gain of the excitation system K_A can reduce the generator terminal voltage fluctuations, it can also introduce negative damping torque to the system at times sufficient to result in instability. To increase the guaranteed region of stability, the DA for this unstable system with saturated feedback controller should be optimized.

3.3 Estimation of the DA

In this section, we address the problem of estimating the DA for a system with actuator constraint and a pre-designed state-feedback law. Consider the system of equations (3.10) with unstable matrix $A \in \mathbb{R}^{n \times n}$ and state-feedback control law defined by $V_s = Fx(t)$, the closed loop system can be expressed as follows:

$$\dot{x}(t) = Ax(t) + B\text{sat}(Fx(t)) \quad (3.20)$$

where the DA with the above transition map of $\phi : (t, x_0) \rightarrow x(t)$ can be defined as

$$\mathcal{D} := \{x_0 \in \mathbb{R}^n : \lim_{t \rightarrow +\infty} \phi(t, x_0) = 0\} \quad (3.21)$$

Without saturation limits, the DA for stable $A + BF$ is \mathbb{R}^n ; however in the presence of saturation, DA is a subset of \mathbb{R}^n and needs to be estimated. There are various methods to approximate the DA [16, 18]. In this research, we follow the work in [19] to obtain the least conservative estimation based on the Lyapunov function. For a matrix $P > 0$ and $\eta > 0$, we can define the ellipsoid $\varepsilon(P, \eta)$ representing the DA as follows:

$$\varepsilon(P, \eta) = \{x \in \mathbb{R}^n, \quad x'Px \leq \eta\} \quad (3.22)$$

which is a contractive invariant set inside the DA.

Theorem 3.1. *If there exists a symmetric positive definite matrix $W \in \mathbb{R}^{n \times n}$, a positive diagonal matrix $S \in \mathbb{R}^{m \times m}$ and a matrix $X \in \mathbb{R}^{m \times n}$ satisfying the following LMIs [19]*

$$\begin{aligned} & \begin{bmatrix} W(A + BF)' + (A + BF)W & BS - Z' \\ SB' - Z & -2S \end{bmatrix} < 0 \\ & \begin{bmatrix} W & WF' - Z' \\ FW - Z & m^2 \end{bmatrix} > 0 \end{aligned} \quad (3.23)$$

then based on quadratic Lyapunov function, the ellipsoid $\varepsilon(P, 1)$, with $P = W^{-1}$ is the domain of attraction for the system with input saturation.

Each eigenvalue of P is related with the length of one axis. Since $\text{trace}(P)$ is the sum of its eigenvalues, its minimization leads to the largest ellipsoid having the same weight in all directions. This problem can be formulated indirectly as the following optimization.

$$\begin{aligned}
& \min_{S, W, Z, M_W} \quad \text{trace}(M_W) \\
& \text{subject to} \quad \begin{bmatrix} M_W & I_n \\ I_n & W \end{bmatrix} > 0 \\
& \quad \begin{bmatrix} W(A + BF)' + (A + BF)W & BS - Z' \\ SB' - Z & -2S \end{bmatrix} < 0 \\
& \quad \begin{bmatrix} W & WF' - Z' \\ FW - Z & m^2 \end{bmatrix} > 0
\end{aligned} \tag{3.24}$$

where S , W and M_W are symmetric positive definite matrices and the ellipsoid $\varepsilon(P, \eta)$ with $P = W^{-1}$ is the estimated DA. In the above optimization, minimizing $\text{trace}(M_W)$ implies the minimization of $\text{trace}(P)$ as the first constraint guarantees that $P < M_W$. The second and third constraints guarantee asymptotic stability of saturated system via a quadratic Lyapunov function. Other size criteria such as maximization of the volume or other geometric characterization can also be considered. The estimated result can be compared with null controllable region \mathcal{C} , which is defined as the region where there exists an admissible bounded control that can steer the system towards the origin. The null controllable region of an unstable system can be found using the following theorem [58].

Theorem: Consider the open loop system (3.10) with unstable matrix A and B that can be partitioned as follows:

$$A = \begin{bmatrix} A_1 & 0 \\ 0 & A_2 \end{bmatrix}, \quad B = \begin{bmatrix} B_1 \\ B_2 \end{bmatrix} \tag{3.25}$$

where $A_1 \in \mathfrak{R}^{n_1 \times n_1}$ is semi-stable and $A_2 \in \mathfrak{R}^{n_2 \times n_2}$ is an unstable subsystem. Then null controllable region of the system can be written as:

$$\mathcal{C} = \mathfrak{R}^{n_1} \times \mathcal{C}_2 \tag{3.26}$$

where \mathcal{C}_2 is the null controllable region of the unstable subsystem. Different cases can be considered to find the boundary of \mathcal{C}_2 ; however, in the case of second order subsystems where A_2 has a pair of unstable complex eigenvalues $+\alpha \pm j\beta$, \mathcal{C}_2 can be characterized as follows:

$$\partial\mathcal{C}_2 = \left\{ \pm \left[e^{-A_2 t} (I + e^{-A_2 T_p})^{-1} (I - e^{-A_2 T_p}) - (I - e^{-A_2 t}) \right] m A_2^{-1} B_2 : t \in [0, T_p) \right\} \quad (3.27)$$

where $T_p = \frac{\pi}{\beta}$ and $\partial\mathcal{C}_2$ is the boundary of the null controllable region of the second subsystem.

Example: Throughout this chapter, the SMIB power system is considered to demonstrate the idea and verify the resulting improvement. Parameters of the machine, excitation system, transformer and transmission lines are:

$$\begin{aligned} X_t &= 0.1, & X_l &= 0.8, & R_e &= 0, & V_\infty &= 1.05 \angle 0^\circ, \\ X_d &= 2.5, & X_q &= 2.1, & X'_d &= 0.39, & V_t &= 1 \angle 15^\circ, \\ T'_{d0} &= 9.6, & H &= 3.2, & D &= 0, & \omega_s &= 377, \\ T_A &= 0.02, & K_A &= 100, & V_s^{\max} &= -V_s^{\min} = 0.05, \end{aligned}$$

Eigenvalue analysis shows that the open loop system has unstable complex eigenvalues of $+0.2423 \pm 7.6064i$ with frequency of 1.21 Hz and damping of -3.18% . The fault considered in this work is a three-phase fault to ground at bus 2 which is applied at $t = 0.1s$ with fault duration of t_f and cleared without line tripping. The CCT can be defined as the maximum allowable time to clear the fault such that system remains stable and gives information regarding the fault ride-through capability of the generator. First without considering the saturation, a state-feedback controller is designed using the LQR method [59] to minimize the following quadratic performance index:

$$J = \frac{1}{2} \int_0^\infty (x^T Q x + u^T R u) dt \quad (3.28)$$

where Q is a positive semi-definite weighted matrix related to state cost and R is a positive definite weighted matrix related to the control cost. The parameters of the LQR controller

are chosen to be $Q = I_{4 \times 4}$ and $R = 0.1$ and the controller gain can be obtained as follows:

$$F_{LQR} = \begin{bmatrix} -0.7047 & 9.4825 & -3.9325 & -3.1523 \end{bmatrix} \quad (3.29)$$

In the practice, these controllers can be implemented based on dynamic state estimation using PMU measurements [60, 61, 62, 63]. The largest guaranteed DA of the SMIB system with the above LQR controller can now be estimated from (3.24). The ellipsoidal DA is given as $\mathcal{D}_{LQR} = \varepsilon(P, 1)$ with:

$$P = \begin{bmatrix} 1.1072 & -0.0679 & 1.2368 & 2.5003 \times 10^{-4} \\ -0.0679 & 2844.6 & -46.7344 & -0.0036 \\ 1.2368 & -46.7344 & 19.6725 & 0.0014 \\ 2.5 \times 10^{-4} & -0.0036 & 0.0014 & 9.4678 \times 10^{-4} \end{bmatrix} \quad (3.30)$$

Using the canonical state-space transformation $z = Tx$ [64], the linear system of equation (3.10) can be transformed to canonical form and then partitioned as stable and unstable parts similar to (3.25). Fig. 3.2 compares cuts of the guaranteed DA of the closed loop system with LQR controller and the null controllable region in the presence of saturation. Using nonlinear simulations, the system with LQR controller has a *CCT* of 0.081 s. Fig. 3.3 shows the estimated DA and the extremal trajectory of the nonlinear SMIB system, which demonstrates the accuracy of estimated DA. In the next section, the optimization problem will be modified to design a state-feedback controller to expand the domain of attraction.

3.4 Enlarging the DA Using State-Feedback Controller

In general, size of the DA depends on the feedback controller and the system constraints, such as, saturation limits. Consequently, the choice of an optimization criterion should include the controller design F in order to enlarge the guaranteed DA. This formulation will introduce bilinear terms of a variable associated with the quadratic Lyapunov function $W = P^{-1}$ and the controller matrix F .

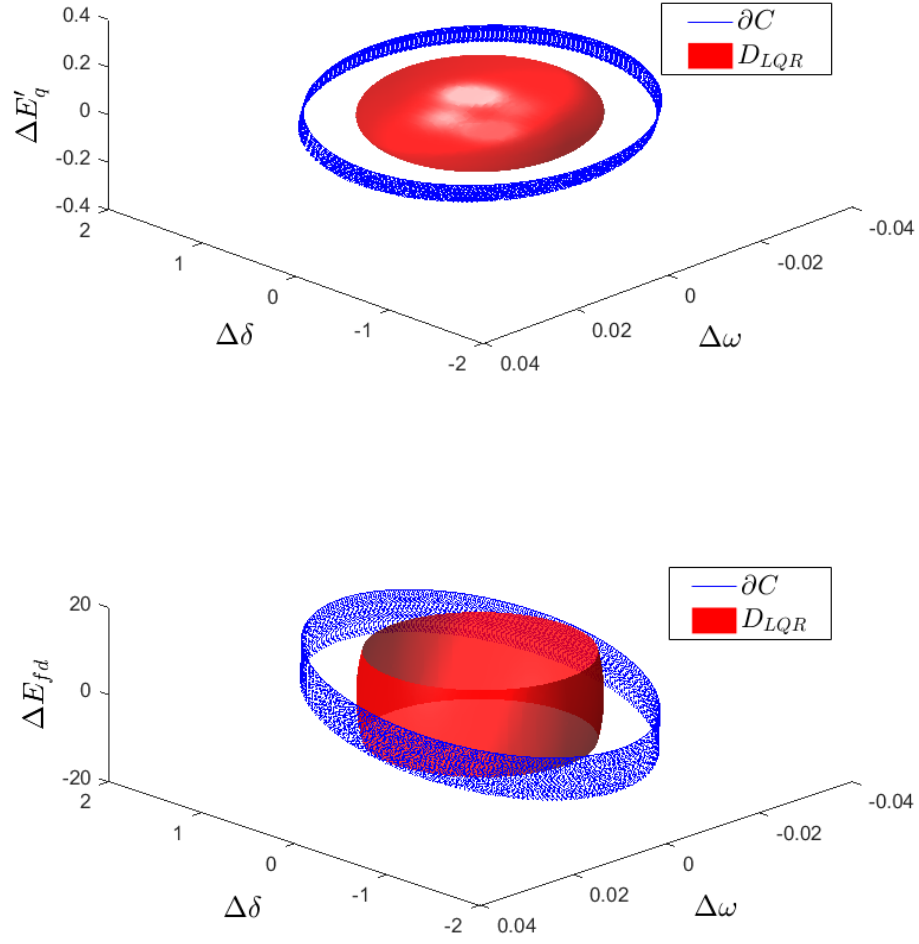


Figure 3.2: Boundary of null controllable region ($\partial\mathcal{C}$) and estimated DA for LQR controller (D_{LQR}) in the presence of saturation.

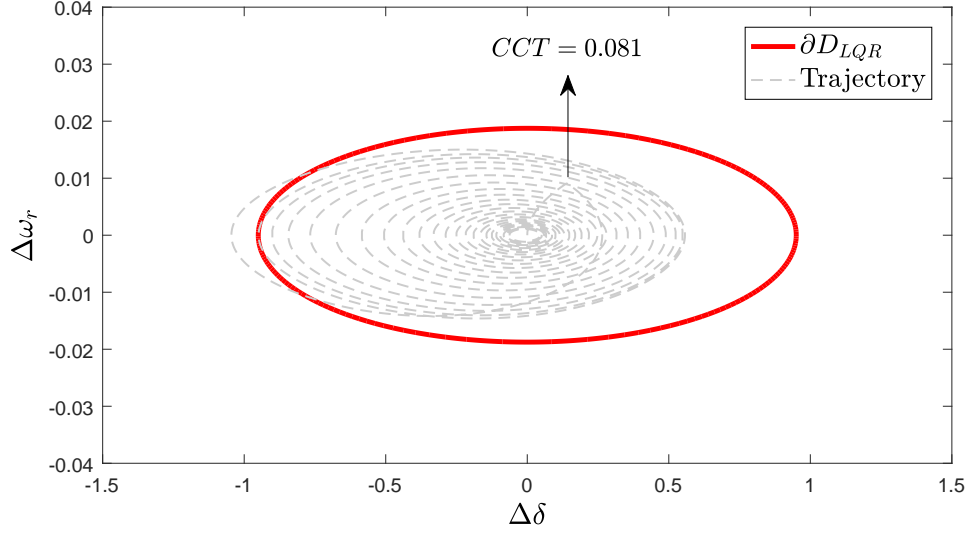


Figure 3.3: Boundary of estimated DA and trajectory of nonlinear SMIB system with LQR controller and critical fault duration of $CCT = 0.081s$.

By introducing an axillary variable $Y = FW$, this problem can be transformed into an LMI problem, namely:

$$\begin{aligned}
 & \min_{S, W, Y, Z, M_W} \text{trace}(M_W) \\
 & \text{subject to} \quad \begin{bmatrix} M_W & I_n \\ I_n & W \end{bmatrix} > 0 \\
 & \quad \begin{bmatrix} WA' + AW + BY + Y'B' & BS - Z' \\ SB' - Z & -2S \end{bmatrix} < 0 \\
 & \quad \begin{bmatrix} W & Y' - Z' \\ Y - Z & m^2 \end{bmatrix} > 0 \\
 & \quad WA' + AW + (Y'\Gamma_j^+ + Z'\Gamma_j^-)B' + B(\Gamma_j^+Y + \Gamma_j^-Z) + 2\alpha_1W < 0 \\
 & \quad WA' + AW + (Y'\Gamma_j^+ + Z'\Gamma_j^-)B' + B(\Gamma_j^+Y + \Gamma_j^-Z) + 2\alpha_2W > 0
 \end{aligned} \tag{3.31}$$

where controller matrix F can be obtained from $F = YW^{-1}$. Matrices Γ^+ and $\Gamma^- \in \Re^{m \times m}$ are diagonal matrices whose diagonal elements take the value 1 or 0, and $\Gamma^- + \Gamma^+ = I_m$ where $j = 1, \dots, 2^m$. For a single input system, these matrices can be either 0 or 1. The last two inequalities in optimization (3.31) are to restrict the pole placement region to a strip of

the complex plane between $-\alpha_1$ and $-\alpha_2$ to avoid high gains in the controller.

Example (continued): Using the above optimization (3.31), a controller can be designed to enlarge the DA of the SMIB system. Assuming $\alpha_1 = 0$ and $\alpha_2 = 80$, the enlarged DA is obtained as $\mathcal{D}_{Enl} = \varepsilon(P, 1)$ with:

$$P = \begin{bmatrix} 0.8411 & 0.6754 & 0.6719 & 0.0015 \\ 0.6754 & 2180.8 & -27.7163 & -0.0454 \\ 0.6719 & -27.7163 & 0.9029 & 0.0018 \\ 0.0015 & -0.0454 & 0.0018 & 3.7605 \times 10^{-6} \end{bmatrix} \quad (3.32)$$

where the optimized state-feedback controller is:

$$F_{Enl} = \begin{bmatrix} -3.3026 & 98.2739 & -3.9459 & -0.0081 \end{bmatrix} \quad (3.33)$$

Fig. 3.4 illustrates the effectiveness of the proposed approach in designing the SDC, which results in a significantly larger DA toward the boundary of null controllable region $\partial\mathcal{C}$ for the closed loop system, in compared to the original LQR controller. Numerical simulations reveal that system with optimized state-feedback controller shows improvement in the *CCT* to 0.109 s. Fig. 3.5 depicts a cut of the enlarged DA and extremal trajectory of the nonlinear SMIB system with optimized controller, which demonstrates the satisfactory accuracy.

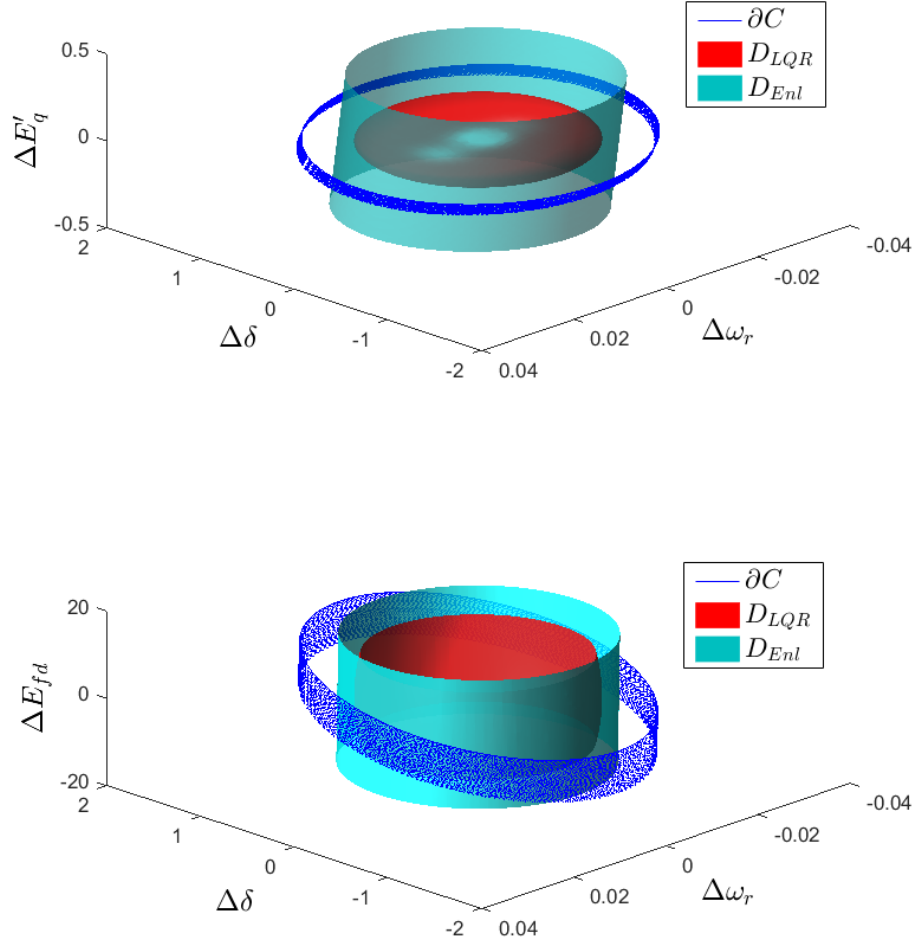


Figure 3.4: Boundary of null controllable region (∂C), estimated DA for LQR controller (D_{LQR}) and enlarged DA (D_{Enl}) in the presence of actuator saturation.

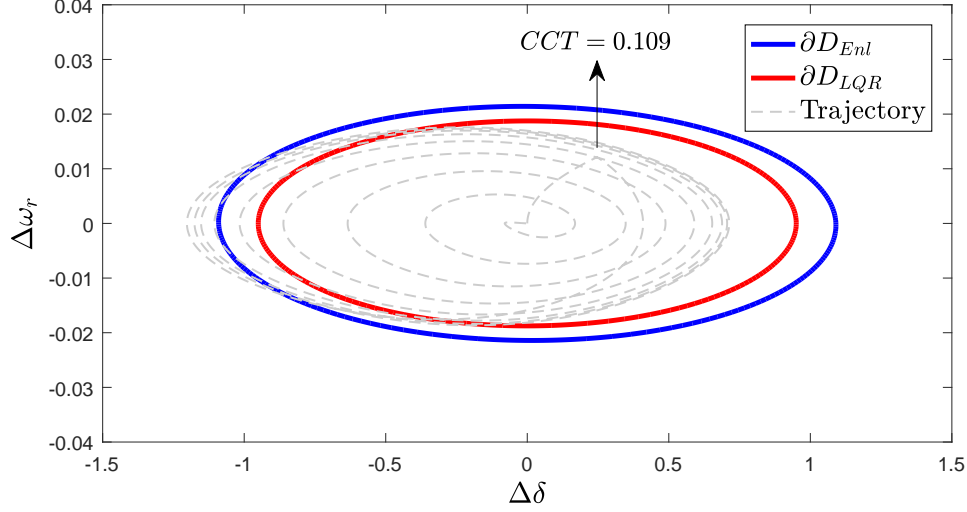


Figure 3.5: Comparison of estimated DA and trajectory of nonlinear SMIB system with LQR controller and critical fault duration of $CCT = 0.109s$.

Moreover, synchronizing and damping components of electrical torque can be used to compare the dynamic performance of the aforementioned controllers. The damping component (proportional to speed change) and the synchronizing component (proportional to angular change) are related to small-signal and transient stability, respectively. The corresponding coefficients are defined according to the following equation:

$$\Delta T_e = K_D \omega_s \Delta \omega_r + K_S \Delta \delta \quad (3.34)$$

where values of parameters K_D and K_S are estimated using the breaking algorithm [65] based on the angle, speed and torque response of the nonlinear system with actuator saturation. As shown in Table 3.1, the system with optimized controller has larger CCT, higher damping ratio and synchronization coefficient. Fig. 3.6 shows a comparison of the transient response of the closed loop system for a fault duration of $t_f = 0.1s$ in the presence of actuator saturation. Fig. 3.7 shows that the proposed controllers use the full feasible control range to enlarge the DA and their performance are close to a bang-bang control law.

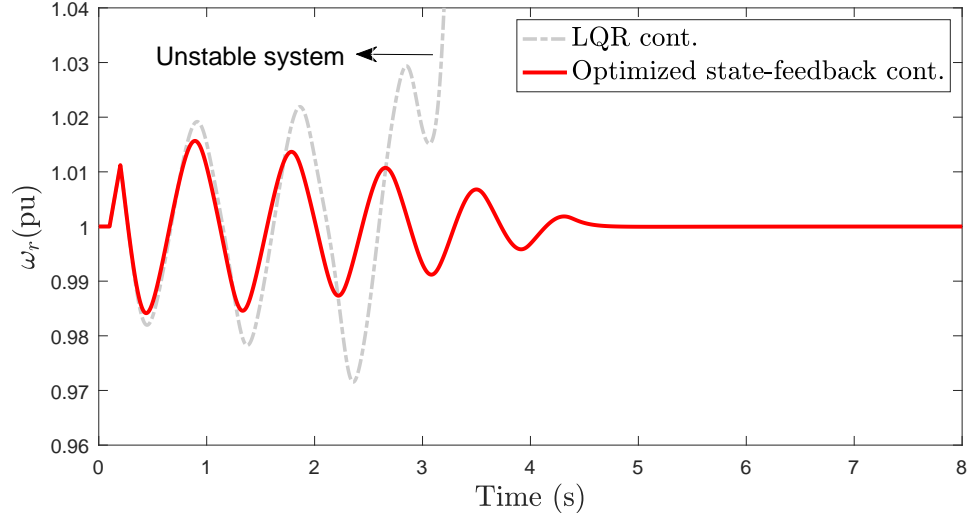


Figure 3.6: Comparison of transient responses for the system with fault duration of $t_f = 0.1s$.

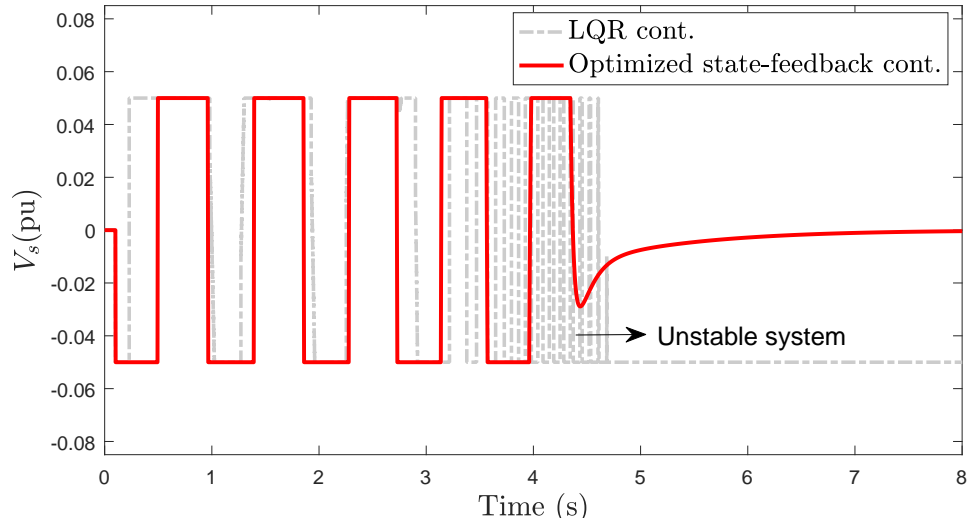


Figure 3.7: Comparison of supplementary control signals for system with fault duration of $t_f = 0.1s$.

Table 3.1: CCT and Coefficient Comparison for SMIB System with Different Controllers.

SDC type	CCT	K_D	K_S
Without controller	0.0 s	-0.00242 pu/(rad/s)	1.0003 pu/rad
LQR controller	0.081 s	0.00223 pu/(rad/s)	0.7078 pu/rad
Optimized output-feedback controller	0.00740 s	0.7548 pu/(rad/s)	0.8091 pu/rad
Optimized state-feedback controller	0.109 s	0.00946 pu/(rad/s)	0.8091 pu/rad

3.5 Enlarging the DA Using Dynamic Output-Feedback Controller

In practical applications for power systems, the full state vector is not available. Consequently, it is desirable to adopt the dynamic output-feedback controller to directly use the measured output signals for damping the oscillation. This type of controller can be defined as:

$$\dot{x}_c(t) = A_c x_c(t) + B_c y \quad (3.35)$$

$$y_c(t) = C_c x_c(t) + D_c y \quad (3.36)$$

where $x_c \in \mathbb{R}^n$ is the controller states, A_c , B_c , C_c , D_c are to be designed, and y_c and y are the controller and system outputs, respectively. In the presence of saturation, this controller yields the following closed loop system.

$$\dot{\hat{x}}(t) = A_{cl} \hat{x}(t) + B_{cl} \phi(y_c(t)) \quad (3.37)$$

$$y_c(t) = C_{cl} \hat{x}(t) \quad (3.38)$$

where $\phi(y_c(t)) = \text{sat}(y_c) - y_c$, $\hat{x}^T = [x^T \quad x_c^T]$ is the augmented system states and closed loop matrices are:

$$\left[\begin{array}{c|c} A_{cl} & B_{cl} \\ \hline C_{cl} & 0 \end{array} \right] = \left[\begin{array}{cc|c} A + BD_c C & BC_c & B \\ B_c C & A_c & 0 \\ \hline D_c C & C_c & 0 \end{array} \right] \quad (3.39)$$

The optimization problem of (3.30) at the bottom of next page can be formulated for the augmented system to design an output-feedback controller in order to enlarge DA of augmented system where S , X and Y are positive definite. These conditions follow with some modification from the results in [19]. Matrix $UV' = I - XY$ and matrix P have the

following structure:

$$P = \begin{bmatrix} X & U \\ U' & \hat{X} \end{bmatrix}, \quad P^{-1} = \begin{bmatrix} Y & V \\ V' & \hat{Y} \end{bmatrix} \quad (3.31)$$

According to (3.31), minimization of $\text{trace}(P)$ can be done by minimizing both $\text{trace}(X)$ and $\text{trace}(\hat{X})$. This can be accomplished indirectly by minimizing $\text{trace}(X) + \mu$ as the first constraint in the optimization guarantees that $\hat{X} < \mu I$ where $\hat{X} = U'(X - Y^{-1})^{-1}U$. The last inequality is added to ensure that U will be nonsingular. Therefore, the output-feedback matrices can be obtained from:

$$A_c = U^{-1}(W' - A' - C'D'_c B' - XBL - XAY - UB_cCY)(V')^{-1} \quad (3.32)$$

$$B_c = U^{-1}(F - XBD_c) \quad (3.33)$$

$$C_c = (L - D_cCY)(V')^{-1} \quad (3.34)$$

To limit the control effort, prevent fast dynamics and avoid high gains in the controller, pole-placement inside the LMI region is also considered by careful selection of matrices l and β . This region can be defined as the intersection of a canonic sector with inner angle 2θ

$$\begin{aligned} & \min_{S, X, Y, U, L, F, W, Z, Z_1, Q, D_c} \text{trace}(X) + \mu \\ & \text{subject to} \quad \begin{bmatrix} \mu I & U' & 0 \\ U & X & I \\ 0 & I & Y \end{bmatrix} > 0, \quad U + U' > 0 \\ & \quad \begin{bmatrix} AY + YA' + BL + L'B' & W & BS - Z' \\ W' & A'X + XA + C'F' + FC & Q - Z'_1 \\ SB' - Z & Q' - Z_1 & -2S \end{bmatrix} < 0 \\ & \quad \begin{bmatrix} Y & I & L' - Z' \\ I & X & C'D'_c - Z'_1 \\ L - Z & D_cC - Z_1 & m^2 \end{bmatrix} > 0 \\ & \quad l_{jk} \begin{bmatrix} Y & I \\ I & X \end{bmatrix} + \beta_{jk} \begin{bmatrix} AY + BL & A + BD_cC \\ W' - (A + BD_cC)' & XA + FC \end{bmatrix}^T \\ & \quad \quad \quad + \beta_{kj} \begin{bmatrix} AY + BL & A + BD_cC \\ W' - (A + BD_cC)' & XA + FC \end{bmatrix} < 0 \end{aligned} \quad (3.30)$$

where $\theta = \cos^{-1}(\xi)$ and a vertical strip of complex plane between $-\alpha_1$ and $-\alpha_2$.

Example (continued): Suppose that all of the states are available through measurements except E'_q and the parameters of the LMI region are assumed to be $\xi = 10\%$, $\alpha_1 = 0.25$ and $\alpha_2 = 100$. An output-feedback damping controller can be designed based on (3.30) and the controller matrices will be:

$$\begin{aligned} A_c &= \begin{bmatrix} -80.01 & 0.0009 & -0.0274 & -0.0101 \\ -0.0014 & -80.33 & -0.0948 & 1.97 \\ 0.0124 & -1.684 & -564.4 & -913.5 \\ -0.037 & -5.064 & -1082 & -2134 \end{bmatrix} \\ B_c &= \begin{bmatrix} -155.1 & -732.4 & -0.0467 \\ 0.0515 & -139.6 & 3.944 \\ -187.8 & -3746 & -2347 \\ -643.2 & -973.8 & -5269 \end{bmatrix} \\ C_c &= \begin{bmatrix} 0 & 0.0004 & 0.1038 & 0.2 \end{bmatrix} \\ D_c &= \begin{bmatrix} -0.3756 & 11.77 & 0.5047 \end{bmatrix} \end{aligned} \quad (3.35)$$

In this case, the estimated DA is obtained for an augmented system with twice the number of state variables of the original system. The results are more usefully compared based on the CCT as visualization of the DA for the high-dimensional augmented system is difficult. Moreover, synchronizing and damping components of electrical torque are also used to compare the performance of the aforementioned controllers.

As shown in Table 3.1, CCT for the closed loop system with optimized output-feedback damping controller is found to be $CCT = 0.103$. This CCT is larger than the system with an LQR controller and it is very close to the system with a full state-feedback controller. As a result, optimized output-feedback controller has enlarged the DA in compare to LQR controller. It can also be seen that the system with state-feedback controller has the highest damping and synchronization coefficient. Fig. 3.8 shows a comparison of the transient response of the closed loop system with different types of SDCs for a fault duration of $t_f = 0.1s$.

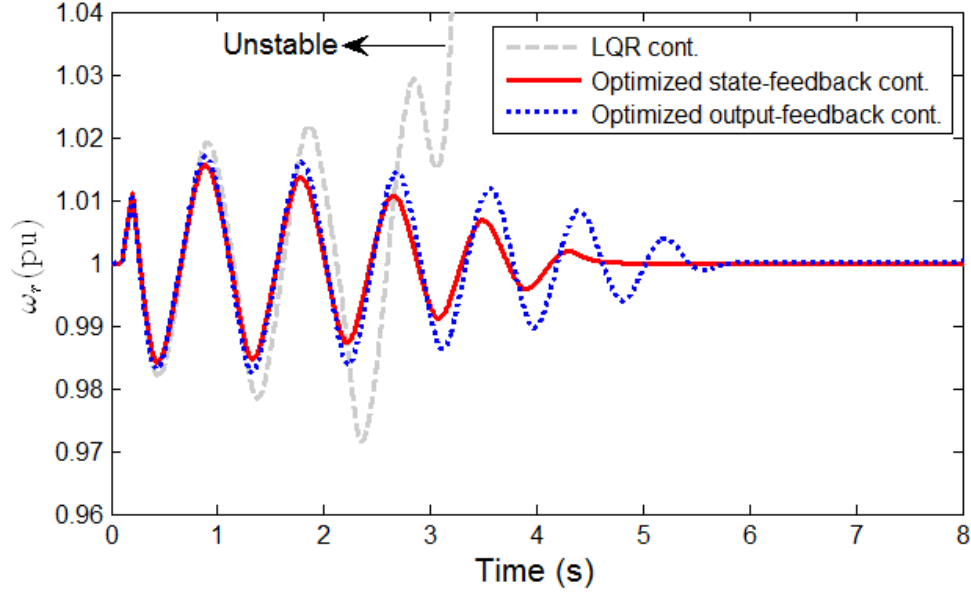


Figure 3.8: Comparison of transient responses for the system with fault duration of $t_f = 0.1s$, employing LQR, optimized state-feedback and optimized output-feedback controllers.

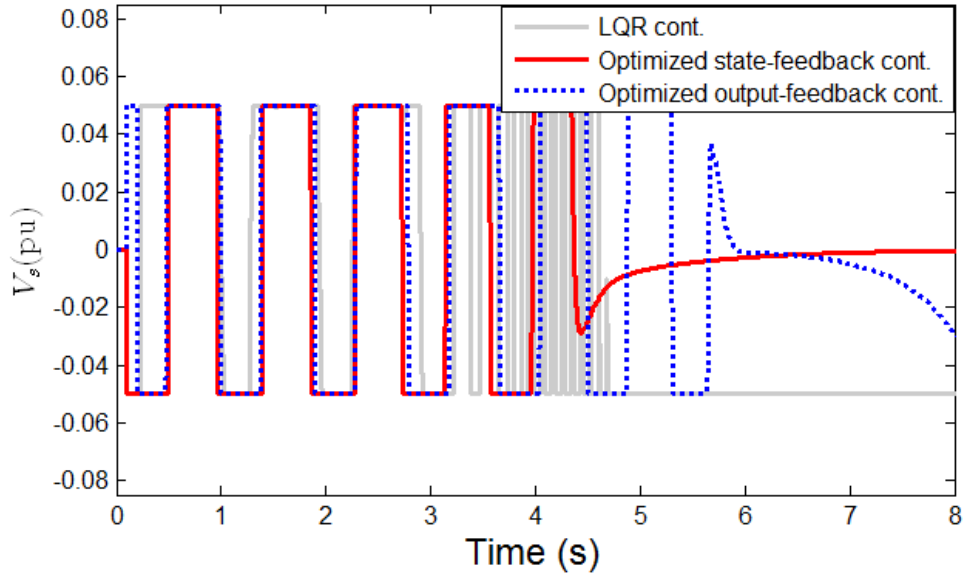


Figure 3.9: Comparison of supplementary control signals for the system with fault duration of $t_f = 0.1s$, employing LQR, optimized state-feedback and optimized output-feedback controllers.

It can be seen that the system with LQR controller will be unstable and the optimized state-feedback controller significantly improves the damping rate. Fig. 3.9 shows that the proposed state-feedback and output feedback controllers use the full feasible range of $[V_s^{\min}, V_s^{\max}]$ to enlarge the DA and their performance are close to a bang-bang control law.

3.6 Summary

In this chapter, a new approach to design supplementary damping controllers by taking into account the effects of saturation limits is introduced. The problem of determining the optimal estimation of DA for SMIB power in the presence of saturation on the control signal is considered. To increase the region of stability, state-feedback controllers are designed to enlarge the guaranteed DA. Consequently, the enlargement of the DA of the post-fault system effectively increases the CCT, which is an important measure of transient stability. Detailed dynamic simulation results demonstrate that the proposed controllers use the available control range to effectively enlarge the DA, improve the damping and enhance the stability in the presence of hard saturation.

Chapter 4

Virtual Actuators for Wide-Area Damping Control

In this chapter, a new approach to design fault-tolerant wide-area damping controllers (WADCs) is presented. Use of actuator redundancy to achieve higher reliability has always been an accepted engineering design technique and is used in this study to help ensure power system security. In our proposed method when an actuator fails or is unavailable (e.g., due to loss of communication), the supervisory controller redistributes the control signals to the remaining actuators. The WADC is initially designed to provide satisfactory damping. In the next step, virtual actuators (VAs) are designed to manage actuator failures without the need to redesign the nominal WADC. By inserting this reconfiguration block between the nominal WADC and the new actuator, there is no need to retune the WADC and the performance of the fault-free system can be recovered. Our proposed block is independent of the nominal WADC and does not need any information beyond that an actuator is unavailable. The approach is applied to Kundur's two-area system, and the 39-bus New England system. Numerical results show the effectiveness of the proposed method subjected to different failures. Part of the results in this chapter appeared in [24].

4.1 Introduction

Development of WADCs includes designs for supplementary control of generator excitation, high voltage direct current (HVDC) links, and FACTS devices. Various design techniques and methodology for WADCs have been reported, e.g., [66, 67, 68]. However, still very few such systems have been deployed in practice at least partly due to the robustness that is required for any closed loop power system controls. In order to transmit remote feedback signals to a central WADC and then to the actuators, highly reliable communications and computations are required. Time delay and communication failures or cyber-attacks can easily degrade the performance of the aforementioned controllers [28, 25]. Moreover, changes in scheduling of generators may mean that some actuators are unavailable. The use of renewable sources to contribute to power system stability may also be limited by the fact that they are not always available. For example, on calm days wind turbines may not be generating electric power if there is insufficient wind to drive the turbines.

Redundancy is a common engineering approach to ensure system resiliency and improve overall reliability. This concept was first introduced by Von Neumann [69] and then commonly used in large commercial and military aircrafts to increase the safety of flight control systems [70]. However, the increase in redundancy also increases the costs and complexity of the system. Increasing interconnections and power demands in modern power systems lead to greater vulnerability to faults and components failures. Thus, to address this issue, the concept of redundant actuators to increase reliability is of great interest. Fault-tolerant control (FTC) systems are needed to maintain nominal controller performance under different faults in the system [71, 72]. An interesting approach to control reconfiguration for FTC is the concept of virtual actuators (VAs). A complete reference on VAs, their applications and details can be found in [73, 74].

This chapter investigates the design of a new fault-tolerant WADC such that the nominal feedback control remains operational after faults in the actuator. In our approach, WADC is designed based on fault-free model and VAs appear as dynamic blocks between the controller and the plant to hide the faults from controller. In normal conditions, the VAs remain inactive and the nominal WADC operates. When faults occur in the system,

the VAs will operate and attempt to maintain the same level of damping performance by redirecting the control signal to other available actuators. This research extends [75, 25] in which unavailability of nominal WADC actuator as result of permanent faults or maintenance has not been considered. Our approach also extends [76] as without using VAs, large communication delay between WADC and actuator can deteriorate the damping performance.

The remainder of this chapter is organized as follows: preliminaries on modeling of power systems are briefly described in Section 4.2. In Section 4.3, a multi-objective LMI with pole placement is presented as one method to design WADC. In Section 4.4, the FTC scheme is applied to power systems with redundant actuators. Time domain simulation results using DSATools software [77] are provided in Section 4.5 to demonstrate the proposed method's ability to increase system resiliency. Concluding remarks are presented in Section 4.6.

4.2 Power System Dynamic Model

The model for a multi-machine interconnected power system including different actuator components equipped with supplementary control such as generators, HVDC links and static VAR compensators (SVCs) is outlined in this section.

4.2.1 Generator Dynamic Model

Each generator is described by the two-axis model [78]:

$$\dot{\delta} = \omega - \omega_s \quad (4.1)$$

$$\frac{2H}{\omega_s} \dot{\omega} = T_M - I_d E'_d - I_q E'_q - (X'_q - X'_d) I_q I_d - D(\omega - \omega_s) \quad (4.2)$$

$$T'_{q0} \dot{E}'_d = -E'_d + (X_q - X'_q) I_q \quad (4.3)$$

$$T'_{d0} \dot{E}'_q = -E'_q - (X_d - X'_d) I_d + E_{fd} \quad (4.4)$$

In the above equations, the notation is as defined in the Nomenclature. Generators are assumed equipped with a high-gain excitation system and supplementary control input:

$$\dot{E}_{fd} = -\frac{E_{fd}}{T_A} + \frac{K_A}{T_A} [V_{ref} + V_p - V + \text{sat}(V_s^{EXC})] \quad (4.5)$$

Saturation nonlinearity should also be considered in the supplementary input control to enforce practical limitations and are usually in the range of ± 0.05 to ± 0.2 per unit which guarantees a modest level of contribution. These limits allow an acceptable control range while providing adequate damping and preventing tripping of the equipment. Standard speed-based PSS model (PSS1A) [79] is used to improve damping of the local modes. Generators are also equipped with steam turbine governor model (TGOV1) which represents the motion of steam through the reheater and turbine stages [80].

4.2.2 HVDC Dynamic Model

The HVDC system considered in this research is based on a Line-Commutated Converter (HVDC-LCC). Supplementary control within the HVDC transmission link is another effective method to enhance small-signal stability. In particular, damping can be increased by modulating the reference current at the rectifier. The following represents dynamic variation of dc power with the supplementary control of HVDC link.

$$T_{dc}\dot{P}_{dc} = -P_{dc} + P_{ref} + \text{sat}(P_s^{HVDC}) \quad (4.6)$$

where P_{dc} will go to the master control system of the HVDC system.

4.2.3 SVC Dynamic Model

Static VAR compensators are mainly used to regulate the voltage and improve voltage stability. Along with voltage regulation, a supplementary input signal can be added to SVC's voltage control loop to provide additional damping for electromechanical modes. In

this work, the following dynamic model is used for the SVC [77].

$$T_{3s}\dot{X}_{1s} = -X_{1s} + \frac{K_s(T_{3s} - T_{1s})}{T_{3s}}[V - V_{ref} + \text{sat}(V_s^{SVC})] \quad (4.7)$$

$$T_{4s}\dot{X}_{2s} = \frac{K_s(T_{4s} - T_{2s})}{T_{4s}}X_{1s} - X_{2s} + \frac{K_sT_{1s}(T_{4s} - T_{2s})}{T_{3s}T_{4s}}[V - V_{ref} + \text{sat}(V_s^{SVC})] \quad (4.8)$$

$$T_{5s}\dot{B}_L = \frac{T_{2s}}{T_{4s}}X_{1s} + (X_{2s} - B_L) + \frac{K_sT_{1s}T_{2s}}{T_{3s}T_{4s}}[V - V_{ref} + \text{sat}(V_s^{SVC})] \quad (4.9)$$

4.3 Multi-Objective Wide-Area Damping Controller Design

In general, remote signals can provide better observability of inter-area modes and can supplement the local control as a WADC. We design the nominal controller based on robust linear control methods but our approach to the VA can accommodate other control approaches. The linearized MIMO system can be represented as:

$$\dot{x}(t) = Ax(t) + Bu(t) + B_d d(t) \quad (4.10)$$

$$Z_\infty(t) = C_\infty x(t) + D_{\infty 2}u(t) + D_{\infty 1}d(t) \quad (4.11)$$

$$Z_2(t) = C_2 x(t) + D_{22}u(t) + D_{21}d(t) \quad (4.12)$$

$$y(t) = Cx(t) \quad (4.13)$$

where $x \in R^n$, $u \in R^m$, $d \in R^q$ and $y \in R^p$ are the vector of state variables, supplementary input signals, disturbances and measured outputs. In this framework, Z_∞ channel relates to the H_∞ performance and is mainly used to guarantee robust performance against model uncertainties while Z_2 relates to the H_2 performance and guarantees satisfactory time domain performance of the system. In our study, a multi-objective damping controller was considered using the LMI optimization techniques introduced in [81] to minimize both H_2 and H_∞ norms concurrently.

Satisfactory closed loop damping can be achieved by using pole-placement objectives to force the open loop poles to lie within a proper sub-region of the left hand plane. Fig. 4.1 shows that pole-placement in a specified region can guarantee a minimum damping ratio of

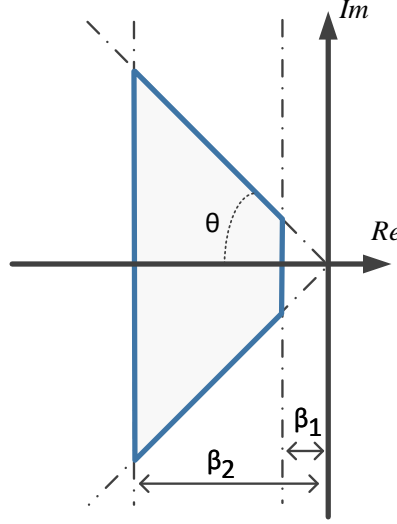


Figure 4.1: Pole-placement in LMI regions.

$\zeta = \cos(\theta)$ along with minimum and maximum decay rate of β_1 and β_2 . However, β_1 must be chosen as a sufficiently small number to avoid large feedback gains and the associated large control efforts. Large gains can also lead the system into saturation. Moreover, in some cases where the controller design is based on a reduced-order model, large gains can result in instability of the full-order system.

In general, our goal for WADC is to design a dynamic output feedback controller to minimize $\Gamma_1 \|T_\infty\|_\infty^2 + \Gamma_2 \|T_2\|_2^2$ along with satisfying the pole-placement requirements. Variables Γ_1 and Γ_2 are positive weightings and T_∞ and T_2 denote the transfer functions from d to Z_∞ and Z_2 , respectively. The choice of these weights depends on the particular application. The WADC can be written as:

$$\dot{\xi}(t) = A_K \xi(t) + B_K y(t) \quad (4.14)$$

$$\bar{u}(t) = C_K \xi(t) + D_K y(t) \quad (4.15)$$

where ξ and \bar{u} are WADC state vectors and outputs (damping signals). In practice, model reduction must be employed to avoid feasibility problems and to realize practical low-order controllers. In this research, the Hankel norm approximation [82] is used to reduce the

open loop model to a lower order. The order of reduction can be determined by comparing the accuracy of frequency response of the full-order and the reduced-order system in the frequency range of interest. In our approach, we design the controller based on the reduced-order model and therefore the controller will have the same order as the reduced model.

Well-known methods such as the geometric measure of controllability gm_c and observability gm_o [75] can be used to choose the input location with the highest controllability for a specific mode and to choose the measurement signals with the highest observability regarding that mode. It is also recommended that measurement signals should have a relatively small gm_o associated with other modes to reduce interaction between different modes. In our study:

$$gm_{ci}(k) = \frac{|b_i^T \Psi_k|}{\|\Psi_k\| \|b_i\|} \quad (4.16)$$

$$gm_{oi}(k) = \frac{|c_i \Phi_k|}{\|\Phi_k\| \|c_i\|} \quad (4.17)$$

where b_i is the i th column of input matrix $B \in R^{n \times m}$ and c_i is the i th row of output matrix $C \in R^{p \times n}$. Matrices $\Psi \in R^{n \times n}$ and $\Phi \in R^{p \times n}$ are the left and right eigenvectors of matrix A , respectively. These geometric measures are effective classifiers, even in cases where inputs and outputs have completely different structures.

Using this concept, outputs regarding H_∞ performance are chosen as the system outputs (measurement signals) to increase the robustness and for H_2 performance are chosen as control inputs (supplementary input signals) of the nominal WADC actuators to limit the control effort and avoid high gains in the controller. In this research, the basic steps of WADC design approach includes the following

1. Perform modal analysis to identify low-frequency modes and determine the critical inter-area modes.
2. Select the nominal damping actuator and remote measurement based on controllability and observability measures.
3. Formulate the generalized plant and obtain the reduced-order model using the Hankel norm approximation.

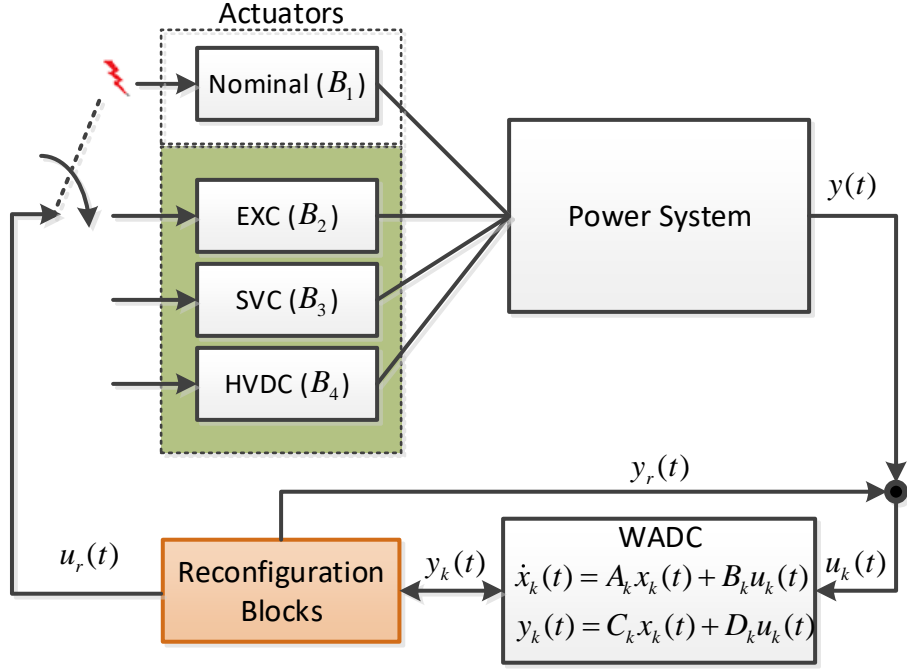


Figure 4.2: Control reconfiguration block diagram (Fault-hiding approach).

4. Design the robust WADC based on the reduced-order model.
5. Verify and evaluate the WADC performance on the full-order model.

4.4 Fault-Tolerant Control Design

In this section, a fault-tolerant scheme for power systems with actuator redundancy is proposed. There is a likelihood that failures in some of the actuators during system operation can deteriorate WADC performance. To achieve a high damping reliability, FTC systems are required to cope with severe faults and enlarge the set of compensable actuator failures through other active actuators. In our proposed approach to enhance reliability in power systems, a greater number of actuation elements along with some reconfiguration control blocks will be used. We use the concept of virtual actuator to benefit from redundancy in the actuator's equipped with supplementary control for our previously designed WADC.

The actuator faults considered arise either when the communication between central

WADC and actuator is lost due to a significant delay, failure due to a cyber-attacks or simply when the actuator is off-line due to maintenance or component faults. In these situations, the actuator is unable to receive the control signal from WADC. A widely used strategy to detect these failures is to use a protocol with an immediate acknowledgment (ACK) for the communication links [83]. As a result, the detection of faults is easy and the problem becomes finding a way to re-route the WADC control signals to other available actuators. Fault detection and diagnosis [84, 85, 86, 87] issues have been extensively investigated in control and power system literatures which are beyond the scope of this research.

The corresponding block diagram of the proposed FTC scheme is shown in Fig. 4.2. The control allocation will depend on the status of different actuators, their controllability measures and time delay associated with the communication link to a specific actuator. By inserting this reconfiguration block between the nominal WADC and the new actuator, there is no need to redesign the WADC to recover the performance of fault-free system. This block is independent of nominal WADC and does not need any information on design specifications. In case that a fault or failure occurs in the nominal actuator ($B_1 = 0_{n \times 1}$) and the supervisory controller will redistribute the control signals to the remaining fault-free actuators (B_2, B_3, \dots). The reconfiguration blocks is a bank of VAs that can be described by following equations:

$$\dot{x}_\Delta(t) = A_\Delta x_\Delta(t) + B_\Delta y_k(t) \quad (4.18)$$

$$u_r(t) = M_r x_\Delta(t) + N_r y_k(t) \quad (4.19)$$

$$y_r(t) = C x_\Delta(t) \quad (4.20)$$

Output y_r goes to the input of the nominal controller, u_r goes to the redundant actuator and state variable x_Δ is related to the VA internal dynamics. We also have

$$A_\Delta := A - B_r M_r \quad (4.21)$$

$$B_\Delta := B_1 - B_r N_r \quad (4.22)$$

Both matrix gains M_r and N_r should be chosen for the above virtual actuator dynamics. In case that fault occurs in the nominal actuator, the corresponding control input changes as follows:

$$(B_r, M_r, N_r) = \begin{cases} (B_1, 0_{1 \times n}, 1) : & \text{Nominal Actuator} \\ (B_2, M_2, N_2) : & \text{EXC VA} \\ (B_3, M_3, N_3) : & \text{SVC VA} \\ (B_4, M_4, N_4) : & \text{HVDC VA} \end{cases} \quad (4.23)$$

Our main goal in designing the VA is to hide the fault from the controller and stabilize the faulty power system. Here, M_r has to be chosen so that eigenvalues of matrix $A - B_r M_r$ have negative real parts. To achieve above objectives, the pair (A, B_r) should be stabilizable and the stabilizing gain M_r can be determined using any state feedback approach such as pole placement technique to keep the deviation x_Δ small. The matrix gain N_r can also be chosen to increase the speed of healthy actuator through bypassing the integrator. At this stage, the fault-tolerant control scheme is completed.

After attaching the virtual actuator to the faulty plant and introduce a new state vector $x(t) = x_\Delta(t) + x_f(t)$, combined state equations can be written as follows:

$$\begin{bmatrix} \dot{x}(t) \\ \dot{x}_\Delta(t) \end{bmatrix} = \begin{bmatrix} A & 0 \\ 0 & A_\Delta \end{bmatrix} \begin{bmatrix} x(t) \\ x_\Delta(t) \end{bmatrix} + \begin{bmatrix} B_1 \\ B_\Delta(t) \end{bmatrix} y_k(t) + \begin{bmatrix} B_d \\ 0 \end{bmatrix} d(t) \quad (4.24)$$

$$u_k(t) = \begin{bmatrix} C & 0 \end{bmatrix} \begin{bmatrix} x(t) \\ x_\Delta(t) \end{bmatrix} \quad (4.25)$$

$$\begin{bmatrix} x(0) \\ x_\Delta(0) \end{bmatrix} = \begin{bmatrix} x_0 + x_{\Delta 0} \\ x_{\Delta 0} \end{bmatrix} \quad (4.26)$$

where from (4.24-4.26) it can be seen that the reconfigured plant dynamics (x) seen by the controller (u_k, y_k) behaves exactly similar to the nominal plant if $x_{\Delta 0} = 0$. Therefore, if $x_{\Delta 0} = 0$ holds, then the fault is hidden from the controller. The state $x_\Delta(t) = x(t) - x_f(t)$ also represents the deviation between the nominal and faulty plant. From the above equations,

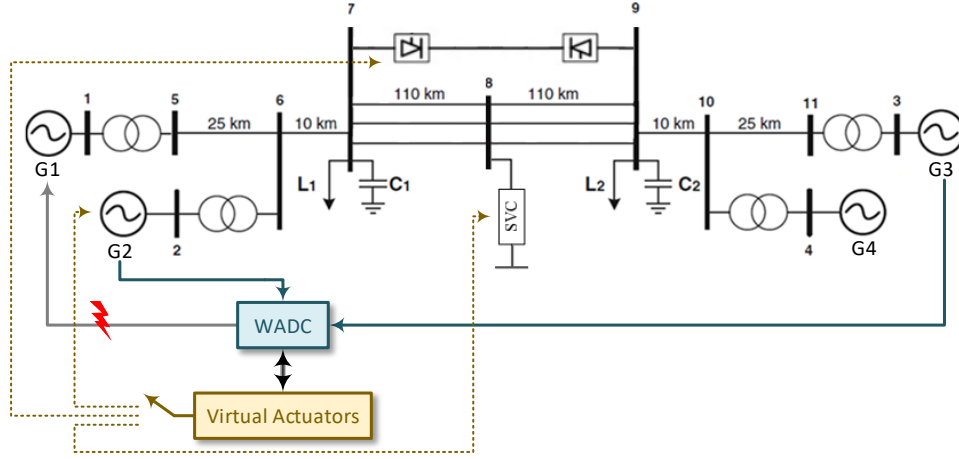


Figure 4.3: Two-area power system with WADC and virtual actuators.

it can be seen that the difference system is structurally unobservable from the controller. Therefore, M_r should be determined by pole placement so that the difference system x_Δ be asymptotically stable and the error vanishes asymptotically.

VAs are designed to handle actuator failures without the need to reconfigure the WADC. In the present work, the reconfigured closed loop is expected to satisfy the nominal control goal without having to change the original controller. The main advantage is that FTC design is independent of nominal WADC and therefore usable with any other controller. It is also more cost efficient than installing new control devices. This FTC scheme will not change the structure of nominal WADC and only modifies the output control signals through virtual actuator dynamics. Therefore, the nominal WADC is suitable for damping purposes via remaining actuators. In summary, this approach will lessen the difficulty of dealing with a faulty system as the reconfigured system recovers the behavior of fault-free system. Numerical simulations are performed in next section to illustrate the effects of this scheme.

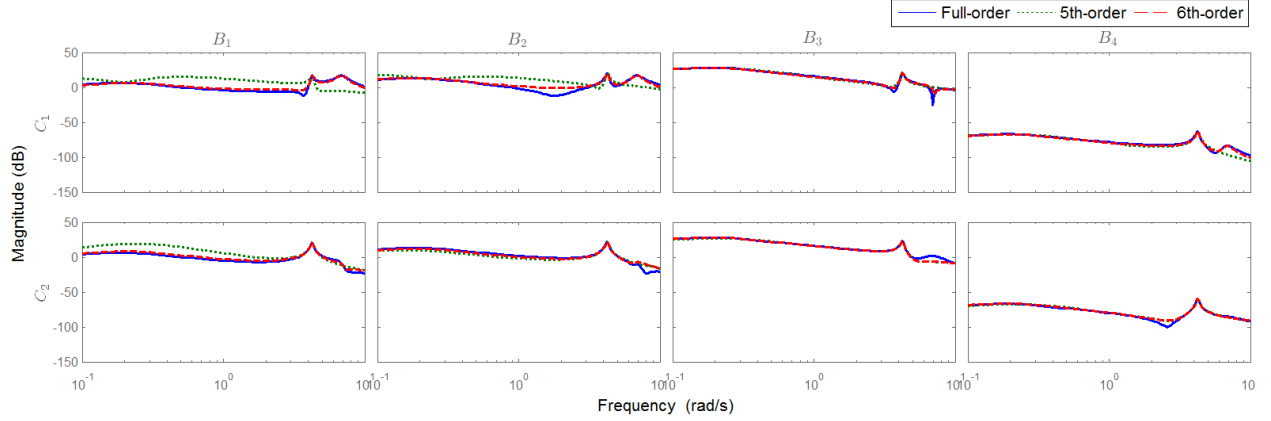


Figure 4.4: Frequency response of full-order and reduced-order system with respect to inputs and output measurement signals.

4.5 Numerical Results

4.5.1 Case Study I: Kundur Two-Area System

In this subsection, the proposed methodology is applied to a modified Kundur two-area system. The modified system is shown in Fig. 4.3. Generators are represented in detail by a fourth-order model and equipped with a high-gain excitation system. Generator G_1 has a turbine-governor model and G_3 is equipped with IEEE standard speed-based PSS to damp the local modes. Area 1 is transferring 550 MW of active power to area 2. An HVDC link connects buses 7 and 9 and is transferring 100 MW. To improve the voltage profile, an SVC with a capacity of ± 400 MVar is connected at bus 8. Details of the original parameters can be found in [4].

The modal analysis summarized in Table 7.2 shows that the system without WADC has a weakly damped inter-area mode at 0.666 Hz and two well-damped local modes. Our main objective in the WADC design is to meet or exceed 11% damping over all inter-area and local modes with $\alpha = -0.05$. Generator supplementary excitation control and speed deviation are chosen as candidates for actuator input and measurement signals of WADC system, respectively. As discussed in Section 4.3, G_1 is chosen as the nominal actuator (B_1) for the WADC system based on the controllability measure (4.16). Speed deviations of G_2 and G_3 are identified as the best candidate input signals for controller, as they have the highest geometric observability measure (4.17) over the first two critical modes.

Table 4.1: Critical Modes of Two-Area System

Mode type	Coherent group	Without WADC		With WADC	
		Freq. (Hz)	Damp. (%)	Freq. (Hz)	Damp. (%)
Inter-area	1,2 vs. 3,4	0.666	1.68	0.657	11.37
Local	1 vs. 2	1.092	5.62	0.971	12.96
Local	3 vs. 4	1.125	16.35	1.119	16.23

The open loop model of this system is 29th-order and is reduced based on the balanced model truncation method. The appropriate order of the reduced-order model can be determined by comparing the frequency responses. Fig. 4.4 illustrates that the 6th-order reduced model can approximate the low-frequency oscillation characteristic and has a closer response to the full-order system relative to the 5th-order model. As a result, the WADC and VAs can be designed based on this 6th-order reduced model. Table 7.2 with the WADC included, shows that the controller satisfactorily improves damping of the full-order system. Details of parameters can be found in Appendix A.1.

In practice, time delay caused by transmission of remote control signal from WADC to the nominal actuator is one of the key factors influencing the performance and stability of the closed loop system. Time delay (T_d) with transfer function e^{-sT_d} can be substituted by a second-order Padè approximation based on minimization of the truncation errors [88] as follows:

$$e^{-sT_d} \approx \frac{1 - \frac{T_d}{2}s + \frac{T_d^2}{12}s^2}{1 + \frac{T_d}{2}s + \frac{T_d^2}{12}s^2} \quad (4.27)$$

The time delay characteristics expressed by the above model can also be considered in the open loop system model to design a controller which can efficiently suppress the negative effects of small time delay. However, delays in communication are often vary within an unbounded range instead of a fixed point and relatively large delay may even cause instability in power systems.

To validate the performance of the designed WADC on the nonlinear system, one of the inter-area lines between bus 7 and 8 trips at $t = 1$ s and then successfully re-closes at $t = 2$ s. Second-order Padè approximation is also considered to demonstrate the effects of delay

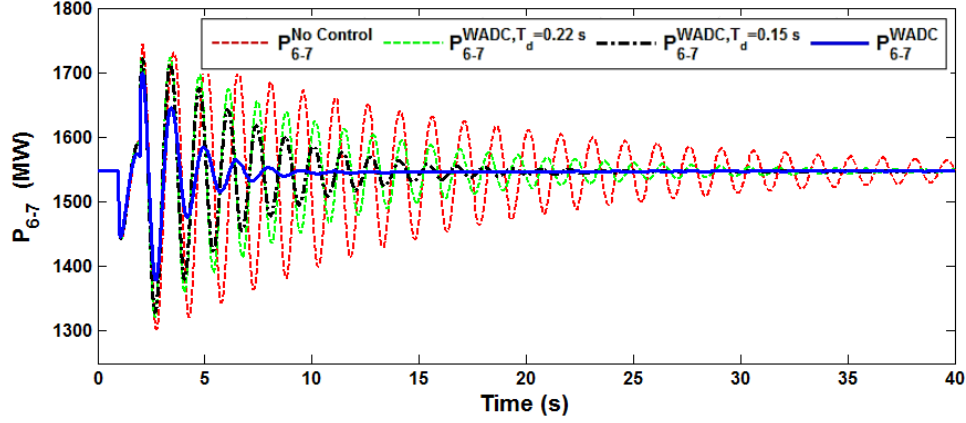


Figure 4.5: Dynamic response of two-area power system to tripping and re-closing one of the tie-lines.

between WADC and the corresponding actuator. Fig. 4.5 shows the active power of one of the tie lines without any control and with WADC in the presence of different communication delays. This figure illustrates the large improvement in the dynamic response of the nonlinear system with WADC even in case of small delay. However, a delay can negatively affect the damping performance and in this case, time delay more than 0.22s may lead to instability. Therefore reconfiguration in the control loop is needed to handle these failures.

Next we assume the primary actuator fails. The reconfiguration block redistributes the control signal to other redundant actuators in the system. We should note that the redundant actuator set is chosen as G_2 , SVC and HVDC link. To evaluate the effects of using this FTC scheme, Fig. 4.6-4.8 illustrate system responses where the WADC signal is redirected by using virtual actuators to supplementary control of G_2 , SVC and HVDC link, respectively. The results reveal the effectiveness of using VAs to damp the oscillations and recovery the performance of fault-free system.

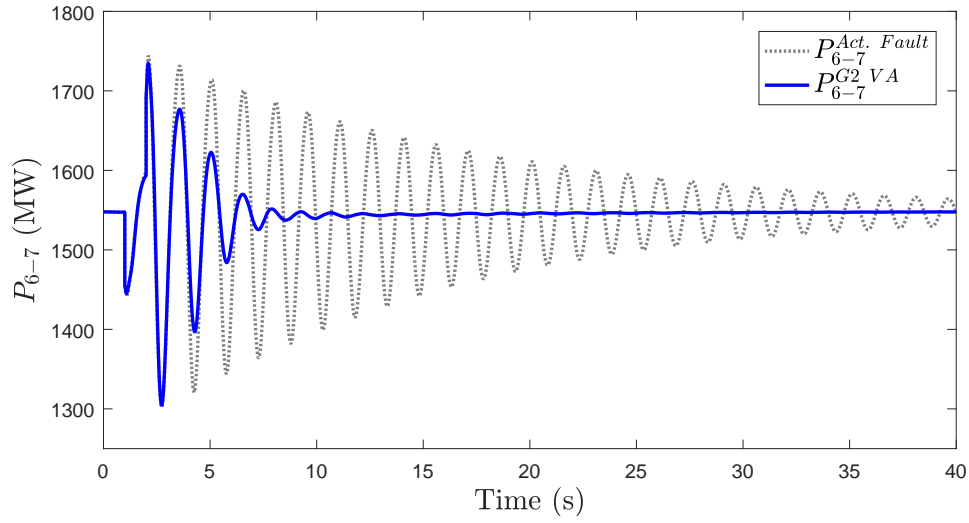


Figure 4.6: Dynamic response of two-area system to tripping and re-closing one of the tie-lines with WADC signal redirected to G_2 .

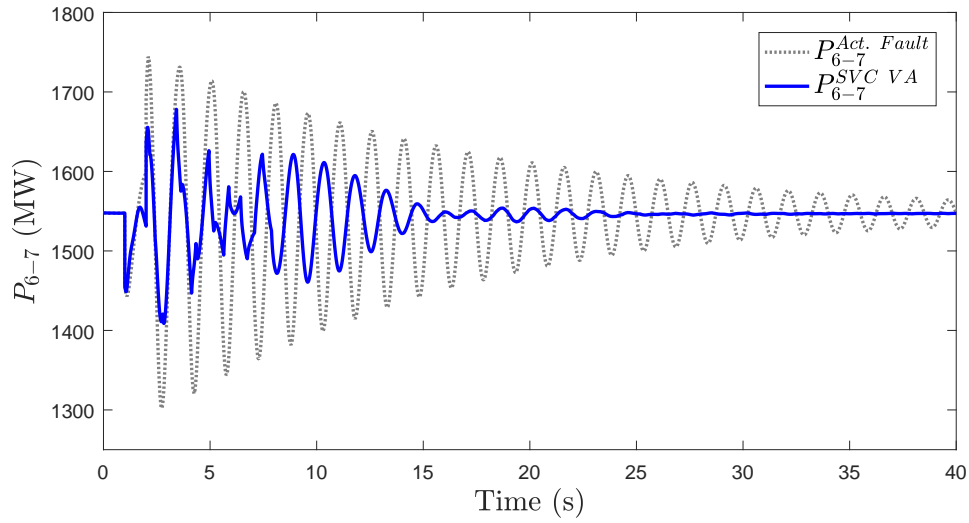


Figure 4.7: Dynamic response of two-area system to tripping and re-closing one of the tie-lines with WADC signal redirected to SVC.

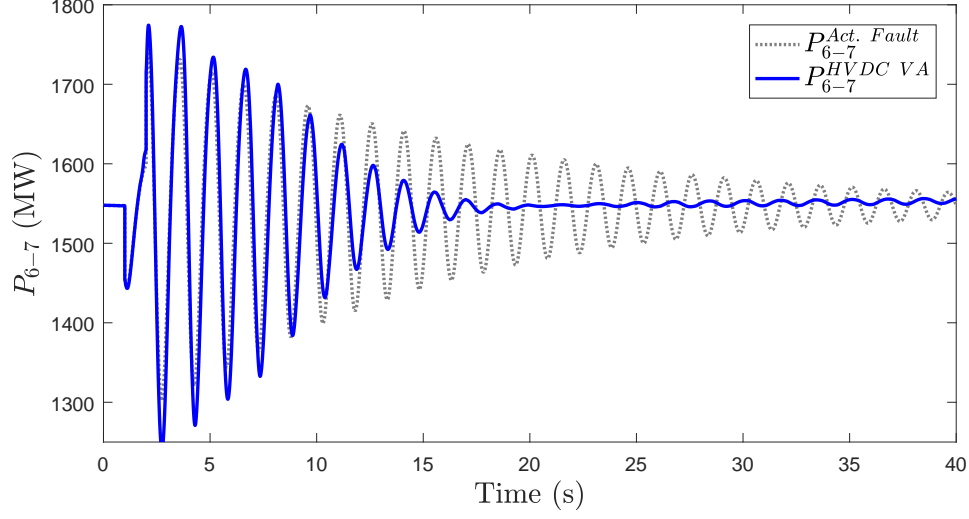


Figure 4.8: Dynamic response of two-area system to tripping and re-closing one of the tie-lines with WADC signal redirected to HVDC.

4.5.2 Case Study II: New England 39-Bus System

To investigate the performance of the proposed approach on a more complex system, the New England ten-machine 39-bus test system was considered. Original details regarding network data, operating conditions and other parameters are given in [89]. The system is modified to have lightly damped inter-area modes. Overview of the proposed system with WADC and virtual actuators is shown in Fig. 4.9. All generators are modeled via a fourth-order model and equipped with an excitation system except for G_{10} which is an equivalent of another large power system. In addition, PSSs are also tuned based on local modes for generators G_1 to G_8 , G_8 has a turbine-governor model and loads are represented as constant power loads. Since bus 16 has the lowest voltage among other buses, an SVC with the capacity of ± 400 MVar is installed to improve the voltage profile. Furthermore, an HVDC link is installed between bus 3 and 19 to increase the transfer capacity by transferring 100 MW power.

Table 4.2 shows two critical inter-area modes with frequency of 0.5716 Hz and 0.7247 Hz. The overall goal in WADC design is to at least achieve 11% damping over all inter-area modes with $\alpha = -0.05$ while reducing the required control efforts. Similar to before, both generators' excitation supplementary control and generators' speed deviation are chosen as candidates for actuator input and measurement signals for WADC.

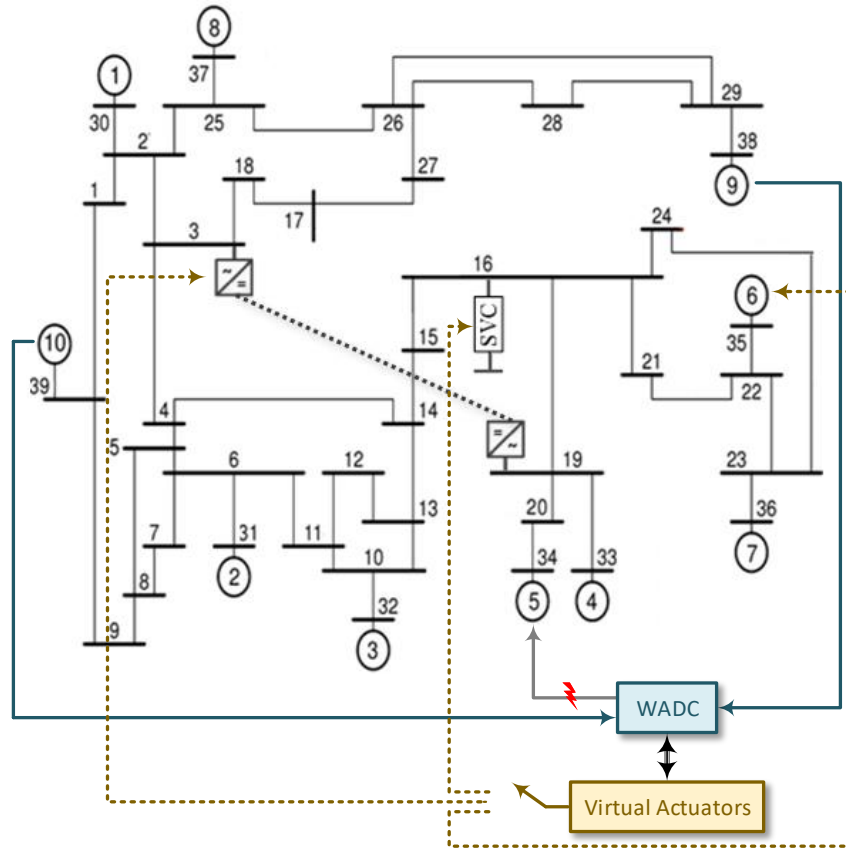


Figure 4.9: New England 10-machine 39-bus system with WADC and virtual actuators.

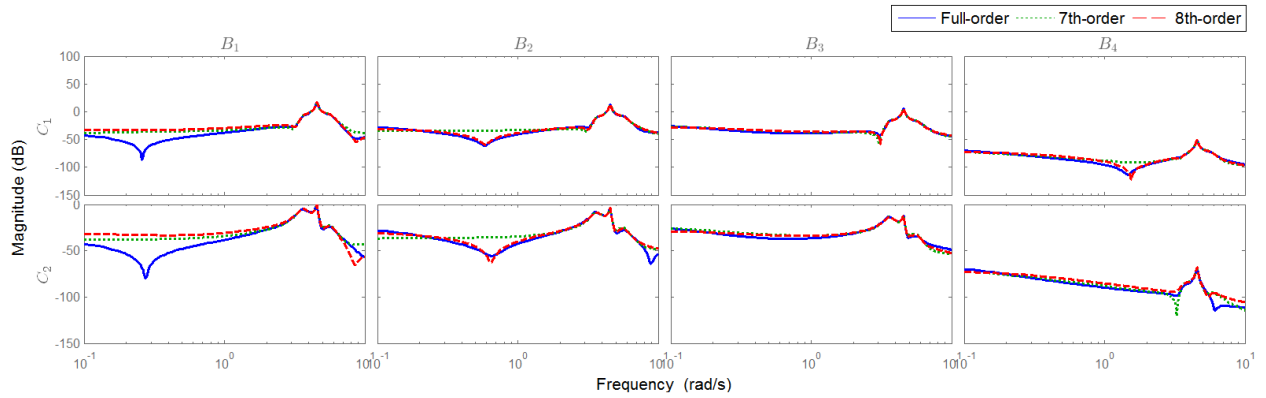
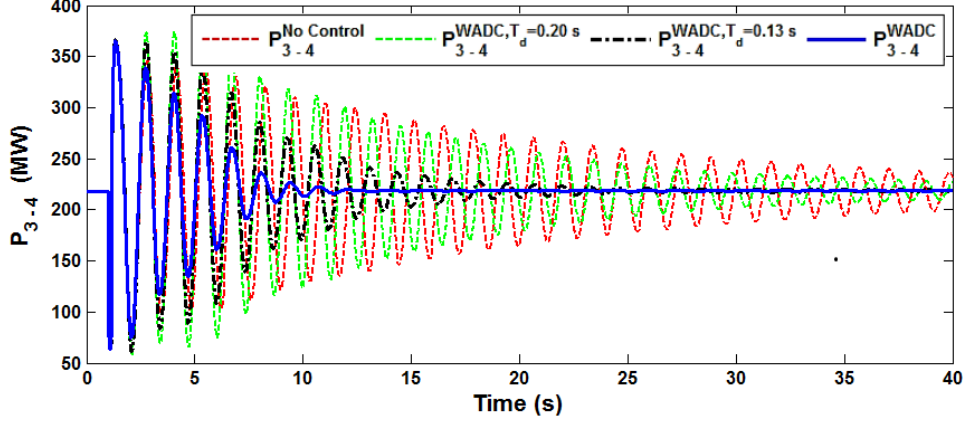


Figure 4.10: Frequency response of full-order and reduced-order system with respect to inputs and output measurement signals.

Table 4.2: Modes of New England Ten-Machine 39-Bus System

Mode type	Coherent group	Without WADC		With WADC	
		Freq. (Hz)	Damp. (%)	Freq. (Hz)	Damp. (%)
Inter-area	1,8,9 vs. 4-7	0.5716	6.99	0.5574	11.09
Inter-area	10 vs. 1-9	0.7247	1.27	0.7069	16.46

**Figure 4.11:** Dynamic responses of New England system to three-phase fault at bus 1.

To obtain the highest damping contribution, G_5 is chosen as nominal actuator (B_1) for WADC system based on controllability measure (4.16). Speed deviations of G_9 and G_{10} are selected as the best candidate signals for our controller, as they have highest geometric observability measure (4.17) over inter-area modes. As shown in following simulations, these two measurement signals are enough to damp out the oscillations.

The open loop model of this system is of 79th-order and has been reduced to an 8th-order using the balanced model truncation method. The appropriate order of the reduced-order model is determined by comparing the frequency responses. Fig. 4.10 depicts that the 8th-order reduced model can cover concerned low-frequency oscillations characteristic and has a close response to the full-order system. Next, according to section 4.3, WADC can be designed based on the 8th-order model. Table 7.2 with WADC included shows that the controller significantly improves damping of the full-order system by achieving at least 11% damping over all inter-area modes. Details of parameters can be found in Appendix A.2.

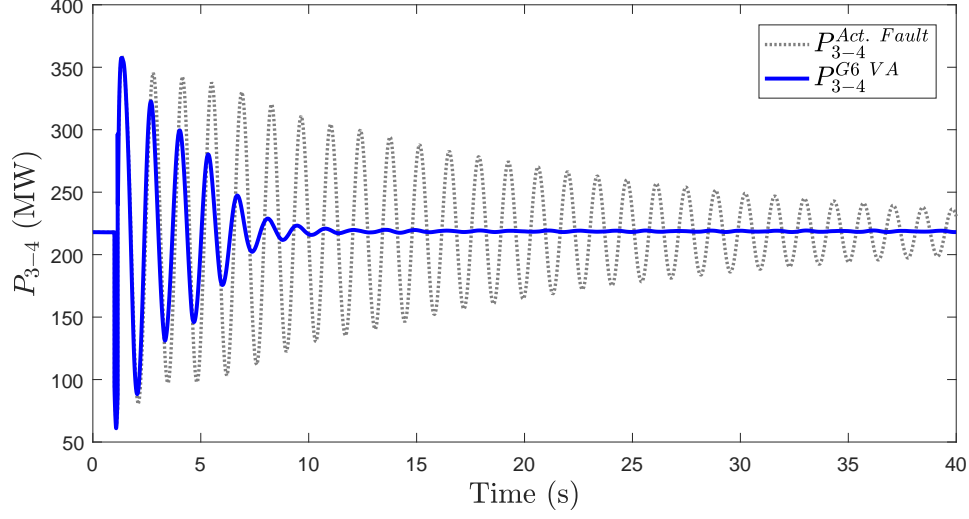


Figure 4.12: Dynamic responses of New England system to three-phase fault at bus 1 when VA redirected WADC signal to G_6 .

To evaluate performance, a symmetrical three-phase fault is applied at bus 1 at $t = 1$ s and cleared after 150 ms. Fig. 4.11 shows the active power of the inter-area line 3-4 for the nonlinear system without any control and with WADC in the presence of different communication delays. According to this figure, the designed WADC remarkably enhances the stability and shows good damping performance. However, large delay can negatively affect the damping performance and in this case communication delay or other severe faults in the actuator may lead to instability. Therefore reconfiguration in the control loop is needed to handle WADC actuator failures.

The redundant actuator set is chosen as G_6 (highest controllability after G_5), SVC, and HVDC link. The pairs (A, B_r) are stabilizable, N_r is assumed to be zero and M_r is chosen by pole placement techniques to stabilize the faulty system. To evaluate the effects of using this FTC scheme, Fig. 4.12-4.14 illustrate the system responses when the WADC signal is redirected by using VAs through G_6 , SVC and HVDC link, respectively. The nonlinear simulation results reveal the effectiveness of the proposed method to damp the oscillations when the communication between central WADC and G_5 is lost or in case that sever fault happens in the nominal WADC actuator.

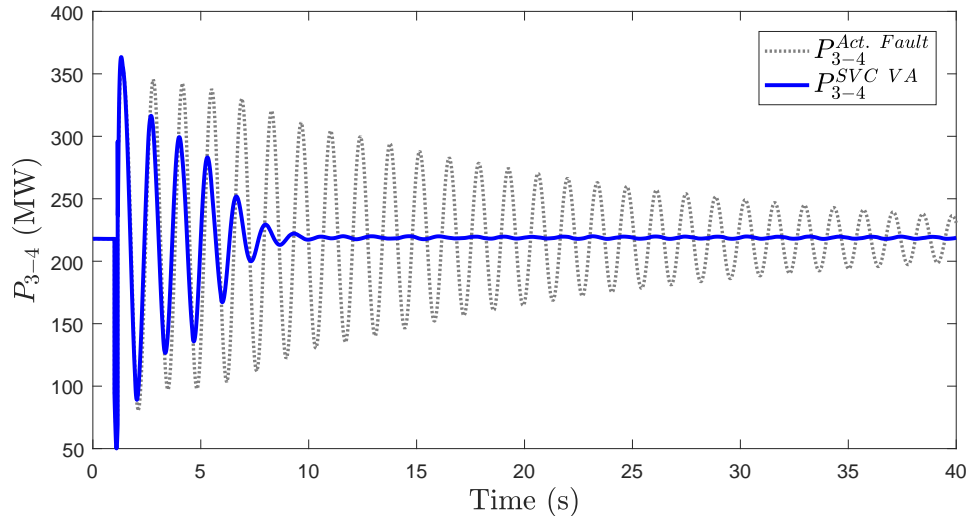


Figure 4.13: Dynamic responses of New England system to three-phase fault at bus 1 when VA redirected WADC signal to SVC.

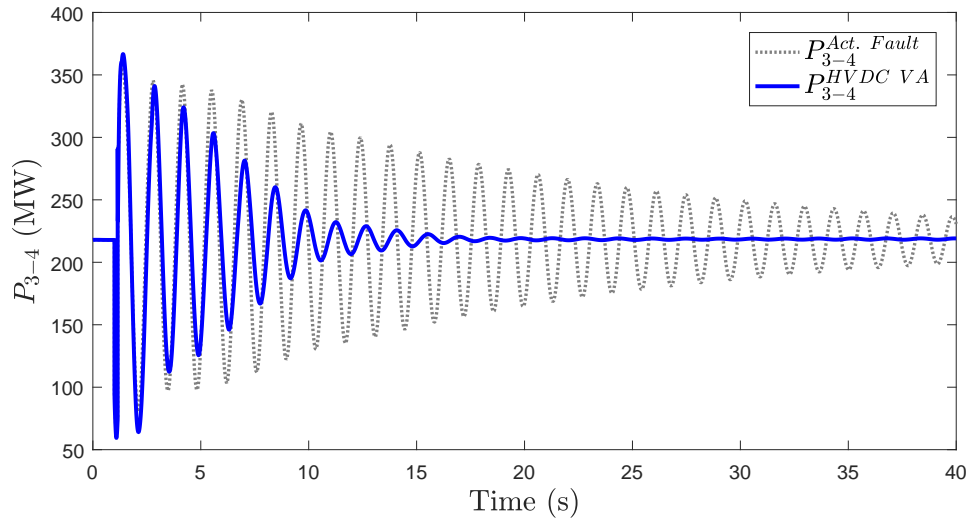


Figure 4.14: Dynamic responses of New England system to three-phase fault at bus 1 when VA redirected WADC signal to HVDC.

4.6 Summary

This research has presented a new fault-tolerant WADC such that nominal controller remain operational after faults in the actuator. Geometric measures of controllability and observability were used to select the most effective measurements and control locations for WADC. The design of nominal WADC carried out using multi-objective H_2/H_∞ optimization with pole placement region to achieve high damping performance. The proposed approach introduces redundancy in actuators to enhance the power system resiliency. The problem of actuator faults is addressed by inserting VAs between the faulty plant and nominal WADC to re-route the control signals to other healthy actuators and recover performance of fault free system without the need to retune the WADC. The design of the proposed method was analyzed in two detailed case studies. Simulation results demonstrate that the proposed approach provides sufficient damping when the system suffers from actuator failures. Further studies will focus on managing actuator redundancy by distributing the control efforts among a redundant set of actuators based on optimal control allocation.

Chapter 5

Dynamic Control Allocation for Damping of Inter-area Oscillations

Use of actuator redundancy to achieve higher reliability is a widely accepted engineering design technique and is used in this study to build resiliency and ensure power system stability in the presence of high levels of renewables. This work presents a new design method for fault-tolerant wide-area damping controllers (WADCs) using modal-based control allocation (MB-CA), which coordinates a set of actuators to contribute to damping of inter-area oscillations. In our proposed method, when an actuator fails or is unavailable (e.g., due to communication failure), the supervisory MB-CA distributes the control signals to the remaining healthy actuators based on effects on the modal system, desired control actions and actuator constraints. Our proposed block offers the benefits of modular design where it is independent of the nominal WADC. The proposed method consists of mainly two design steps. The first step is to design a WADC based on a fault-free model using robust control methods. The second step is to design an MB-CA to manage actuator availability and constraints. To validate the feasibility and demonstrate the design principles, a set of comprehensive case studies are conducted on a modified 192-bus Western Electricity Coordinating Council (WECC) system. Numerical results verify the effectiveness of the proposed approach in ensuring resiliency to different actuator failures and actuator availability. Part of the results in this chapter appeared in [56].

5.1 Introduction

Small-signal instability problems such as inter-area oscillations have become increasingly common in large power grids and may restrict the available transmission capacity between different areas [90]. In recent years, wide-area measurement systems (WAMSs) have been deployed that allow inter-area modes to be easily observed and identified [7]. As a result, low frequency oscillations can be observed globally and then appropriately designed wide-area damping controllers (WADCs) can be deployed. Many control strategies and design techniques have been reported for WADCs including designs for supplementary damping control of generators [75, 91, 24], renewable sources [92, 93, 94, 95, 96], high-voltage direct current (HVDC) links [68, 97, 98] and FACTS devices [76, 99, 66]. Still, the practical implementation of such WADCs face significant challenges to satisfy the reliability requirements of modern grids.

In order to transmit remote feedback signals to a WADC and then to the actuators, highly reliable communications and computations are required. Communication failures, measurement distortions, time delays or cyber-attacks can degrade the performance of the aforementioned controllers [25, 76]. Moreover, changes in scheduling of generators may mean that some actuators are temporarily unavailable. Recently, the use of doubly-fed induction generator (DFIG) wind farms for damping inter-area oscillations through active/reactive power modulation has been discussed in literatures [95, 96].

However, the availability of these weather dependent renewable resources could cause significant reliability issues. If the wind blows strongly, wind farms may efficiently contribute to damping of inter-area oscillations while on calm days the turbines may be below cut-in speeds and so actuation must come from conventional generators. Moreover, mode switching [100, 101] may also affect the capability limits of the DFIG wind farm. Therefore, the controller should be capable of maintaining the stability and acceptable damping performance in the event of these actuator unavailabilities.

Redundancy is a common engineering approach to ensure safety, resiliency and improve overall reliability and was first introduced by Von Neumann [69]. The increase in actuator redundancy also increases the complexity of the system and control allocation (CA)

techniques are needed for distributing a given control action to individual actuators and maintaining the nominal performance under different actuator faults. Considerable research has been conducted in this area primarily for commercial and military aircraft [102, 103, 104], spacecrafts [105, 106, 107] and marine vessels [108, 109]. Similarly, modern power systems have been equipped with various actuators that are useful for distinct purposes. These actuators can contribute to damping inter-area oscillations (through supplementary controls) based on size of the plant (rating), operating mode, location, and how their controls impact system dynamics. We wish to take advantage of this existing built-in redundancy in power system to enhance the reliability and satisfy security requirements.

In this research, a new modal-based control allocation (MB-CA) method is proposed to coordinate multiple actuators to optimally contribute to damping of inter-area modes and achieve a fault-tolerant WADC. In our approach, WADC is designed based on a fault-free model and the supervisory MB-CA distributes the control signals to healthy actuators based on the effects on different modes, desired control actions, total cost, and actuator limitations. This work generalizes the control allocation methods reported in [102, 103, 104] by considering the effects of virtual control on a modal system and extending its application to damping low-frequency oscillations in power systems.

This technique allows us to give the highest priority to the control efforts associated with the critical inter-area modes. Moreover, to the best knowledge of the authors, this is the first time the control allocation concept has been applied to inter-area oscillations. This work also extends the work in [75, 91, 94, 95, 96] in which unavailability of a nominal WADC actuator as a result of permanent faults, maintenance, large communication delay or loss of communication has not been considered. To validate the feasibility and demonstrate the design principles, a set of comprehensive case studies are conducted on a modified 192-bus Western Electricity Coordinating Council (WECC) system with high wind penetration.

The reminder of this chapter is as follows: a multi-objective LMI with pole-placement is presented in section 5.2 as one approach for WADC design. In section 5.3, a modal-based control allocation method is proposed for over-actuated systems. Section 5.4 briefly discusses the dynamic model of the test system. Time domain simulation results are provided

in section 5.5 to verify the feasibility of the proposed method and its ability to increase resiliency. Finally, concluding remarks are made in section 5.6.

5.2 Multi-Objective Wide-area Damping Controller Design

In general, remote signals can provide better observability of inter-area modes and supplement the local control through WADC. We design the nominal WADC based on robust multi-objective LMI optimization technique described in chapter 4.3. However, our approach to CA in section 5.3 can accommodate other methods. The controller is designed based on the reduced order model to avoid feasibility problems and realize practical low-order controllers. Although the above WADC is designed using robust control methods, failure in the communication links or in the actuators will lead to poor damping performance

5.3 Modal-based Control Allocation

Control allocation is an approach to manage actuator redundancy and faults for an over-actuated system, where the number of actuators (m) is greater than the number of states (n). Considering the input matrix $B \in R^{n \times m}$ in equation (7.7), a group of redundant actuators $rank(B) = n < m$ needs to be available to guarantee a set of feasible control commands. In general, this assumption is not true for the full-order model of many practical systems, and in particular power grids. As a result, we consider the CA problem based on the reduced-order model described in the previous section. It is assumed that the reduced-model captures the dominant contribution of damping actuators to the low-frequency modes of interest. Using an appropriate transformation matrix $z = \psi x$ where $\psi \in R^{n \times n}$, the modal realization can

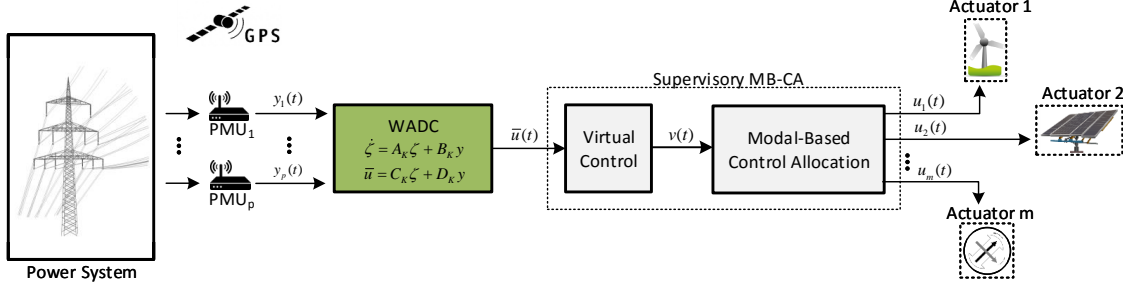


Figure 5.1: Control block diagram of the feedback loop with Supervisory MB-CA embedded.

be obtained as

$$\dot{z}(t) = \Lambda z(t) + \psi B u(t) \quad (5.1)$$

$$\Lambda = \begin{bmatrix} \sigma_1 & \omega_1 & 0 & \dots \\ -\omega_1 & \sigma_1 & 0 & \\ 0 & 0 & \iota_1 & \\ \vdots & & & \ddots \end{bmatrix} \quad (5.2)$$

where $\Lambda = \psi A \psi^{-1}$ is a block diagonal matrix having the complex eigenvalues of $\sigma_i \pm \omega_i j$ or real eigenvalue ι_i along its diagonal. Introducing a new virtual control input $v \in R^n$, (5.1) can be separated into two components which leads to a modular design.

$$\dot{z}(t) = \Lambda z(t) + I_n v(t) \quad (5.3)$$

$$v(t) = \psi B u(t) \quad (5.4)$$

Virtual control $v(t)$ will be generated based on the WADC in Section 5.2 and MB-CA distributes the effort among available actuators via the command vector $u(t)$. The overall structure of the feedback loop with supervisory MB-CA is illustrated in Fig. 5.1. In this work, we consider analytical or model-based redundancy in the actuators as physical redundancy (e.g. replicating an actuator) is not cost effective in power systems. Given an n^{th} -order reduced model where $n < m$, matrix ψ is full rank and $rank(\psi B) = n$. Hence, the system can now represent an over-actuated system and the resulting matrix ψB has null space

of dimension $m - n$ in which u can be perturbed without significant impact on dynamic response.

The proposed modal-based control allocation method with proper filtering to reduce the variations can be formulated as the following constrained optimization problem

$$\begin{aligned}
& \min_{u_t} \quad \|W_u u_t\|^2 + \|W_s(u_t - u_{t-T_s})\|^2 \\
& \text{s. t.} \quad \psi B u_t = v_t \\
& \quad \quad u_{\min} \leq u_t \leq u_{\max}
\end{aligned} \tag{5.5}$$

where $W_u \in R^{m \times m}$ (resp. $W_s \in R^{m \times m}$) is a positive definite diagonal matrix, and represent the weighting for distributions (resp. variations) of the control signal and T_s is the time step. In the proposed method, the virtual control vector v_t (derived from the nominal WADC at time t) is distributed among all actuators considering the total cost, modal effects, actuator rates and limitations such as, saturation. This technique allows us to give the highest priority to the control efforts associated with the critical inter-area modes and obtain the feasible regions in modal coordinates.

In general, the key to control allocation is to take advantage of all the healthy actuators without having to redesign the WADC system. For power systems, the most likely actuators for damping inter-area oscillations are conventional generators, wind farms and FACTS devices equipped with supplementary control input. In case that a fault or failure occurs in the i th actuator, the i th column of matrix B can be substituted by $(1 - \Sigma)b_i$ where $\Sigma \in [0, 1]$ denotes the loss of effectiveness. For example, a complete communication failure to an actuator can be modeled by choosing $\Sigma = 1$ and the i th column will be equal to zero.

To simplify the optimization problem (5.3), the cost function can be computed as follow and constant terms which do not affect the optimal minimizer can be omitted.

$$\begin{aligned}
& \|W_u u_t\|^2 + \|W_s(u_t - u_{t-T_s})\|^2 \\
& = u_t^T W_u^2 u_t + (u_t - u_{t-T_s})^T W_s^2 (u_t - u_{t-T_s}) \\
& = u_t^T (W_u^2 + W_s^2) u_t - 2u_t^T W_s^2 u_{t-T_s} + \text{const.} \\
& = \|W(u_t - u_d)\|^2 + \text{const.}
\end{aligned} \tag{5.6}$$

where

$$u_d = W_s^2(W_u^2 + W_s^2)^{-1}u_{t-T_s}, \quad W = (W_u^2 + W_s^2)^{\frac{1}{2}} \quad (5.7)$$

The optimization can then be written in the form of a constrained least square problem

$$\begin{aligned} \min_{u_t} \quad & \|W(u_t - u_d)\|^2 \\ \text{s. t.} \quad & \psi B u_t = v_t \\ & u_{\min} \leq u_t \leq u_{\max} \end{aligned} \quad (5.8)$$

with u_d and W from (5.7). Utilizing the Lagrangian multiplier ρ^2 , the cost function can be expressed in the form

$$\begin{aligned} & \|W(u_t - u_d)\|^2 + \rho^2 \|W_v(\psi B u_t - v_t)\|^2 = \\ & \left\| \begin{pmatrix} \rho W_v \psi B \\ W \end{pmatrix} u_t - \begin{pmatrix} \rho W_v v_t \\ W u_d \end{pmatrix} \right\|^2 \end{aligned} \quad (5.9)$$

Finally, the augmented cost function (5.9) yields the following optimization problem.

$$\begin{aligned} \min_{u_t} \quad & \left\| \begin{pmatrix} \rho W_v \psi B \\ W \end{pmatrix} u_t - \begin{pmatrix} \rho W_v v_t \\ W u_d \end{pmatrix} \right\|^2 \\ \text{s. t.} \quad & u_{\min} \leq u_t \leq u_{\max} \end{aligned} \quad (5.10)$$

Assuming there is no saturation constraint, it is possible to find the optimal distribution of control signals. With saturation constraints, the above optimization can be solved using algorithm 1 which is based on active set method [102, 110]. This algorithm can be implemented to be solved in real-time as this active set algorithm has a high efficiency given estimates of the output u_t and the set of saturated actuators \mathcal{S} are available. In our optimization problem for damping the low-frequency modes, the optimal solution at each step does not change much from the previous sampling time based on the low frequency range of the critical inter-area modes. Therefore, a hot-start can be used to initialize the optimization

using the previous results and the number of iterations can be reduced significantly.

In summary, the following major steps are involved in supervisory MB-CA

1. Select a redundant set of actuators based on the controllability measure and identify their limits.
2. Choose appropriate weightings for (5.10).
3. Construct the virtual control block based on the WADC design structure to generate vector $v(t)$ from WADC.
4. Design the MB-CA block based on (5.10) and run the algorithm 1 in real-time to obtain vector $u(t)$.
5. Send the control command $u_i(t)$ to the i th actuator.

5.4 Dynamic Model of the WECC Test System

A modified WECC power grid with high level of wind penetration rate (20% by energy) is considered in this work to verify the effects of redundant damping actuators over low-frequency modes. Original details regarding network data, operating conditions and dynamic parameters are given in [111]. The system with WECC boundaries can be seen in Fig. 5.2. It consists of 31 conventional generators with total generation of 48.49 GW and 11 wind farms with generation of 13.5 GW. Loads are considered to be constant power. In the following, dynamic models of different actuator components equipped with supplementary control inputs are outlined to formulate the problem of actuator constraints and failures.

5.4.1 Generator Dynamic Model

Generators are represented by a two-axis model described in chapter 4.2. The notation is as defined in the Nomenclature. Standard speed-based PSS model (PSS1A) [79] is used to improve damping of the local modes and governors are modeled by the IEEE1 steam turbine model [80].

Algorithm 1 Active set algorithm for optimization (5.10):

1. Initialization:

Let $u_t = (u_{\max} + u_{\min})/2$, the set of free actuators be $\mathcal{R} := \{1, 2, \dots, m\}$ and the set of saturated actuators be $\mathcal{S} := \{\emptyset\}$

2. Main loop:

begin repeat

Compute the unconstrained optimum in free variables:

$$\min_d \left\| \begin{pmatrix} \rho W_v \psi B \\ W \end{pmatrix} (u_t + d) - \begin{pmatrix} \rho W_v v_t \\ W u_d \end{pmatrix} \right\|^2$$

where $d_i = 0, \quad i \in \mathcal{S}$

if $u_{\min} \leq u_t + d \leq u_{\max}$ for all \mathcal{R}

Set $u_t = u_t + d$ and for free actuators, compute the Lagrange multiplier λ as

$$\lambda := \begin{pmatrix} \rho W_v \psi B \\ W \end{pmatrix}^T \left[\begin{pmatrix} \rho W_v \psi B \\ W \end{pmatrix} u_t - \begin{pmatrix} \rho W_v v_t \\ W u_d \end{pmatrix} \right]$$

if $\mathcal{S} = \emptyset$ or all $\lambda \geq 0$

Go to step 3 and vector u_t is optimal.

else

Move the index associated to the most negative λ from \mathcal{R} to \mathcal{S} .

else

Compute the maximum step length α such that $u_{\min} \leq u_t + \alpha d \leq u_{\max}$ and move the index of primary bounding constraint into \mathcal{S} .

end

3. Hot-start:

Use the previous optimal solution u_t and working sets \mathcal{R} and \mathcal{S} as the initial conditions in step 2.

The generators are assumed to be equipped with high-gain AVR systems and supplementary control inputs as shown in Fig. 5.3. Saturation nonlinearity on the field voltage E_{fd} is also considered in the design process. In high-gain excitation systems, typical values of time constant T_A are in the range of 0.01 – 0.05 s. Therefore, T_A is negligible and limits on the field voltage can be modeled by limits of $K_A^{-1}E_{fd\min} - K_A^{-1}E_{fd\max}$ pu on the output of summation block. As a result, the following saturation limits can be considered on the supplementary input u_i .

$$\eta K_A^{-1}E_{fd\min} \leq u_i \leq \eta K_A^{-1}E_{fd\max} \quad (5.11)$$

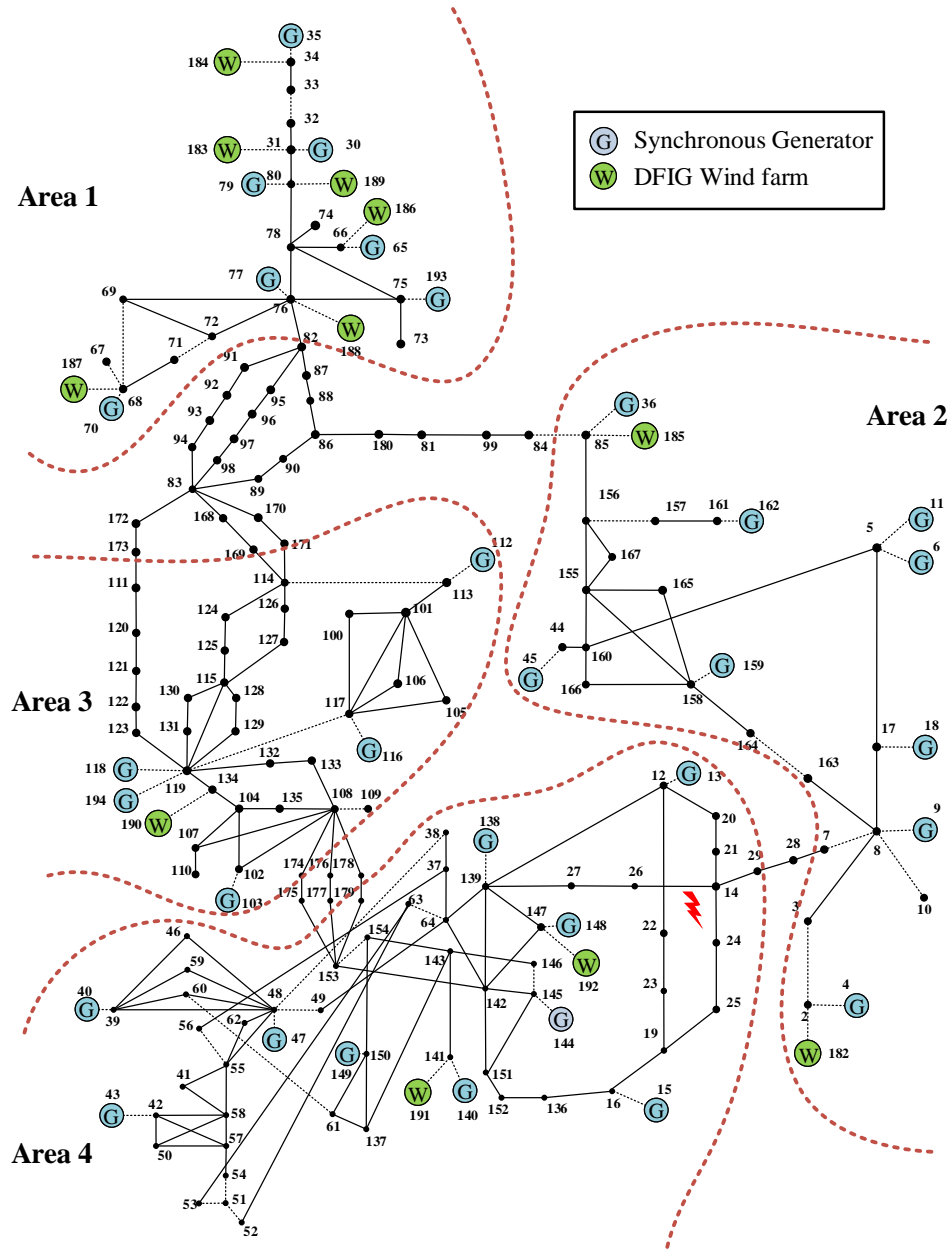


Figure 5.2: Single-line diagram of the modified 192-bus WECC system with DFIG wind farms.

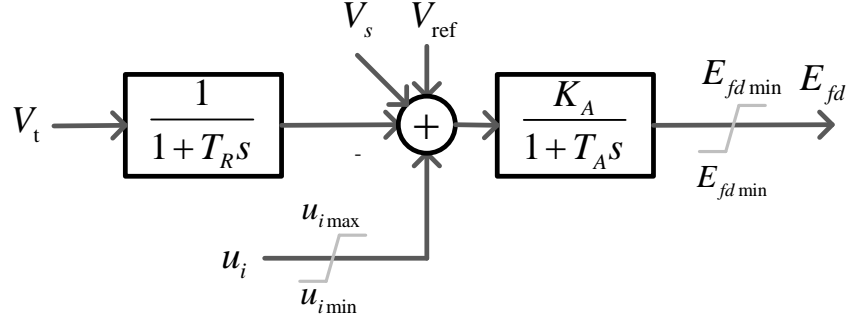


Figure 5.3: Schematic of the high-gain AVR system with supplementary input u .

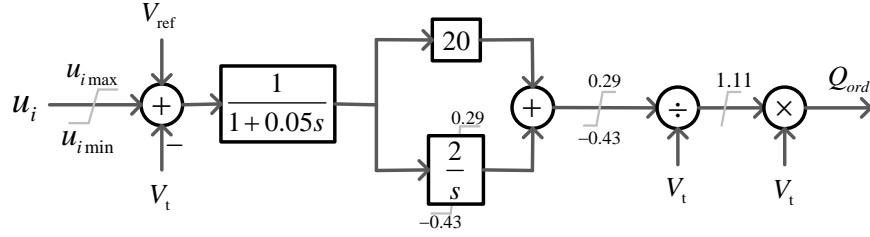


Figure 5.4: Schematic of DFIG reactive power control loop with supplementary input u .

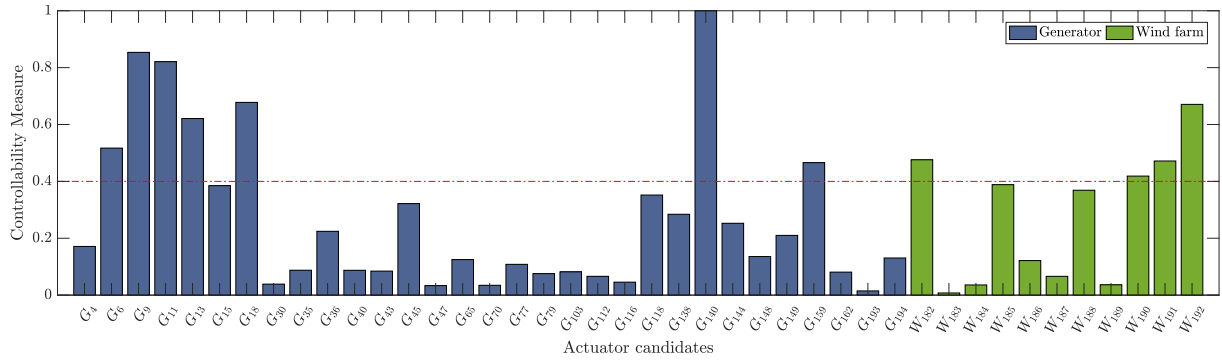


Figure 5.5: Normalized controllability measure associated with inter-area mode 3 for all possible actuators.

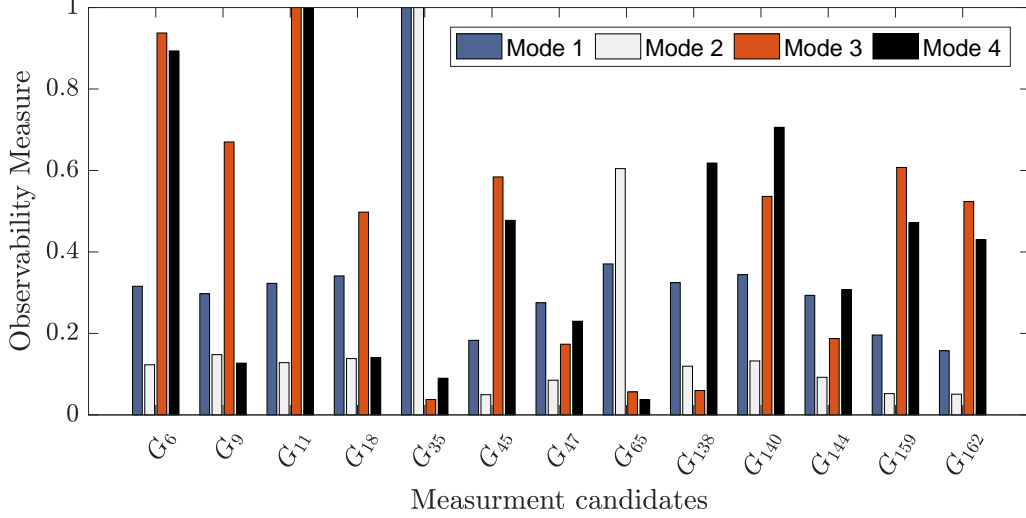


Figure 5.6: Normalized observability measure associated with modes 1-4.

where $\eta \in [0, 1]$ should be chosen to allow an acceptable control range and provide adequate damping while prevent tripping of the generator. Moreover, these limits also minimize the negative effects of damping controllers on voltage regulatory response and are usually in the range of ± 0.05 to ± 0.1 pu which guarantees a modest level of contribution.

5.4.2 DFIG-based Wind Farm Model

A large wind farm may consist of several hundred DFIG wind turbines. Representing each individual unit in the wind farm model can be difficult and unnecessary for large system studies. By aggregation, an equivalent lumped model of a wind farm can be represented by a large DFIG. In this work, the base power of each wind farm is scaled based on the total number of wind turbines while the parameters are assumed to be constant. Each DFIG unit considered in this research is rated at 1.67 MVA and 1.5 MW. It is also assumed that the reactive power capability of each DFIG unit is in the range of -0.432 to 0.29 pu and more comprehensive parameters can be found in [112]. Details of the wind farms outputs are given in Table 5.1 There are different options in DFIG wind farms to add a damping controller. In this study, we consider the reactive power modulation for supplementary damping proposes. Fig. 5.6 illustrates the reactive power control loop where Q_{ord} is input to the master control system of the DFIG. The limits on the supplementary input u are typically in the range of

Table 5.1: DFIG Wind Farms Outputs in the WECC Test System.

Bus No.	Base MVA	MW	MVAr	PF
182	600	400	-114	-0.96
183	1500	1062	164	0.98
184	1410	1000	175	0.98
185	1050	700	41	0.99
186	1410	1000	-317	-0.95
187	1140	880	183	0.97
188	3600	2369	576	0.97
189	3600	3000	423	0.99
190	1500	1068	-36	-0.99
191	1500	1050	235	0.97
192	1350	980	148	0.98

± 0.1 pu. However, depending on the grid requirements for power factor (PF), the amount of available reactive power might be limited by the active power.

5.5 Numerical Results

To illustrate the design principles and verify the effectiveness of the proposed approach, simulations and analysis are carried out on a detailed nonlinear model of the WECC test system described in previous section.

5.5.1 Modal Analysis

In practice, phasor measurement units (PMUs) can be used for identification of power system dynamic models and critical modes of instability [113]. In this research, however, the nonlinear system is linearized around the nominal operating point using the SSAT program [114] to perform modal analysis. Table 5.2 shows a summary of low frequency oscillation modes where the mode 3 with frequency of 0.570 Hz and low damping ratio of 1.047%, represents the critical inter-area mode between area 2 vs. 4. Fig. 5.5 illustrates the controllability measure (4.16) for all possible actuators and the set of actuators with strong enough controllability (assume the threshold variable 0.4) over mode 3 can be chosen

Table 5.2: Modal Analysis of the WECC Test System with 20% Wind Penetration.

Mode Index	Participating Generators	Without WADC		With WADC	
		f (Hz)	ζ (%)	f (Hz)	ζ (%)
1	Area 1 vs. Area 2, 4	0.359	9.946	0.367	8.741
2	G_{35} vs. G_{65}	0.483	15.14	0.481	14.04
3	Area 2 vs. Area 4	0.570	1.047	0.569	7.804
4	Area 2 vs. Area 3, 4	0.722	5.065	0.715	5.918

as follow

$$\mathcal{A} = \{G_6, G_9, G_{11}, G_{13}, G_{18}, G_{140}, G_{159}, W_{182}, W_{190}, W_{191}, W_{192}\} \quad (5.12)$$

where the i th element of vector \mathcal{A} is associated with the i th column of matrix B . Hence, there will always be a trade-off between the degree of fault-tolerance and infrastructure costs such as communication links. To obtain the highest damping contribution, G_{140} (associated with b_6) with the highest controllability measure is chosen as the nominal actuator for WADC. Based on observability measure (4.17), the speed deviations of G_9 is selected as the remote measurement since it has a high observability over the critical mode 3 and also relatively small observability to other modes.

5.5.2 Model Reduction and Design of WADC

With previously identified candidate signals as input and output of the system, the original 417th-order model can be reduced while preserving the larger Hankel singular values. The appropriate order of the reduced-order model is determined by comparing the frequency responses. Fig. 5.7 shows that the 6th-order reduced model represents the low-frequency characteristics of mode 3 and has a close frequency response to the full-order system for interesting input candidates. The nominal WADC is designed based on the 6th-order model to meet or exceed 7% damping mainly over the critical mode 3. The design parameters of the multi-objective WADC are given as $\Gamma_1 = 1$, $\Gamma_2 = 10$, $\beta_1 = -0.005$, $\beta_2 = -50$. The controller matrices can be found in equation (5.13). The choice of design variables usually depends upon the individual application and design requirements, such as, low control effort.

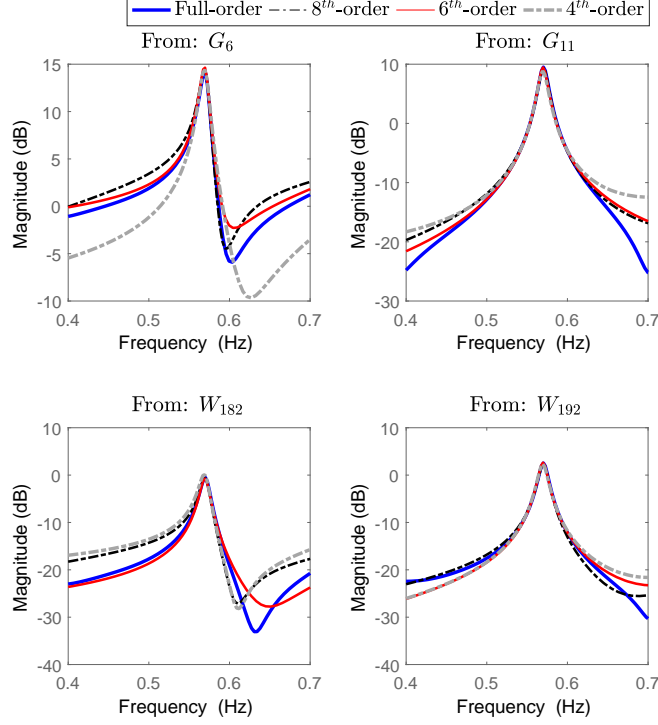


Figure 5.7: Frequency response of the full-order and reduced order models of the WECC system from supplementary inputs.

Table 5.2 also shows a significant improvement in damping ratio of the critical mode 3 with WADC while only slightly affecting the other modes. Since MB-CA offers the advantages of modular design, the output of the WADC controller $\bar{u}(t)$ can be used to generate the virtual control vector $v(t) = \psi b_6 \bar{u}(t)$. This block is just a gain matrix and depends on the WADC design structure.

5.5.3 Design of Modal-Based Control Allocation

The proposed MB-CA is implemented as a user-defined model (UDM) [112] in TSAT [77] by using dynamically linked blocks (DLBs) and the optimization algorithm 1 is implemented using C/C++ with fixed time step of $T_s = 0.02$ s. The weighting functions and gains are chosen as follows: $W_u := \text{diag}(1, 1, 1, 1, 1, 0.5, 1, 1, 1, 1, 1)$, $W_s := 5W_u$, $W_v := \text{diag}(2, 2, 4, 4, 8, 8)$ and $\rho := 10$. The weighting W_u is chosen such that deviation of the nominal actuator is penalizing less than other actuators. This choice of weighting matrix prioritizes the use of the nominal WADC actuator in normal condition to reduce the

$$\begin{aligned}
A_K &= \begin{bmatrix} -0.757 & 0.460 & -0.343 & 6.254 & 0.182 & -0.405 \\ -0.460 & -0.144 & 5.981 & -2.658 & -0.173 & 0.320 \\ -0.343 & -5.981 & -0.244 & 19.66 & 0.195 & -0.488 \\ -6.254 & -2.658 & -19.66 & -51.20 & -4.252 & 7.237 \\ 0.182 & 0.173 & 0.195 & 4.252 & -0.501 & 6.998 \\ 0.405 & 0.320 & 0.488 & 7.237 & -6.998 & -3.321 \end{bmatrix}, \\
B_K &= \begin{bmatrix} -1.682 \\ -0.376 \\ -0.475 \\ -5.745 \\ 0.207 \\ 0.443 \end{bmatrix}, \quad C_K = \begin{bmatrix} -1.682 \\ 0.376 \\ -0.475 \\ 5.745 \\ 0.207 \\ -0.443 \end{bmatrix}^T, \quad D_K = 0
\end{aligned} \tag{5.13}$$

cost. Moreover, the choice of W_v gives the highest priority to the control efforts regarding the critical mode 3. We choose $T_R = 0$, $T_A = 0.02$, $K_A = 50$, $\eta = 0.5$, $E_{fd\max} = -E_{fd\min} = 7.5$ pu so hard limits for the generators are $u_{\max} = -u_{\min} = 0.075$ pu. Additionally, hard limits of $u_{\max} = -u_{\min} = 0.1$ pu are imposed on the supplementary damping signals of wind farms.

5.5.4 Discussion

Nonlinear time domain simulations are conducted using TSAT program. Different variables are monitored and Prony analysis is performed based on the nonlinear response to estimate damping ratio and frequency of the critical modes. To evaluate the performance, different faults are considered in both actuators and the physical system. A symmetrical three-phase fault is applied to bus #14 (marked in Fig. 5.2) near the tie-line connecting the areas 2 and 4. The fault occurs at $t = 1$ s and is cleared after 10 cycles. In this study, the time frame of analysis (oscillation) is restricted to a few seconds and so reasonable to assume that the wind speed remains constant throughout the simulation period.

Without control allocation, the system responses are as been shown in Fig. 5.8 and 5.9. Using Prony analysis of the nonlinear response, it can be observed that WADC can significantly improve the damping from 1.149% to 7.806%. If there is any failure in the nominal WADC actuator, the system will illustrate a similar response to the no control system with damping of 1.149%. Note that results from Prony analysis are slightly different from the linearized results in Table 5.2 because of the nonlinear nature of the system.

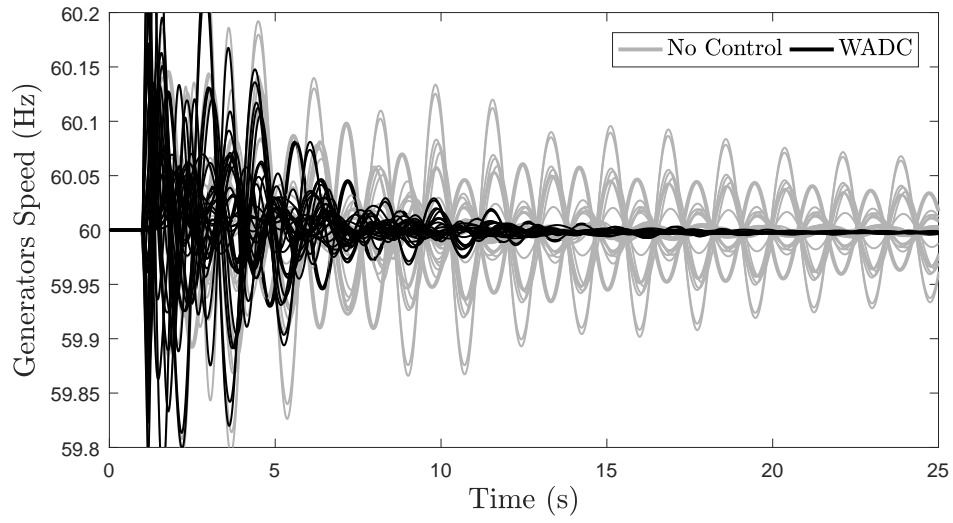


Figure 5.8: Dynamic response of the system to three-phase fault at bus #14.

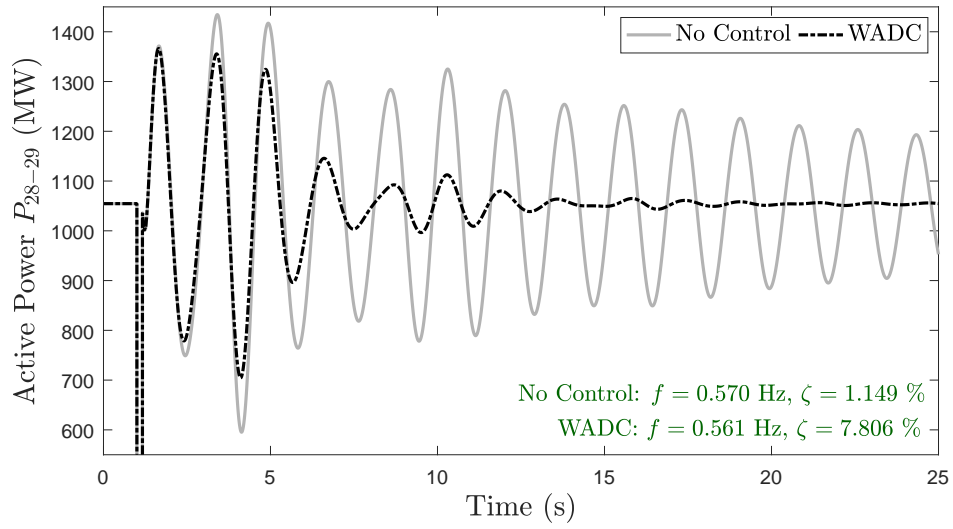


Figure 5.9: Power flow on the tie-line connecting the areas 2 and 4 after a three-phase fault at bus #14.

In case with modal-based control allocation, the system responses are shown in Fig. 5.10 and 5.11 for the following cases.

- Case A: No faulty actuators $\mathcal{F} = \{\emptyset\}$;
- Case B: Faults in the nominal actuator $\mathcal{F} = \{G_{140}\}$, hard limits $u_{\max} = -u_{\min} = 0.05$ pu for all wind farms;
- Case C: Faults in six random actuators $\mathcal{F} = \{G_6, G_{13}, G_{18}, G_{140}, W_{182}, W_{192}\}$;

It can be seen that in case A, where there is no faulty actuator, MB-CA mainly use the nominal damping actuators and can compensate the effects of hard limits on the actuators. In case B, the nominal WADC actuator suffers a loss of communication and hard limits on wind farms are narrowed by 50%. MB-CA successfully recovers the performance of the system. In case C, where more than half of the actuators have failed, the wind farm W_{182} is disconnected and the rest face a communication failure, MB-CA will damp the oscillations by distributing the control signal to healthy actuators and maintain a sufficient damping of 4.035%. Comparing these results, it can be seen that even though the damping performance in case C is not as good as Case A and B, it is far better than without MB-CA. The proposed method clearly enhances fault tolerance of the WADC system. Figs. 5.12, 5.13 and 5.14 illustrate the MB-CA outputs in Case A, B and C, respectively and effects of actuator faults and limits are clearly observed.

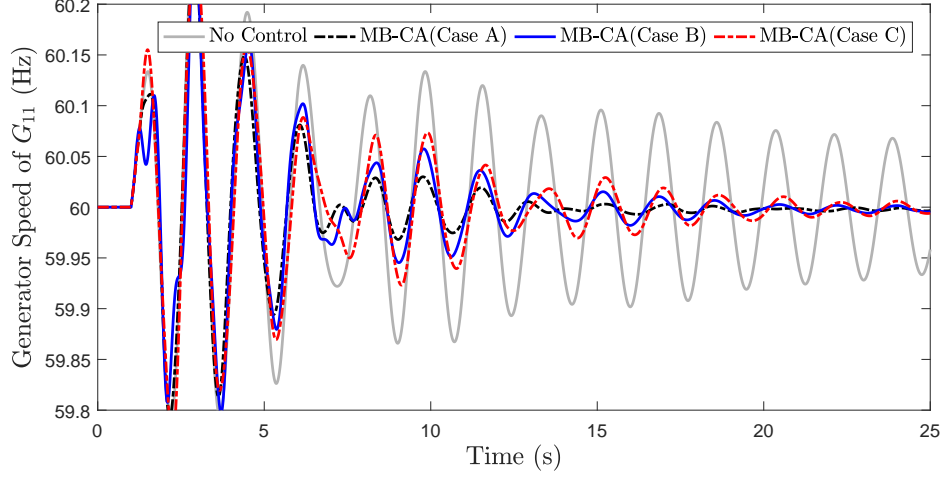


Figure 5.10: Dynamic response of the system to three-phase fault at bus #14 when MB-CA redirects the WADC signal to healthy actuators.

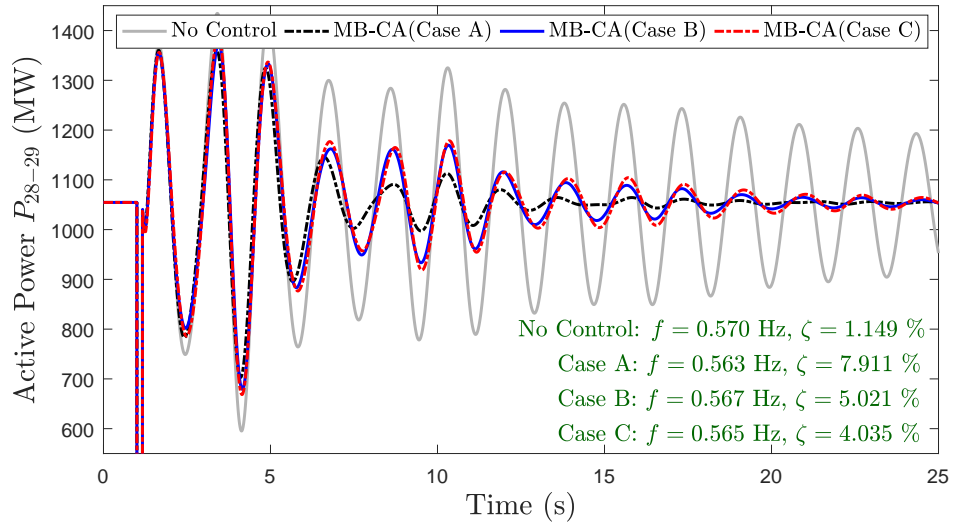


Figure 5.11: Power flow on the tie-line connecting areas 2 and 4 to a three-phase fault at bus #14 when MB-CA redirects WADC signal to healthy actuators.

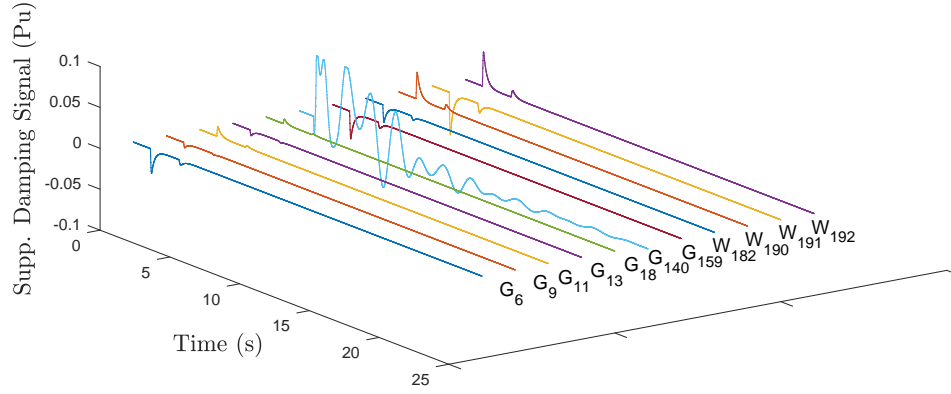


Figure 5.12: Supplementary signals (MB-CA outputs) in Case A.

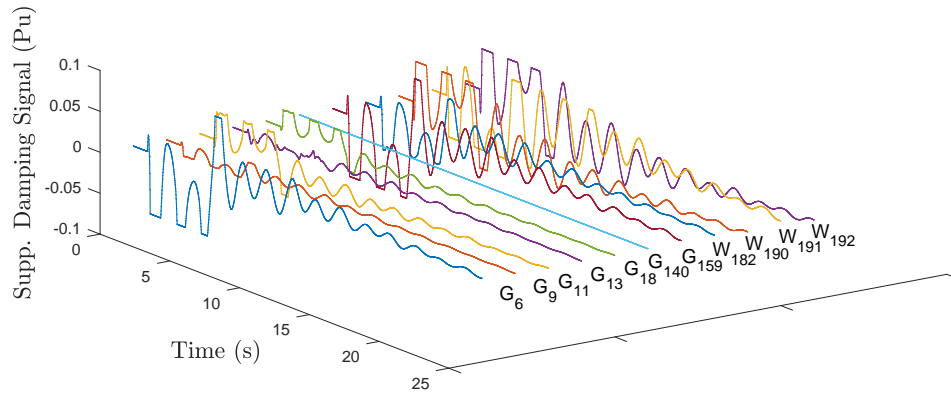


Figure 5.13: Supplementary signals (MB-CA outputs) in Case B.

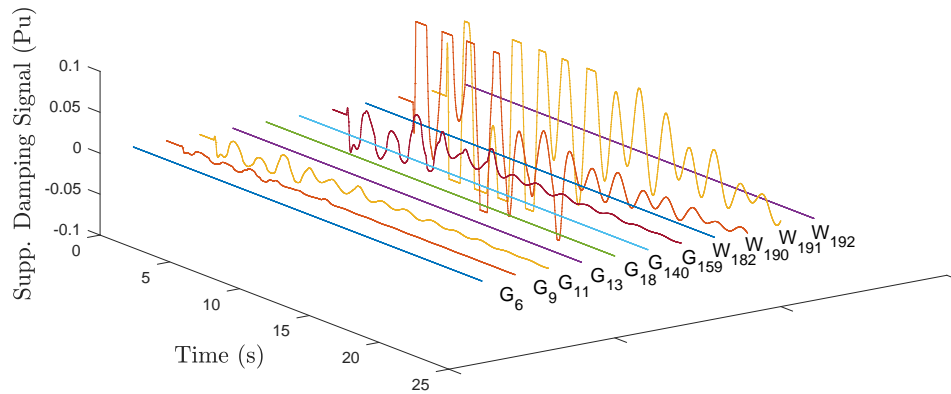


Figure 5.14: Supplementary signals (MB-CA outputs) in Case C.

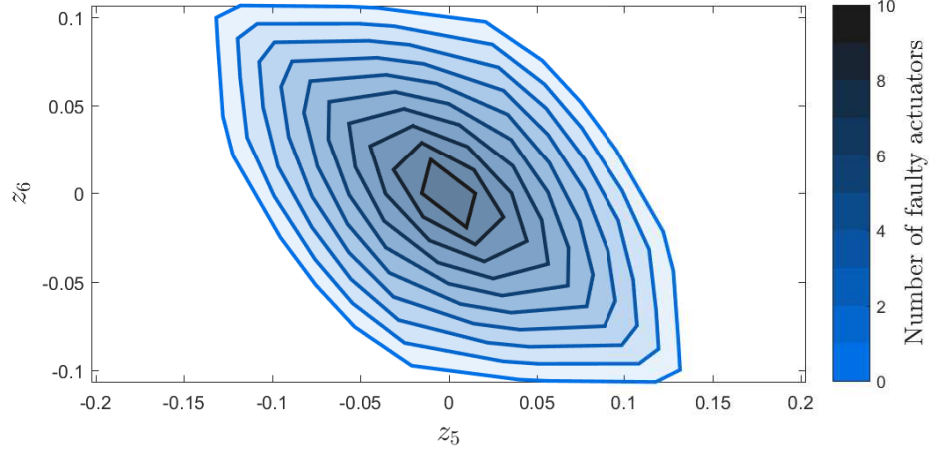


Figure 5.15: Effects of actuator faults on feasible virtual control region for inter-area mode 3.

Various results with respect to different controllers and fault combinations are included in Table 5.3. In all cases, the nominal WADC actuator G_{140} is assumed to be faulty. It is shown that the proposed MB-CA tolerates multiple failures and maintains the minimum acceptable damping of 3.329% over the critical mode in compare to 1.467% damping in case where all modes have identical weights. In general, the optimal solution may not be feasible for all virtual control inputs, constraints and failures. Fig. 5.15 visualizes the average feasible virtual control regions in modal coordinates for the critical mode 3 considering all failure scenarios. These regions can be obtained considering the actuator constraints in (5.5) and provides insight to the degree of fault tolerance. Different faults in the actuators or adding more constraints can further reduce the area of feasible region, which is related to the attainable damping ratio.

In this work, the previous optimization results are used as the starting point to solve the MB-CA problem for the next sampling time. Fig. 5.16 depicts the distribution of the number of iterations required by the algorithm in Case B, with and without warm-start. It clearly indicates that in case of warm-start, the algorithm can converge mostly in one iterations and significantly improve the performance.

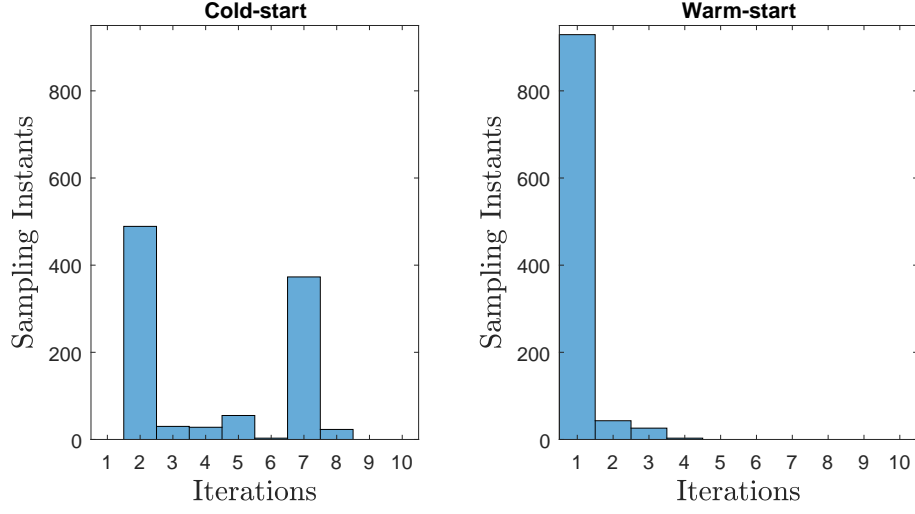


Figure 5.16: Histogram showing the number of iterations required by the optimization algorithm in Case B from $t = 1$ s to $t = 6$ s.

Table 5.3: Damping Ratio of Mode 3 with Respect to Different Controllers and Fault Combinations.

Faulty Actuator Set \mathcal{F}	Damping Ratio (%)		
	MB-CA	CA	WADC
\emptyset	7.911	7.907	7.806
G_{140}	5.052	4.759	1.149
G_6, G_{140}	4.950	4.624	1.149
G_6, G_{140}, W_{182}	4.899	4.353	1.149
$G_6, G_{18}, G_{140}, W_{182}$	4.316	3.744	1.149
$G_6, G_{18}, G_{140}, W_{182}, W_{192}$	4.086	3.103	1.149
$G_6, G_{18}, G_{140}, W_{182}, W_{190}, W_{192}$	3.817	2.949	1.149
$G_6, G_{11}, G_{18}, G_{140}, W_{182}, W_{192}$	3.329	1.467	1.149

5.6 Summary

In this research, a new approach to designing a fault-tolerant WADC using modal-based control allocation is proposed to coordinate a group of actuators to optimally contribute to damping of inter-area oscillations. In our proposed method when an actuator fails or is unavailable, the supervisory MB-CA distributes the control signals to the remaining healthy actuators based on the effects on modal system, the desired control action and actuator constraints. The WADC design is carried out using multi-objective H_2/H_∞ optimization with pole-placement region to achieve high damping performance. In the next step, the MB-CA is designed to manage actuator failures and constraints without redesigning the nominal WADC. The feasibility and performance of the proposed method is analyzed using the WECC system. Numerical results have verified the effectiveness of the proposed method to provide sufficient damping and build in resiliency to different faults.

Chapter 6

Sparse Control Allocation for Wide Area Coordinated Damping

In this work, a modal-based sparse control allocation (SMB-CA) is proposed for coordinated and fault-tolerant wide-area damping controllers (WADCs). In our proposed method, the supervisory sparse CA only communicates with necessary actuators to achieve the required damping performance and in case of actuator failures (e.g., due to loss of communication or scheduling), capabilities of the remaining actuators are fully used before the nominal performance is degraded. This method offers the advantages of modular design where WADC is initially designed to achieve satisfactory damping without the detailed knowledge of actuators. In the next step, sparse CA is designed to manage actuator failures and limitations without the need to redesign the nominal WADC. The proposed approach is applied to a modified 286-bus Western Electricity Coordinating Council (WECC) system to verify the feasibility on a complex power system. Simulation results indicate the effectiveness of the proposed method in coordinating multiple actuators and building resiliency. The results in this chapter appeared in [\[55\]](#).

6.1 Introduction

Traditional power system topology is changing and a large number of small-scale renewable sources are being installed throughout the system. In this aspect, spatial distributions of wind farms are crucial to reduce the need for new transmission infrastructure. These wind farms could be selected as WADC actuators and contribute to damping inter-area oscillations through active/reactive power modulation [94]. In contrast with a large wind farm in a concentrated location, deployment of multiple small-scale wind farms will require special techniques for actuator coordination as none could be used individually to achieve adequate damping. Moreover, the availability of these weather dependent renewable resources could pose design challenges for reliability of critical controllers.

Considering reactive power modulation in Type 4 wind turbines (i.e., full converter asynchronous generators), the amount of available reactive power depends upon the operating mode, converter rating and grid code requirements. This may mean that some WADC actuators become temporarily unavailable (failed) or have more limited capabilities. Moreover, communication failures such as packet loss, excessive time delay and cyber-attacks may also lead to failures in these geographically-dispersed actuators. Thus, developing robust controllers to accommodate such failures and maintain the system stability is an important challenge in deploying WADCs.

In this chapter, a sparse CA method is developed to optimally coordinate a set of actuators to damp the inter-area modes and achieve a fault-tolerant WADC. In our approach, the damping controller is designed based on a fault-free model and the supervisory sparse CA distributes the control signals to necessary actuators based on the desired control actions, total cost, effects on different modes of the system and actuator constraints. This chapter generalizes the previous methods chapter on control allocation and previous work [102, 103, 115, 55] by considering the temporal sparsity and the effects of virtual control on the modal system. This technique allows us to give the highest priority to the control efforts associated with the critical inter-area modes. In [94, 116], an attempt to coordinate multiple wind farms was addressed but without considering the effects of actuator failures, capabilities and limits. This chapter also extends [7, 75, 23, 25, 117] in which unavailability

of WADC actuators has not been considered. Feasibility of the proposed approach has been verified on a modified 286-bus Western Electricity Coordinating Council (WECC) system with multiple small-scale wind farms.

This chapter is organized as follows. In section 6.2, a modular control allocation technique is developed for system with redundant actuators and a multi-objective synthesis is presented as one method to design damping controller. Preliminaries on dynamic modeling of a WECC system with distributed wind farms are described in section 6.3. Nonlinear time-domain simulations are presented in section 6.4 to demonstrate the effectiveness of the proposed method in coordinating multiple actuators. Concluding remarks are given in section 6.5.

6.2 Modal-based Sparse Control Allocation

Similar to chapter 5.3, the Hankel norm approximation [82] can be used to obtain the reduced-order model and the order of model reduction can be determined by examining the Hankel singular values. Considering the reduced-order system with state variables $x_r \in R^n$, using an appropriate transformation $z = \psi x_r$ where $\psi \in R^{n \times n}$, the realization in modal form can be written as

$$\dot{z}(t) = \Lambda z(t) + \psi B_r u(t) \quad (6.1)$$

$$y(t) = C_r \psi^{-1} z(t) \quad (6.2)$$

$$\Lambda = \begin{bmatrix} \iota_1 & 0 & 0 & \dots \\ 0 & \sigma_1 & \omega_1 & \\ 0 & -\omega_1 & \sigma_1 & \\ \vdots & & & \ddots \end{bmatrix} \quad (6.3)$$

where $\Lambda = \psi A_r \psi^{-1}$ is a block diagonal matrix whose elements are eigenvalues of A_r (assuming no repeated eigenvalues), $u \in R^m$ denotes the input and $y \in R^p$ is the measured output. Real eigenvalue ι_i appears on diagonal and complex conjugate eigenvalues $\sigma_i \pm \omega_i j$ appear as a 2-by-2 block on the diagonal of Λ . By introducing the virtual control input $v \in R^n$, the

system equations can be expressed as

$$\dot{z}(t) = \Lambda z(t) + I_n v(t) \quad (6.4)$$

$$y(t) = C_r \psi^{-1} z(t) \quad (6.5)$$

$$v(t) = \psi B_r u(t) \quad (6.6)$$

which decomposes the system into two parts and leads to a modular design where WADC generates the virtual control signal v and control allocator distributes the effort among the available actuators. Matrix ψ is full rank and $\text{rank}(\psi B_r) = n < m$, hence ψB_r has null space of dimension $m - n$ in which u can be perturbed without affecting the response.

Based on the order of the reduced model, the system can now represent an over-actuated system and the problem of modal-based sparse control allocation with proper filtering to reduce the variations can be represented as follows

$$\begin{aligned} \min_{u_t} \quad & \|W_u u_t\|_2^2 + \|W_s (u_t - u_{t-T_s})\|_2^2 + \lambda \|u_t\|_1 \\ \text{s. t.} \quad & \psi B_r u_t = v_t \\ & u_{\min} \leq u_t \leq u_{\max} \end{aligned} \quad (6.7)$$

where W_u and W_s are positive definite matrices, usually diagonal, and represent the weighting for distributions and variations in the control signal, respectively. The term $\|u_t\|_1 = \sum_{i=1}^m |u_{t,i}|$ denotes the ℓ_1 norm of control vector u_t and $\lambda \geq 0$ is the regularization parameter [118]. Virtual control input v_t is derived from the nominal WADC at time t and T_s denotes the time step. We designed a multi-objective damping controller based on LMI optimization technique introduced in [81] but our approach to the sparse CA can accommodate other control approaches. The damping controller designed by the above methodology can be written as:

$$\dot{x}_k(t) = A_k x_k(t) + B_k y(t) \quad (6.8)$$

$$v(t) = C_k x_k(t) + D_k y(t) \quad (6.9)$$

The key feature of the proposed control allocation strategy is that the temporal sparse control vector u_t is directed to actuators considering total cost, actuator rates, modal effects and actuator limitations, which leads to a constrained optimization problem (6.7). This method is based on prior knowledge of control limits and sparse CA only communicates with necessary actuators to achieve the damping requirement.

The cost function of the above optimization can then be simplified to

$$\begin{aligned}
& \|W_u u_t\|_2^2 + \|W_s(u_t - u_{t-T_s})\|_2^2 + \lambda \|u_t\|_1 \\
&= u_t^T W_u^2 u_t + (u_t - u_{t-T_s})^T W_s^2 (u_t - u_{t-T_s}) + \lambda \|u_t\|_1 \\
&= u_t^T (W_u^2 + W_s^2) u_t - 2u_t^T W_s^2 u_{t-T_s} + \lambda \|u_t\|_1 + \text{const.} \\
&= \|W(u_t - u_d)\|_2^2 + \lambda \|u_t\|_1 + \text{const.}
\end{aligned} \tag{6.10}$$

where

$$u_d = W_s^2 (W_u^2 + W_s^2)^{-1} u_{t-T_s}, \quad W = (W_u^2 + W_s^2)^{\frac{1}{2}} \tag{6.11}$$

Since constant terms in the objective function will not affect the optimal solution, they can be removed and the optimization can be cast in the form of least square optimization with ℓ_1 norm regularization

$$\begin{aligned}
& \min_{u_t} \quad \|W(u_t - u_d)\|_2^2 + \lambda \|u_t\|_1 \\
& \text{s. t.} \quad \psi B_r u_t = v_t \\
& \quad \quad u_{\min} \leq u_t \leq u_{\max}
\end{aligned} \tag{6.12}$$

with u_d and W from (6.11). The problem can be approximated by utilizing the first constraint in the cost function using the Lagrangian multiplier ρ and weighting function W_v .

$$\begin{aligned}
& \|W(u_t - u_d)\|_2^2 + \rho^2 \|W_v(\psi B_r u_t - v_t)\|_2^2 + \lambda \|u_t\|_1 = \\
& \left\| \begin{bmatrix} \rho W_v \psi B_r \\ W \end{bmatrix} u_t - \begin{bmatrix} \rho W_v v_t \\ W u_d \end{bmatrix} \right\|_2^2 + \lambda \|u_t\|_1
\end{aligned} \tag{6.13}$$

Finally, we obtain the following optimization problem

$$\begin{aligned} \min_{u_t} \quad & \left\| \begin{bmatrix} \rho W_v \psi B_r \\ W \end{bmatrix} u_t - \begin{bmatrix} \rho W_v v_t \\ W u_d \end{bmatrix} \right\|_2^2 + \lambda \|u_t\|_1 \\ \text{s. t.} \quad & u_{\min} \leq u_t \leq u_{\max} \end{aligned} \quad (6.14)$$

In the control literature, there exist other methods to distribute the control signal based on cost [103] or actuator limits [115], but these have not considered the effects on modal system or sparsity. This technique allows us to give the highest priority to the control efforts associated with the critical inter-area modes by using the weighting function W_v and obtain the feasibility regions in modal coordinates. By decomposing the control vector u_t to positive and negative components, we introduce nonnegative variables u_t^+ , u_t^- and $q_t = \begin{bmatrix} u_t^+ & u_t^- \end{bmatrix}^T$ such that

$$u_t = u_t^+ - u_t^- = \begin{bmatrix} I_m & -I_m \end{bmatrix} q_t; \quad u_t^+, u_t^- \geq 0 \quad (6.15)$$

The ℓ_1 norm can then be modeled as $\|u_t\|_1 = \bar{1}^T q_t$ (with $\bar{1}$ being a vector of ones) and the ℓ_1 -regularized least square problem can be transformed into a quadratic programming with simple box constraints as follow

$$\begin{aligned} \min_{q_t} \quad & q_t^T \begin{bmatrix} \mathcal{A}^T \mathcal{A} & -\mathcal{A}^T \mathcal{A} \\ -\mathcal{A}^T \mathcal{A} & \mathcal{A}^T \mathcal{A} \end{bmatrix} q_t + (2 \begin{bmatrix} -\mathcal{A}^T \mathcal{B} \\ \mathcal{A}^T \mathcal{B} \end{bmatrix}^T + \lambda \bar{1}^T) q_t \\ \text{s. t.} \quad & \bar{0} \leq q_t \leq \begin{bmatrix} u_{\max} \\ -u_{\min} \end{bmatrix} \end{aligned} \quad (6.16)$$

where

$$\mathcal{A} = \begin{bmatrix} \rho W_v \psi^T B_r \\ W \end{bmatrix}, \quad \mathcal{B} = \begin{bmatrix} \rho W_v v_t \\ W u_d \end{bmatrix} \quad (6.17)$$

These quadratic programs can be solved efficiently using interior-point or active-set methods. Note the transformed problem is an optimization over $2m$ -dimensional vector space.

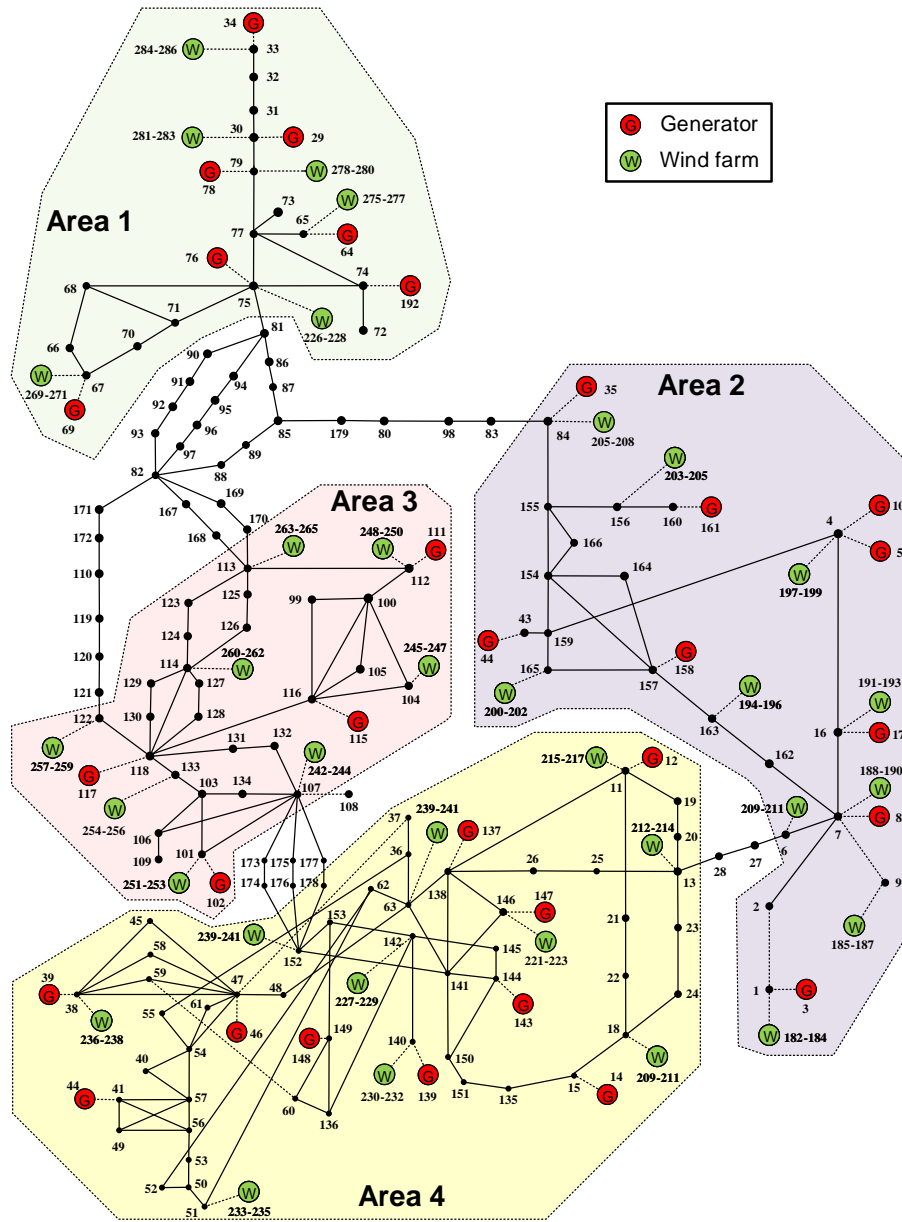


Figure 6.1: One-line diagram of a WECC power system with Type 4 wind farms.

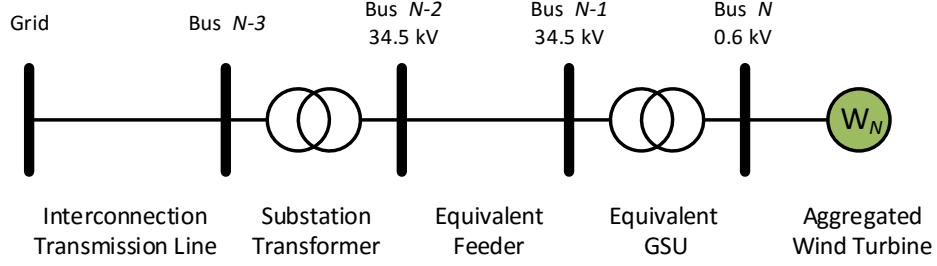


Figure 6.2: Single-generator representation of aggregated wind farm model.

6.3 Dynamic Model of the WECC Test System

A modified 286-bus WECC system is used in this study to capture the effects of redundant actuators over the inter-area modes. As shown in Fig. 6.1, this system consists of 31 synchronous generators with generation of 60.25 GW and 35 small-scale wind farms, each rated at 60 MVA and 50 MW, with total generation of 1.75 GW. Each generator is represented using a two-axis model equipped with a high-gain AVR system and a power system stabilizer (PSS1A) to damp the local oscillation modes. All loads are assumed to be constant power and original parameters regarding the network data and operating conditions are given in [119].

Wind farms are represented by an aggregated model of Type 4 wind turbines. In this work, the base power of each wind farm is scaled based on the total number of wind turbines while the parameters are assumed to be constant. The equivalent circuit is shown in Fig. 6.2 and further details on network and model parameters can be found in [119]. In this study, the damping controller is performed by adding a supplementary signal u to the reactive power control loop for reactive power modulation. We assume each wind farm is constrained to run within a specific power factor range, for example 0.9 lagging to 0.9 leading which is typical for Type 4 machines [120]. As a result, a hard limits of $u_{\max} = -u_{\min} = 0.4$ pu are imposed on the supplementary signal of each wind farm.

Table 6.1: Low-Frequency Modes of the Modified WECC System, Base Case with no Controllers.

Mode No.	Participating Generators	Freq. (Hz)	Damp. (%)
1	Area 1 vs. Area 2,4	0.327	6.99
2	G_{34} vs. G_{64}	0.442	11.62
3	Area 2 vs. Area 4	0.564	0.98

6.4 Numerical Results

Detailed studies based on a nonlinear model of the WECC system described in the previous section are performed to verify the performance of the proposed control allocation method.

6.4.1 Linear Analysis and Design of WADC

This system exhibits several low-frequency oscillation modes that are characterized in Table 6.1. Critical mode 3 with frequency of 0.564 Hz and a low damping ratio of 0.98% is of high interest and represents the inter-area mode between area 2 and 4. Based on an observability measure, speed deviation of G_{10} is selected as the best candidate signal for our controller as it has the highest observability over the critical mode (details of this approach are given in chapter 4.3). The test system has 490 states and the order of the reduced model is chosen as $n = 6$ to preserve the largest Hankel singular values as shown in Fig 6.3. The WADC is designed based on the 6th-order model to meet or exceed 6% damping over the inter-area modes.

6.4.2 Design of Modal-Based Control Allocation

The proposed sparse CA is implemented as a user-defined model (UDM) in TSAT [77] and the optimization algorithm (6.16) is performed using dynamically linked blocks (DLBs) and MATLAB with a fixed time step of $T_s = 0.02$ s and interior-point method. The available small-scale wind farms are chosen as the set of redundant actuators as follows

$$\mathcal{R} = \{W_{184}, W_{187}, W_{190}, \dots, W_{286}\} \quad (6.18)$$

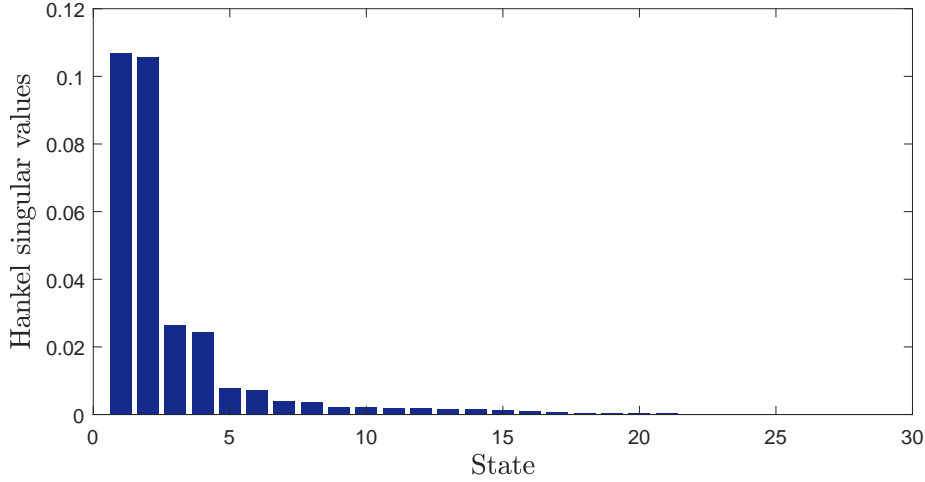


Figure 6.3: Hankel singular values of the modified WECC system.

where i^{th} element of vector \mathcal{R} is associated with the i^{th} column of matrix B_r . The weighting functions and gains are chosen as $W_u := I_{35}$, $W_s := 2W_u$, $W_v := \text{diag}(2, 2, 4, 4, 8, 8)$, $\lambda := 1$ and $\rho := 100$. This choice of weighting matrix W_v gives the highest priority to the control efforts regarding the critical mode 3. Moreover, the weighting W_u can also be chosen based on the reliability of each actuator and the corresponding communication link.

6.4.3 Nonlinear Simulations

Nonlinear transient studies were performed using TSAT and Prony analysis is used to extract the damping coefficient of the inter-area oscillation based on the nonlinear response. In this study, the time frame of analysis (oscillation) is restricted to a few seconds, so it is reasonable to assume that the wind speed remains effectively constant during this period. Cases of interest include faults in both the physical system and actuators. In the physical system, a symmetrical three-phase fault is applied at bus #139, which is a severe disturbance.

To illustrate the benefit of sparse control allocation, three control cases were evaluated and compared during transient response. First, the system with no control is considered. Second, a WADC with fixed allocation $u(t) = (\psi B_r)^\dagger v(t)$ is considered based on pseudo-inverse calculation. Finally, a sparse control allocation is considered to include hard limits and actuator status in the design. Active power of the inter-area transmission line 6 – 27 is shown in Figs 6.4, 6.5 and 6.6 for the following cases

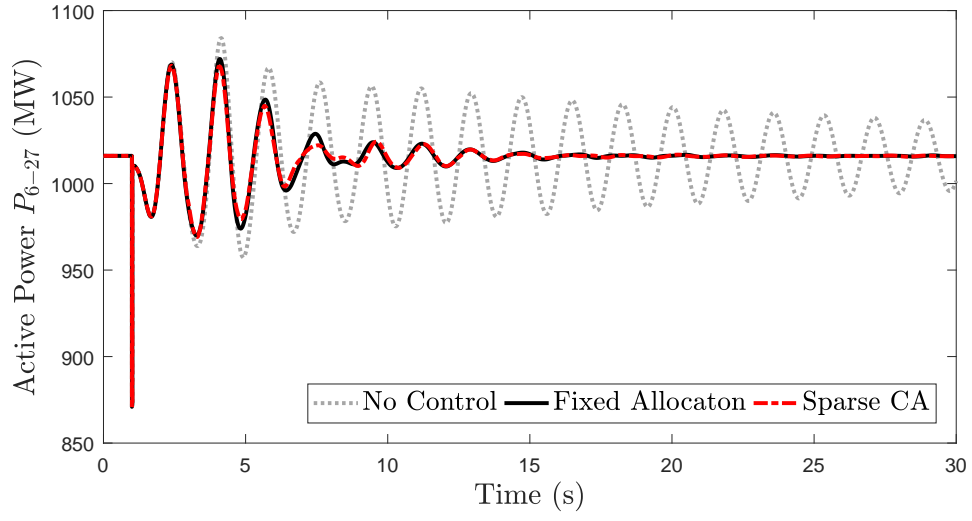


Figure 6.4: Responses of the WECC system to three-phase fault at bus #139 in case A.

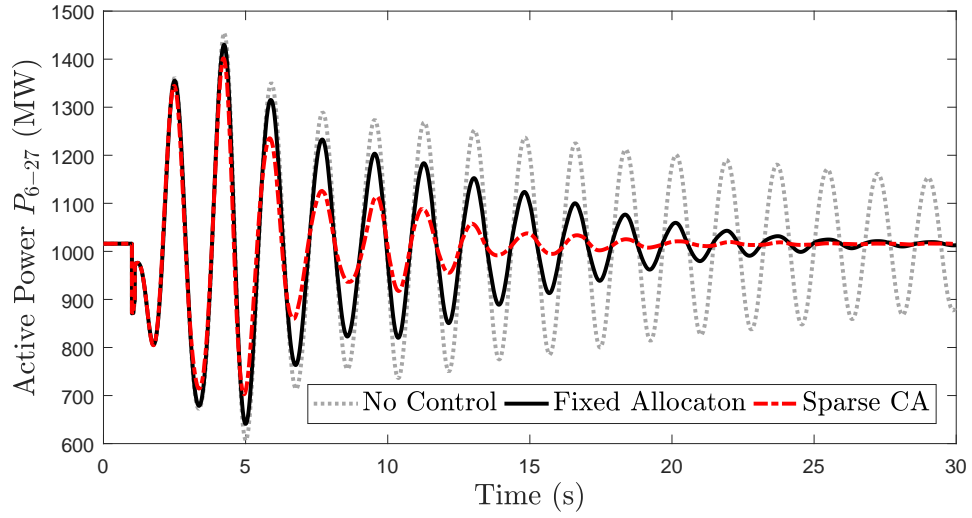


Figure 6.5: Responses of the WECC system to three-phase fault at bus #139 in case B.

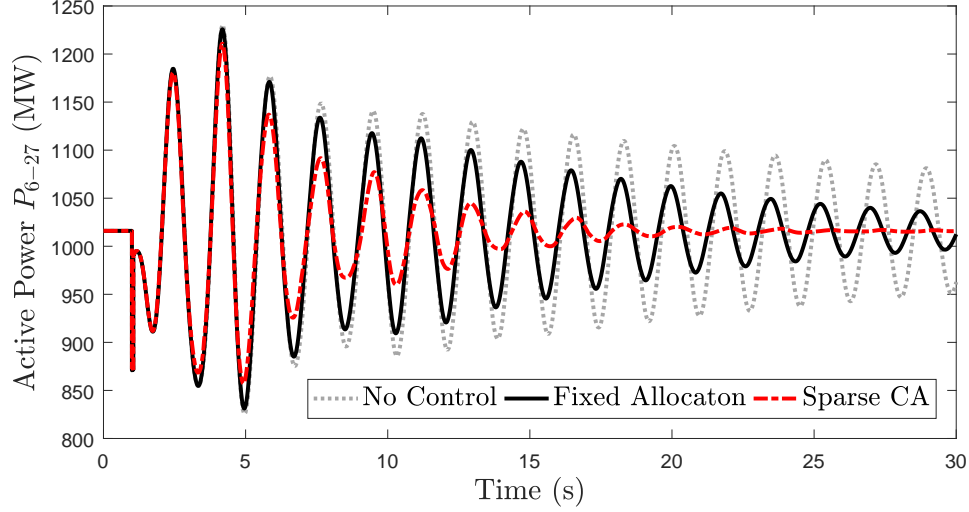


Figure 6.6: Responses of the WECC system to three-phase fault at bus #139 in case C.

- Case A: No faulty actuators and fault duration of 1 cycle;
- Case B: No faulty actuators and fault duration of 6 cycles;
- Case C: Faults in 70% of the actuators and fault duration of 3 cycles;

It can be seen that in case A, where fault duration is short and the required control effort is less, both sparse CA and fixed allocation method can improve the damping to 7.2% compared to the open-loop damping of 0.98%. In case B, where fault duration is longer and requires extensive control efforts, the damping ratio of the fixed allocation method reduces to 2.82%. However, the sparse CA achieves a damping ratio of 5.55% as it considers the actuator limitations in control redistribution. In case C with a shorter fault duration but 70% actuator failures (either from multiple wind farms are disconnected, communication congestions, changes in wind speed), the sparse sparse CA will again dampen the oscillations by redistributing the control signal to healthy actuators and maintain sufficient damping of 4.89% compared to 2.03% under a fixed allocation. Comparing these results, it can be seen that the proposed method enhances fault-tolerance of the WADC system.

Figs. 6.7 and 6.8 illustrate the sparse sparse CA outputs in case A and B, respectively. It can be seen that the control signal u is temporally sparse relative to the fixed control allocation method. Additional results for different actuator fault combinations are presented in Table 6.2. In all cases, the physical fault is assumed to be with a duration of 3 cycles.

Table 6.2: Damping Ratio of the Critical Mode for Different Actuator Fault Combinations.

Actuator Failure (%)	Damping Ratio (%)		
	sparse CA	Fixed Alloc.	No Control
0	6.79	5.12	0.97
10	6.56	4.62	0.97
30	6.43	4.01	0.97
50	5.80	3.04	0.97
70	4.89	2.03	0.97
80	4.33	1.59	0.97

It can be observed that our proposed method tolerates various combinations of failures and maintains a higher damping ratio over the critical inter-area mode.

6.5 Summary

This work proposes a sparse control allocation technique for fault-tolerant wide-area damping controllers and coordinated control of multiple actuators. This method leads to a modular design process where the damping controller generates the virtual control signal and the supervisory sparse CA distributes the control efforts to the necessary actuators based on the desired control actions, actuator limits and modal effects. The proposed approach is applied to a modified 286-bus Western Electricity Coordinating Council (WECC) system with distributed small-scale wind farms. Simulation results show significant improvement in resiliency due to various system failures.

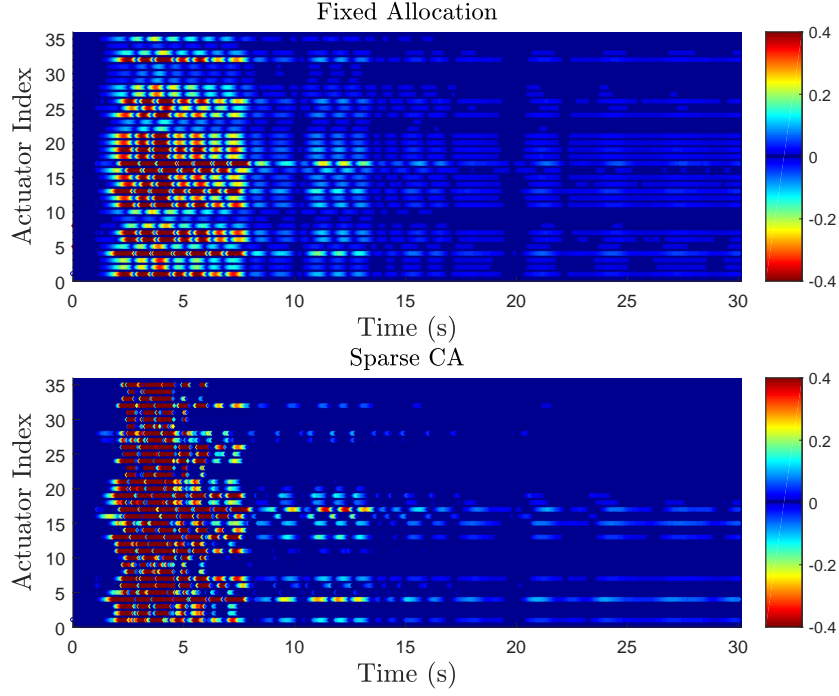


Figure 6.7: Supplementary control signal u for different actuators in response to three-phase fault at bus #139 in case A.

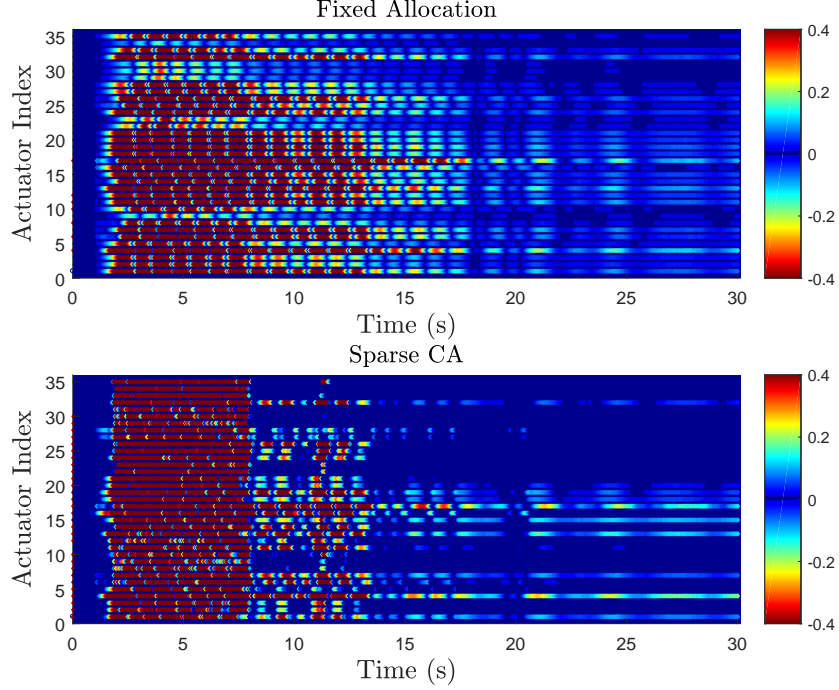


Figure 6.8: Supplementary control signal u for different actuators in response to three-phase fault at bus #139 in case B.

Chapter 7

Stability of Wide Area Controls with Intermittent Information Transmission

This chapter investigates the stability problem of wide area damping controllers with intermittent information transmission. Due to the interruption in communication links between remote measurements and damping controllers or from the controller to the damping actuators, the closed loop system might become unstable. To estimate instability, this chapter uses discrete-continuous time models and the stability conditions are derived using time scale theory. This method allows us to handle discrete and continuous models under the same framework on a particular time scale, such that the system switches between a continuous time subsystem (when the communication occurs) and a discrete-time system (when the communication fails). The focus of this chapter is on application of the developed method for power systems and more details on time scale preliminaries and formulations can be found in [121]. The contribution is in quantifying the maximum time of interruption in order to guarantee exponential stability. The findings are useful in specifying the minimum requirements for communication infrastructure and the time to activate remedial action schemes. Simulations are performed based on both linear and nonlinear systems to validate the theoretical development.

7.1 Introduction

Traditionally, PMU data has been primarily used for off-line post event analysis. However, with recent advancement in communications (e.g. faster communication channels) and processing power, it is now possible to use these geographically dispersed PMUs for real-time applications in power systems [122]. PMUs can be used to address the problem of inter-area oscillations that may require wide-area supervision and control schemes. In these applications, usually damping controllers, sensors (e.g., PMUs) and actuators (e.g., synchronous generators, FACTS devices and energy storage systems) are located remotely and can must communicate over a communication network as depicted in Fig. 7.1.

Implementation of damping controllers in a network, such that, portions of the control system are located remotely, create challenges in analysis as the closed loop performance is highly dependent on the communication network. In this study, we aim to consider the effect of the communication intermittency. The main question is what happens when communication experiences constant or time varying delays [29], packet dropouts [30] or packet disordering [31]. Hence, the communication introduces additional uncertainty in the operation of the closed-loop system.

The theory of dynamical systems on an arbitrary time scales appears to be a promising approach to analyze this problem. By using time scale theory, it will be shown that the problem can be converted to an asymptotic stabilization problem for a particular switched system on a non-uniform time domain formed by the union of disjoint intervals with variable lengths and variable gaps [123, 124]. Indeed, the closed loop system evolves some continuous time intervals when the communication occurs, and when the communication fails, the control may not be updated and the system is discretized with a variable step size. Thus, it would be valuable to have a unified framework for a combined continuous-time and discrete-time system [125, 126, 127, 128].

In power systems, communication network effects are often ignored [66, 67]. Reference [129] studied the impact of induced network delays using LMIs and only for state feedback controllers. In [130, 131], simple models were considered to capture the effects of communication failure with known lower and upper bounds. In fact, existing methods based

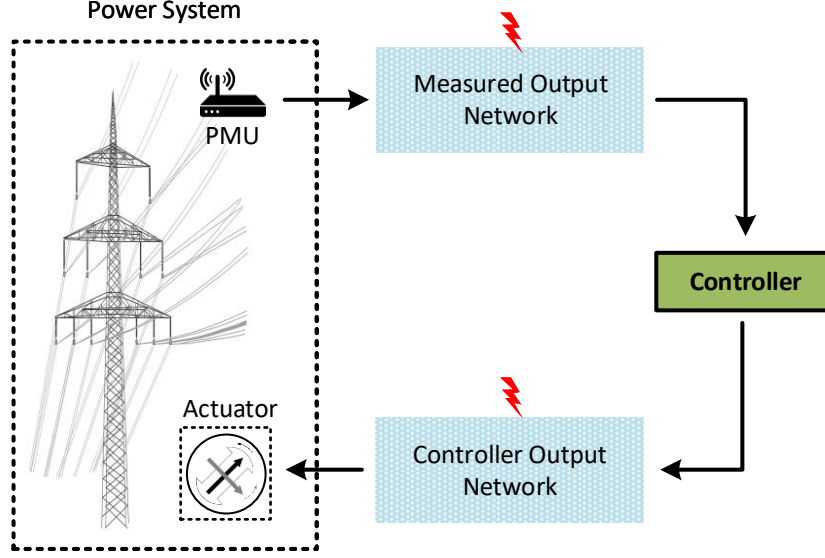


Figure 7.1: A networked control system with components that are remotely operated over a communication network.

on LMIs or common quadratic Lyapunov functions lead to highly conservative results. In this chapter, new stability conditions are derived using time scale theory to determine the maximum time of interruption in information transmission in order to guarantee exponential stability of the closed loop power system. The findings are useful in specifying the minimum requirements for communication infrastructure and the time to activate remedial action schemes [90]. Moreover, we explore practical cases involving sensor-to-controller and/or controller-to-actuator communication failures.

The remainder of this chapter is organized as follows. Some background on time scale theory is presented in Section 7.2. In Section 7.3, it is shown that the stability problem of linear system with intermittent information transmission is equivalent to the stabilization of a switched system consisting of a linear continuous-time and linear discrete-time subsystems. A set of conditions on the maximum time of interruption to guarantee the exponential stability of the closed-loop power system is derived in Section 7.3. Finally, numerical results and conclusions are presented in Section 7.4 and Section 7.5, respectively.

7.2 Preliminaries on Time Scale Theory

Basic notations and properties of time scales theory [121, 132, 125, 123] are presented in this section. A *time scale*, noted \mathbb{T} is an arbitrary nonempty closed subset of \mathbb{R} . The usual integer subsets \mathbb{Z} and \mathbb{N} , the real numbers \mathbb{R} and any discrete subset or any combination of discrete points united with closed intervals, are an examples of time scales. For $t \in \mathbb{T}$, the *forward jump operator* $\sigma(t) : \mathbb{T} \rightarrow \mathbb{T}$ is defined by

$$\sigma(t) := \inf\{s \in \mathbb{T} : s > t\} \quad (7.1)$$

The mapping $\mu : \mathbb{T} \rightarrow \mathbb{R}^+$, called the *graininess function*, is defined by

$$\mu(t) = \sigma(t) - t \quad (7.2)$$

In particular, if $\mathbb{T} = \mathbb{R}$, $\sigma(t) = t$ and $\mu(t) = 0$ and If $\mathbb{T} = h\mathbb{Z}$, $\sigma(t) = t + h$ and $\mu(t) = h$. The Δ -*derivative* of f is defined as

$$f^\Delta(t) = \lim_{s \rightarrow t} \frac{f(\sigma(t)) - f(s)}{\sigma(t) - s} \quad (7.3)$$

The Δ -*derivative*, unify the derivative in the continuous sense and the difference operator in the discrete sense. If $\mathbb{T} = \mathbb{R}$, $\sigma(t) = t$ and $f^\Delta(t) = \dot{f}(t)$. If $\mathbb{T} = h\mathbb{Z}$, $\sigma(t) = t + h$ and $f^\Delta(t) = \frac{f(t+h) - f(t)}{h}$. In particular, if $h = 1$, $f^\Delta(t) = f(t + 1) - f(t) = \Delta f(t)$, the difference operator. We notice that the Δ -derivative, generalize the continuous and the discrete derivatives.

A function $f : \mathbb{T} \rightarrow \mathbb{R}$ is *regressive* if $1 + \mu(t) f(t) \neq 0$, $\forall t \in \mathbb{T}^\kappa$. A matrix A is called *regressive*, if $\forall t \in \mathbb{T}^\kappa$, the matrix $(I + \mu(t)A)$ is invertible, where I is the identity matrix (equivalently, if and only if $(1 + \mu(t)\lambda_i) \neq 0$, for all λ_i the eigenvalues of A [132]). Let A be a regressive matrix. The unique matrix-valued solution of

$$x^\Delta(t) = A x(t), \quad x(t_0) = x_0, \quad t \in \mathbb{T}, \quad (7.4)$$

The dynamical system (7.4) is exponentially stable on an arbitrary time scale \mathbb{T} , if there exists a constant $\beta \geq 1$ and a negative constant $\lambda \in \mathcal{R}^+$, such that the corresponding solution satisfies

$$\|x(t)\| \leq \beta \|x_0\| e_\lambda(t, t_0), \quad \forall t \in \mathbb{T}. \quad (7.5)$$

where the generalized exponential function denoted by $e_A(t, t_0)$ [121]. This characterization is a generalization of the definition of exponential stability for dynamical systems defined in \mathbb{R} or $h\mathbb{Z}$. To study the stability of linear dynamical systems on time scale \mathbb{T} , a particular open set of the complex plane called the *Hilger circle* is defined for all $t \in \mathbb{T}$ as

$$\mathcal{H}_{\mu(t)} := \left\{ z \in \mathbb{C} : |1 + z\mu(t)| < 1, z \neq -\frac{1}{\mu(t)} \right\} \quad (7.6)$$

When $\mu(t) = 0$, we define $\mathcal{H}_0 = \{z \in \mathbb{C} : \operatorname{Re}(z) < 0\} = \mathbb{C}^-$, the open left-half complex plane. The smallest Hilger circle (denoted \mathcal{H}_{\min}) is the Hilger circle associated with $\mu(t) = \mu_{\max} = \sup_{t \in \mathbb{T}} \mu(t)$. A regressive time-invariant matrix A is called Hilger stable if $\operatorname{spec}(A) \subset \mathcal{H}_{\min}$ (i.e all eigenvalues of A are in \mathcal{H}_{\min}) [126].

7.3 Wide Area Control with Intermittent Information

We aim to consider the effects of the communication network in the stability analysis. First, nonlinear power system models can be linearized around the operating point which leads to the following generalized form

$$\dot{x}(t) = Ax(t) + Bu(t) \quad (7.7)$$

$$y(t) = Cx(t) \quad (7.8)$$

where $x \in \mathbb{R}^n$, $A \in \mathbb{R}^{n \times n}$ and $B \in \mathbb{R}^{n \times m}$ are constant real matrices such that (A, B) is stabilizable and $u \in \mathbb{R}^m$ is the control input. The goal in this section is to estimate the maximum time of interruption and analyze what happens when the communication network is no longer perfect due to packet loss, delay or any other common communication failure.

Two general schemes can be found in the literature to compensate for intermittent

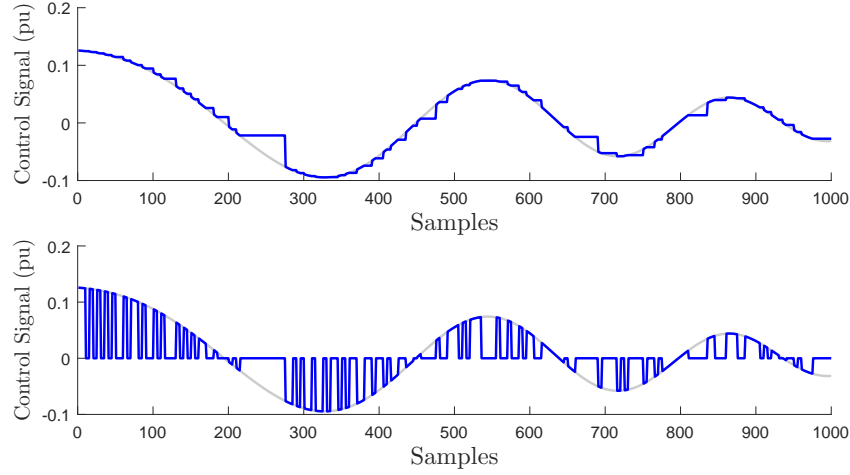


Figure 7.2: Sample of control signal with intermittent communication transmissions using hold strategy (top sub-figure) and zero strategy (bottom sub-figure).

communication as shown in Fig. 7.2: the zero strategy, in which the input/measurement of the plant is set to zero if a packet is dropped; and the hold strategy, in which the latest arrived/measured packet is kept constant until the next packet arrives [133]. In this chapter, the hold strategy is used in control and measurement loops in which the states before communication failure are held and continues to be used when packet dropouts happen. If the failure becomes large, the system may become unstable. Hence, the goal is to estimate the maximum time of interruption in order to maintain the stability of the system.

7.3.1 State Feedback Problem Formulation

Consider the particular time scale $\mathbb{T} = \cup_{k=0}^{\infty} [\sigma(t_k), t_{k+1}]$, where $\sigma(\cdot)$ is the forward jump operator, such that, $\sigma(t_0) = t_0$ and the graininess function $\mu(t_k) = \sigma(t_k) - t_k, \forall k \in \mathbb{N}^*$. To solve the power system problem under intermittent information transmission between generators, we assume that the duration of a communication failure is bounded by a known value $\mu \in \mathbb{R}^+$. The following switching control law is applied

$$u(t) = \begin{cases} Kx(t), & \text{if } t \in \cup_{k=0}^{\infty} [\sigma(t_k), t_{k+1}) \\ Kx(t_{k+1}), & \text{if } t \in \cup_{k=0}^{\infty} [t_{k+1}, \sigma(t_{k+1})) \end{cases} \quad (7.9)$$

where K is an appropriate state feedback controller. The union of time intervals over which the communication occurs is represented by $\cup_{k=0}^{\infty}[\sigma(t_k), t_{k+1})$. The remaining intervals represent the time intervals over which the feedback does not evolve (i.e., is constant to its value at the switching times instants t_{k+1}) due to the absence of local information. The time sequence $\{t_1, t_2, t_3, \dots\}$ characterizes the time when the communication failure occurs and suppose that there is no accumulation points. The duration of a communication failure equal to $\mu(t_k)$ which is assumed to be variable and bounded, $\forall k \in \mathbb{N}^*$. With the control law (7.9), the dynamical system (7.7) is equivalent to

$$\dot{x}(t) = \begin{cases} (A + BK)x(t), & \text{if } t \in \cup_{k=0}^{\infty}[\sigma(t_k), t_{k+1}) \\ Ax(t) + BKx(t_{k+1}), & \text{if } t \in \cup_{k=0}^{\infty}[t_{k+1}, \sigma(t_{k+1})) \end{cases} \quad (7.10)$$

Since the feedback does not evolve when local information is not available, the study of system (7.10) is not trivial. There exist previous works dealing with the stabilization of linear systems under variable sampling period. The approaches are usually based on linear matrix inequalities, derived using Lyapunov-Razumikhin stability conditions, which are rather complex to verify [134]. To reduce the conservatism and facilitate the analysis, the problem (7.10) is converted to switched system on time scale $\mathbb{T} = \cup_{k=0}^{\infty}[\sigma(t_k), t_{k+1}]$, such that, during the communication failures, only the behavior of the solution of (7.10) at the discrete times $\{t_{k+1}\}$ and $\{\sigma(t_{k+1})\}$ is considered. The second subsystem of (7.10) is discretized at times $\{t_{k+1}\}_{k \in \mathbb{N}}$ as follows (for more detail see [135]).

For $t \in [t_{k+1}, \sigma(t_{k+1}))$, $k \in \mathbb{N}$, we have

$$\dot{x} = Ax(t) + Bu(t_{k+1}) \quad (7.11)$$

such that $u(t_{k+1}) = Kx(t_{k+1})$ is constant on the time interval $[t_{k+1}, \sigma(t_{k+1}))$. The solution of (7.11) is given by

$$\begin{aligned} x(t) &= e^{A(t-t_{k+1})} [x(t_{k+1}) + A^{-1}Bu(t_{k+1})] - A^{-1}Bu(t_{k+1}) \\ &= e^{A(t-t_{k+1})} [I + A^{-1}BK] x(t_{k+1}) - A^{-1}BKx(t_{k+1}) \end{aligned}$$

At time $t = t_{k+1}$, the Δ -derivative of $x(t)$ is given by

$$\begin{aligned} x^\Delta(t_{k+1}) &= \frac{x(\sigma(t_{k+1})) - x(t_{k+1})}{\sigma(t_{k+1}) - t_{k+1}} \\ &= \left(\frac{e^{A\mu(t_k)} - I}{\mu(t_k)} \right) [I + A^{-1}BK] x(t_{k+1}). \end{aligned}$$

By using the above development, the closed-loop system (7.10) is modelled as the following switched linear system

$$x^\Delta = \begin{cases} (A + BK)x(t), & t \in \cup_{k=0}^{\infty} [\sigma(t_k); t_{k+1}) \\ \left(\frac{e^{A\mu(t)} - I}{\mu(t)} \right) (I + A^{-1}BK) x(t), & t \in \cup_{k=0}^{\infty} \{t_{k+1}\} \end{cases} \quad (7.12)$$

on $\mathbb{T} = \cup_{k=0}^{\infty} [\sigma(t_k); t_{k+1}]$, where the system commutes between a continuous-time linear subsystem and a discrete-time linear subsystem during a period of time $\mu(t)$, which corresponds to the interruption time of the control evolution. Notice that, the stability of switched system (7.12) depend strongly on $\mu(t)$. The objective is to determine the maximum time of interruption of communication to be respected in order to maintain stability of the switched system.

7.3.2 Stability Criteria

In this subsection, the stability criteria is briefly presented to guarantee the stability of the switched system (7.12) with respect to the duration of interruption of communication $\mu(t)$. Consider the switched system (7.12), and suppose that the following assumptions are fulfilled [121]:

- i) The matrix control law K is determined such that $(A + BK)$ is stable. Existence of K is guaranteed since (A, B) is assumed stabilizable.
- ii) The discrete subsystem is regressive for all $\mu(t)$ and can be Hilger stable or unstable.

iii) Let $\tau(t_i) = t_{i+1} - \sigma(t_i)$ be the duration of each continuous-time subsystem, such that, $\forall 0 \leq i \leq k$ we have

$$\|e^{(A+BK)\tau(t_i)} [I + (e^{A\mu(t_i)} - I)(I + A^{-1}BK)]\| < 1 \quad (7.13)$$

Then the switched system (7.12) is exponentially stable.

7.3.3 Extension to Dynamic Output-feedback

In practical applications for power systems, the full state vector is not available. Consequently, it is desirable to adopt the dynamic output-feedback controller to directly use the measured output signals for damping the oscillations. This type of controller can be defined as

$$\dot{x}_k(t) = A_k x_k(t) + B_k u_k(t) \quad (7.14)$$

$$y_k(t) = C_k x_k(t) + D_k u_k(t) \quad (7.15)$$

where $x_k \in \mathbb{R}^n$ is the controller states, A_k, B_k, C_k, D_k are an appropriate matrices to be designed, u_k and y_k are the controller input and output, respectively. This controller yields with (7.7) and (7.8) to the following closed loop matrix

$$A_{cl} = \begin{bmatrix} A + BD_k C & BC_k \\ B_k C & A_k \end{bmatrix} \quad (7.16)$$

where $\hat{x}^T = [x^T \quad x_k^T]$ is the augmented system states. Consider the case where communication failure happens in control signal as is shown in Fig. 7.3, the augmented system can be written as

$$\dot{\hat{x}}(t) = \begin{bmatrix} A & 0 \\ B_k C & A_k \end{bmatrix} \hat{x}(t) + \begin{bmatrix} B \\ 0 \end{bmatrix} u(t) \quad (7.17)$$

$$y_k(t) = \begin{bmatrix} D_k C & C_k \end{bmatrix} \hat{x}(t) \quad (7.18)$$

and can be reformulated on time scale $\mathbb{T} = \cup_{k=0}^{\infty} [\sigma(t_i), t_{i+1}]$ as follow

$$\dot{\hat{x}}(t) = \begin{cases} \begin{bmatrix} A + BD_k C & BC_k \\ B_k C & A_k \end{bmatrix} \hat{x}(t), & \text{if } t \in \cup_{k=0}^{\infty} [\sigma(t_i), t_{i+1}) \\ \begin{bmatrix} A & 0 \\ B_k C & A_k \end{bmatrix} \hat{x}(t) + \begin{bmatrix} B \\ 0 \end{bmatrix} u(t_{i+1}), & \text{if } t \in \cup_{i=0}^{\infty} [t_{i+1}, \sigma(t_{i+1})) \end{cases} \quad (7.19)$$

which is equivalent to

$$\dot{\hat{x}}(t) = \begin{cases} \begin{bmatrix} A + BD_k C & BC_k \\ B_k C & A_k \end{bmatrix} \hat{x}(t), & \text{if } t \in \cup_{k=0}^{\infty} [\sigma(t_i), t_{i+1}) \\ \begin{bmatrix} A & 0 \\ B_k C & A_k \end{bmatrix} \hat{x}(t) + \begin{bmatrix} B \\ 0 \end{bmatrix} [D_k C \quad C_k] \hat{x}(t_{i+1}), & \text{if } t \in \cup_{i=0}^{\infty} [t_{i+1}, \sigma(t_{i+1})) \end{cases} \quad (7.20)$$

such that the controller $y_k(t_{i+1}) = [D_k C \quad C_k] \hat{x}(t_{i+1})$ is constant on $[t_{i+1}, \sigma(t_{i+1}))$. Similarly to the above analysis, the system can be rewritten as follows

$$\hat{x}^{\Delta}(t) = \begin{cases} \begin{bmatrix} A + BD_k C & BC_k \\ B_k C & A_k \end{bmatrix} \hat{x}(t), & \text{if } t \in \cup_{k=0}^{\infty} [\sigma(t_i), t_{i+1}) \\ \left[\frac{e \begin{bmatrix} A & 0 \\ B_k C & A_k \end{bmatrix}^{\mu(t)} - I}{\mu(t)} \right] \left[I + \begin{bmatrix} A & 0 \\ B_k C & A_k \end{bmatrix}^{-1} \begin{bmatrix} BD_k C & BC_k \\ 0 & 0 \end{bmatrix} \right] \hat{x}(t), & \text{if } t \in \cup_{i=0}^{\infty} \{t_{i+1}\} \end{cases} \quad (7.21)$$

The stability criteria (7.22) at the bottom of next page can be formulated for the augmented system with output-feedback controller and communication failures in the control signal.

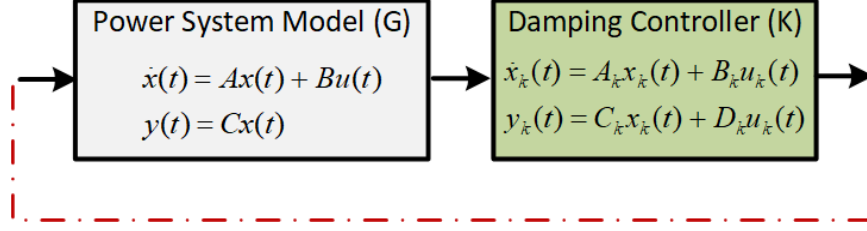


Figure 7.3: Block diagram of communication failure in control signal.

Similarly, for case where a communication failure happens in the measurement signal, as is shown in Fig. 7.4, the augmented system can be rewritten as follows

$$\dot{\hat{x}}(t) = \begin{bmatrix} A & BC_k \\ 0 & A_k \end{bmatrix} \hat{x}(t) + \begin{bmatrix} BD_k \\ B_k \end{bmatrix} u_k(t) \quad (7.23)$$

$$y(t) = \begin{bmatrix} C & 0 \end{bmatrix} \hat{x}(t) \quad (7.24)$$

such that $y(t_{i+1}) = \begin{bmatrix} C & 0 \end{bmatrix} \hat{x}(t_{i+1})$ is constant on time interval $[t_{i+1}, \sigma(t_{i+1}))$ when the communication fails. Similarly, the switched system on time scale $\mathbb{T} = \cup_{i=0}^{\infty} [\sigma(t_i), t_{i+1}]$ will be

$$\hat{x}^{\Delta}(t) = \begin{cases} \begin{bmatrix} A + BD_k C & BC_k \\ B_k C & A_k \end{bmatrix} \hat{x}(t), & \text{if } t \in \cup_{k=0}^{\infty} [\sigma(t_i), t_{i+1}) \\ \left[\frac{e^{\begin{bmatrix} A & BC_k \\ 0 & A_k \end{bmatrix} \mu(t)} - I}{\mu(t)} \right] \left[I + \begin{bmatrix} A & BC_k \\ 0 & A_k \end{bmatrix}^{-1} \begin{bmatrix} BD_k C & 0 \\ B_k C & 0 \end{bmatrix} \right] \hat{x}(t), & \text{if } t \in \cup_{i=0}^{\infty} \{t_{i+1}\} \end{cases} \quad (7.25)$$

$$\left\| e^{\begin{bmatrix} A + BD_k C & BC_k \\ B_k C & A_k \end{bmatrix} \tau(t_i)} \left[I + \left(e^{\begin{bmatrix} A & 0 \\ B_k C & A_k \end{bmatrix} \mu(t_i)} - I \right) \left(I + \begin{bmatrix} A & 0 \\ B_k C & A_k \end{bmatrix}^{-1} \begin{bmatrix} BD_k C & BC_k \\ 0 & 0 \end{bmatrix} \right) \right] \right\| < 1, \quad \forall 0 \leq i \leq k \quad (7.22)$$

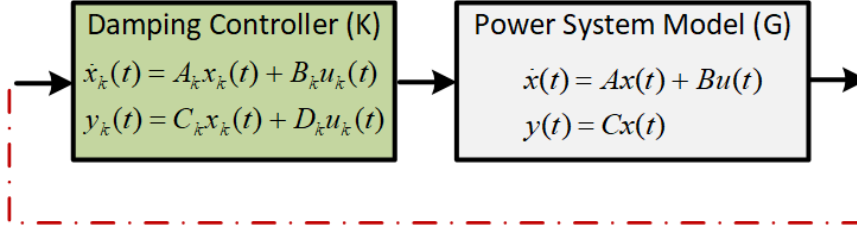


Figure 7.4: Block digram of communication failure in measurement signal.

Finally, the stability criteria (7.26) at the bottom of next page is formulated for the augmented system with output-feedback controller and communication failure in measurement signal.

7.4 Numerical Results

To verify and evaluate the accuracy of the developed stability conditions, a Single-Machine Infinite Bus (SMIB) system and Kundur's two-area systems are considered in this section. Both systems are modified to have undamped inter-area modes.

7.4.1 Case Study I: SMIB Power System

In this subsection, a SMIB power system model is considered. As shown in Fig. 7.5, simple power system model consists of a synchronous generator connected through two transmission lines to an infinite bus that represents an approximation of a large system. More detail on the dynamic equation can be found in chapter 3.3. The SMIB power system is considered to demonstrate the idea and verify the resulting improvement. The parameters of the machine,

$$\left\| e^{\begin{bmatrix} A + BD_k C & BC_k \\ B_k C & A_k \end{bmatrix} \tau(t_i)} \left[I + \left(e^{\begin{bmatrix} A & BC_k \\ 0 & A_k \end{bmatrix} \mu(t_i)} - I \right) \left(I + \begin{bmatrix} A & BC_k \\ 0 & A_k \end{bmatrix}^{-1} \begin{bmatrix} BD_k C & 0 \\ B_k C & 0 \end{bmatrix} \right) \right] \right\| < 1, \quad \forall 0 \leq i \leq k \quad (7.26)$$

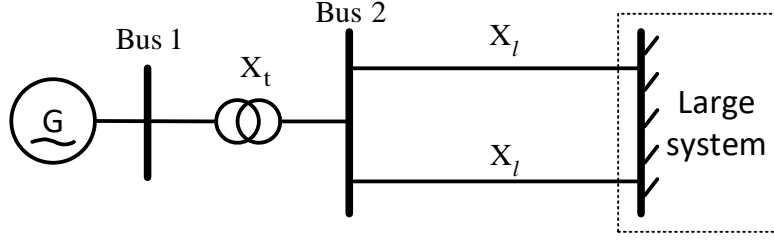


Figure 7.5: A single-machine infinite-bus power system.

excitation system, transformer and transmission lines are listed as follows

$$\begin{aligned}
 X_t &= 0.1, & X_l &= 0.8, & R_e &= 0, & V_\infty &= 1.05\angle 0^\circ, \\
 X_d &= 2.5, & X_q &= 2.1, & X'_d &= 0.39, & V_t &= 1\angle 15^\circ, \\
 T'_{d0} &= 9.6, & H &= 3.2, & D &= 0, & \omega_s &= 377, \\
 T_A &= 0.02, & K_A &= 100, & V_s^{\max} &= -V_s^{\min} = 0.05,
 \end{aligned}$$

The above nonlinear model can be linearized around the nominal operating point and expressed in the following fourth order state-space representation with state variables $\Delta\delta$, $\Delta\omega_r$, $\Delta E'_q$ and $\Delta E'_{fd}$.

$$A = \begin{bmatrix} 0 & \omega_s & 0 & 0 \\ -\frac{K_1}{2H} & -\frac{D\omega_s}{2H} & -\frac{K_2}{2H} & 0 \\ -\frac{K_4}{T'_{d0}} & 0 & -\frac{1}{K_3 T'_{d0}} & \frac{1}{T'_{d0}} \\ -\frac{K_A K_5}{T_A} & 0 & -\frac{K_A K_6}{T_A} & -\frac{1}{T_A} \end{bmatrix}, B = \begin{bmatrix} 0 \\ 0 \\ 0 \\ \frac{K_A}{T_A} \end{bmatrix} \quad (7.27)$$

and K_1 – K_6 are the well-known linearization constants based on the system parameters.

Eigenvalue analysis shows that the open loop system has unstable complex eigenvalues of $+0.2423 \pm 7.6064i$ with a frequency of 1.21 Hz and damping of -3.18% . Using modal transfer, the system is written into stable and unstable parts and the LQR state-feedback damping controller is designed [50] to enhance the damping performance by regulating the exciter.

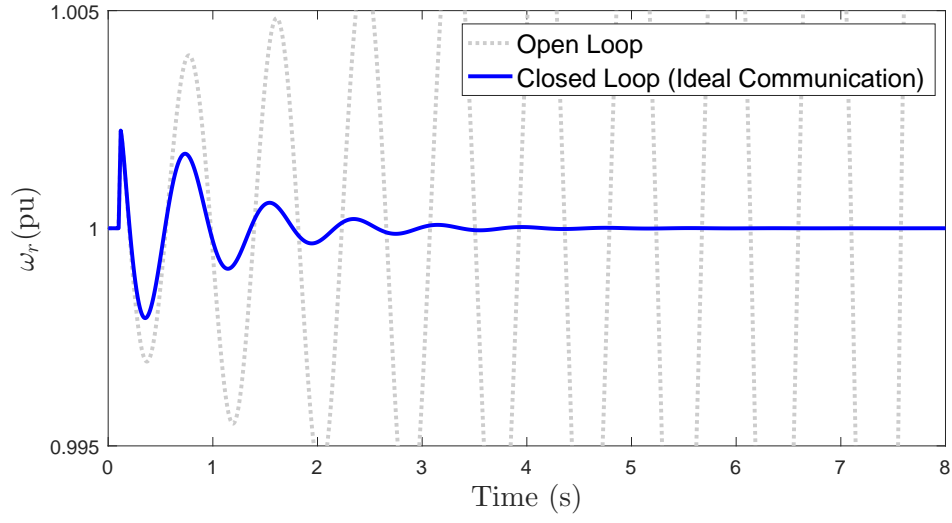


Figure 7.6: Speed deviation of SMIB power system in case of ideal communication network.

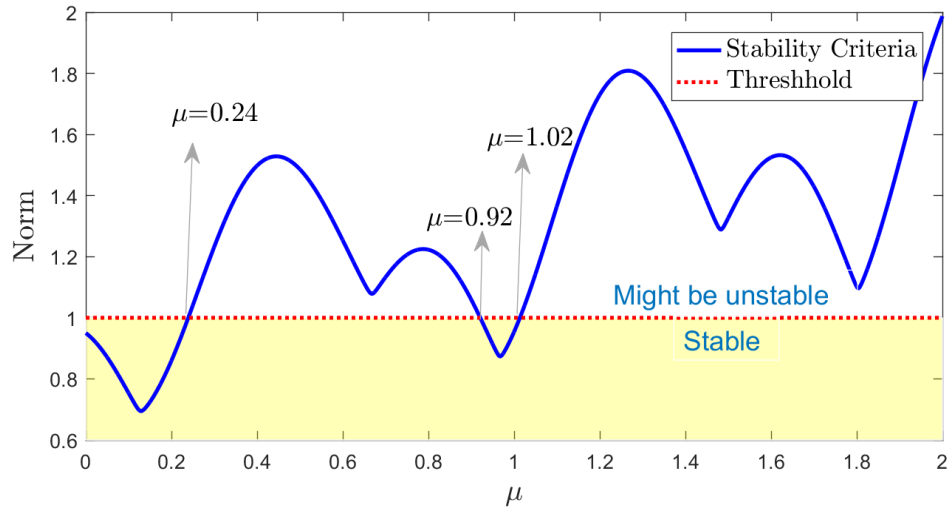


Figure 7.7: Stability criteria for SMIB power system.

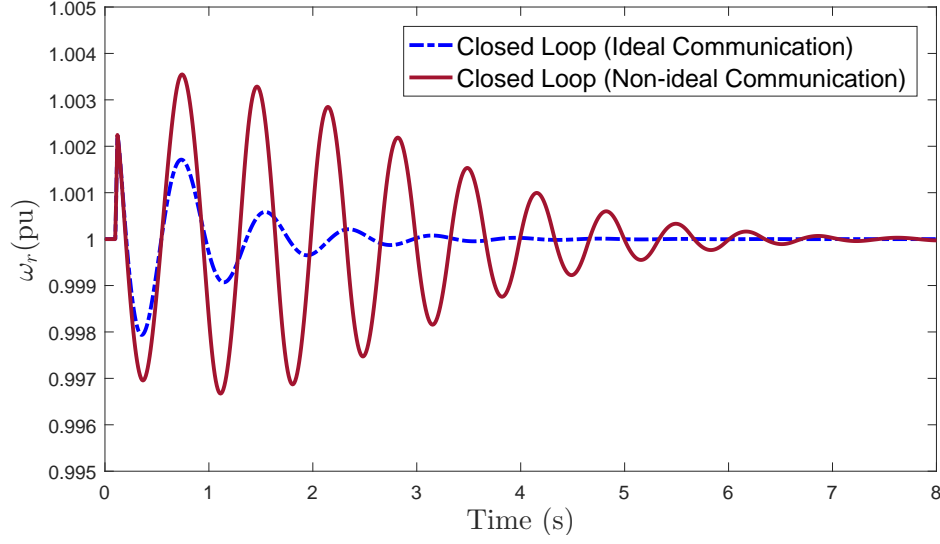


Figure 7.8: Speed deviation of closed loop and open loop SMIB power system in case of ideal and non-ideal ($\tau = 0.1$ and $\mu = 0.23$) communication network.

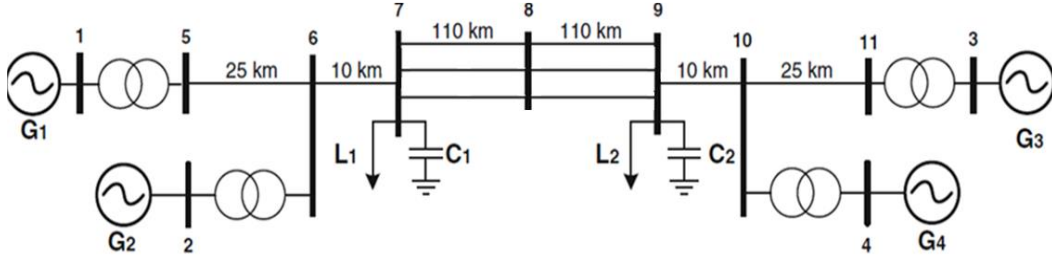
$$K = [-0.22 \quad 7.75 \quad -0.28 \quad -0.0006] \quad (7.28)$$

For ideal communications network, the performance of the closed-loop system is shown in Fig. 7.6. First, it is assumed that the perfect communication time is $\tau = 0.1$ s. Then using the developed stability criteria (7.13), two separate intervals can be found analytically (without simulation) for the maximum time of interruptions μ as shown in Fig 7.7. In Table 7.1, these intervals are compared with the real values using trial and error simulations. Compared to the developed stability criteria, excessive effort is needed to identify the unstable regions.

From Table 7.1 it can be seen that the stability condition is conservative but reasonably characterizes the limits. The system response for the case of perfect communication time $\tau = 0.1$ s and communication failure $\mu = 0.23$ s is also shown in Fig 7.8. It can be seen that the performance of damping controller with non-ideal communication network has been degraded significantly. In practice, in case of violation of these intervals (e.g., having a longer communication failure), these stability intervals could be used as thresholds for activating remedial action [90].

Table 7.1: Communication Failure Duration for Stable SMIB System.

	First Interval μ	Second Interval μ
Stability Condition	(0, 0.24)	(0.92, 1.02)
Simulation (Linear System)	(0, 0.48)	(0.8, 1.18)
Simulation (Nonlinear System)	(0, 0.42)	(0.85, 1.12)

**Figure 7.9:** A two-area Kundur power system.

7.4.2 Case Study II: Kundur's Two-Area System

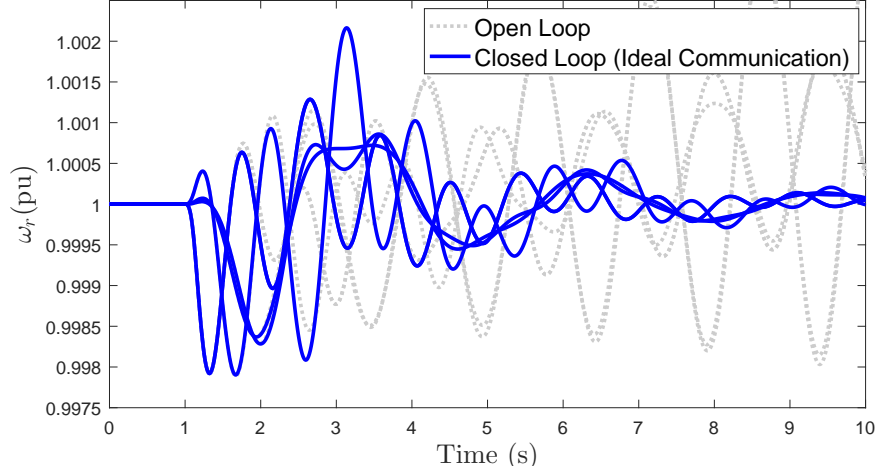
In this subsection, the developed stability condition is applied to a modified Kundur two-area system [4], shown in Fig.7.9. Area 1 is transferring 550 MW of active power to area 2. Generators are represented by a fourth-order model and equipped with a high-gain excitation system. Generators G_1 and G_3 are equipped with IEEE standard speed-based PSS to damp the local modes. More details of the parameters can be found in [4].

The modal analysis summarized in Table 7.2 show that the system without a controller has a negatively damped inter-area mode at 0.68 Hz with damping ratio of -2.52% and two damped local modes. The generator supplementary excitation control and speed deviation are chosen as candidates for actuator and measurement signals of WADC system, respectively. G_1 is chosen as the nominal actuator for damping controller. Based on the controllability measure, speed deviation of G_3 is identified as the best candidate measurement signals for the controller, as it has the highest geometric observability over the first critical mode [24].

Hankel norm approximation [82] is used to obtain the reduced-order model where the order of the model reduction can be determined by examining the Hankel singular values. The

Table 7.2: Critical Modes of Two-Area System

Mode type	Without WADC		With WADC	
	Freq. (Hz)	Damping (%)	Freq. (Hz)	Damping (%)
Inter-area	0.68	-2.52	0.78	12.76
Local	1.16	6.64	1.17	6.75
Local	1.12	6.07	1.09	5.74

**Figure 7.10:** Speed deviation of two-area Kundur power system in case of ideal communication network.

linear model is reduced to a second-order model and the following output feedback controller is designed using multi-objective optimization to meet or exceed 11% damping over all inter-area and local modes, more details can be found in [24]. For ideal communication network, the performance of the closed loop system with ideal communication is shown in Fig. 7.10.

Assuming the maximum time of perfect communication as $\tau = 0.2$ s and using the developed stability criteria (7.22), one interval can be found analytically (without any simulations) for the maximum time of interruption in control signal as shown in Fig 7.11. The system response for the case of perfect communication time $\tau = 0.2$ s and communication failure $\mu = 0.39$ s is also shown in Fig 7.12. It can be seen that the performance of damping controller with non-ideal communication network has been degraded significantly. In Table 7.3, these intervals are compared with the real values using try and error simulation. It can be seen that the stability condition is again conservative but reasonably characterizes the limit.

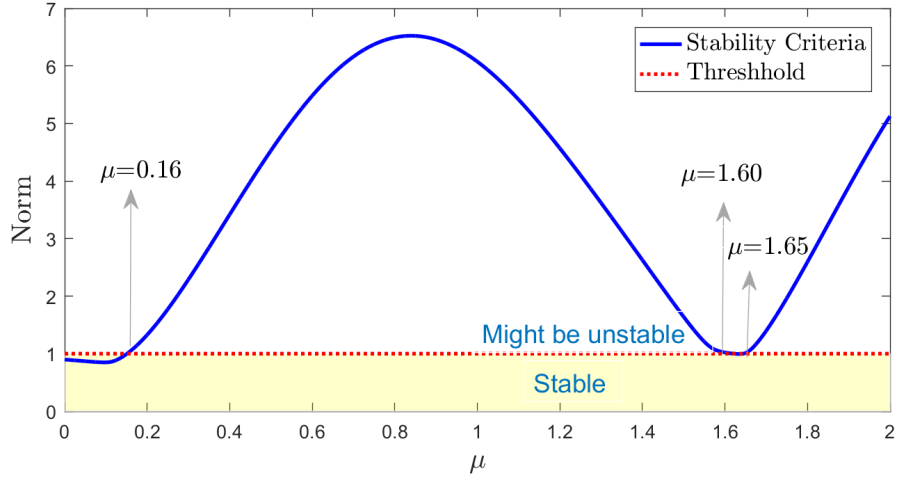


Figure 7.11: Stability criteria for two-area Kundur power system.

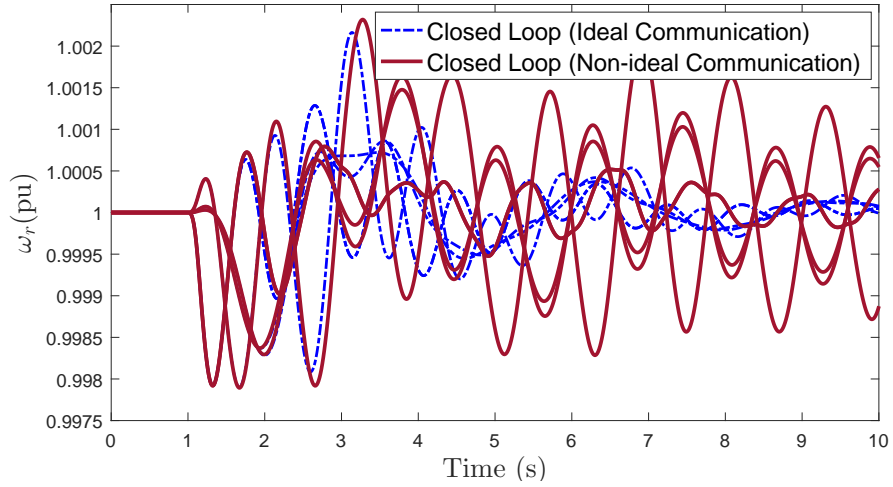


Figure 7.12: Speed deviation of closed loop and open loop two-area Kundur power system in case of ideal and non-ideal ($\tau = 0.2$ and $\mu = 0.39$) communication network.

Table 7.3: Communication Failure Duration for Kundur's two-area system

	First Interval μ	Second Interval μ
Stability Condition	(0.0, 0.16)	(1.60, 1.65)
Simulation (Linear System)	(0.0, 0.41)	(1.50, 1.81)
Simulation (Nonlinear System)	(0.0, 0.40)	(1.53, 1.76)

7.5 Summary

In this research, the problem for wide area control of power systems with intermittent information transmission is analyzed using time scale theory. This problem is formulated as the stability of a switched linear system which consists of a set of linear continuous-time and discrete-time systems on a particular time scale. Using the developed stability criteria, the upper limit on the communication failure time has been computed which guarantees the stability of the system in case of state-feedback and output-feedback controllers. Numerical results show the effectiveness of the proposed scheme. It is also found that the results based on the linear model are reasonably accurate for the nonlinear system. Further research is needed to model the stochastic process of intermittent transmission and random packet loss.

Chapter 8

Conclusion

In this dissertation, decentralized, fault-tolerant and coordinated wide-area controllers have been developed to improve the reliability of power systems. At the very beginning, this dissertation introduced the basic introduction that describes the previous works, motivations and contributions.

Generally, decentralized controllers are the only feasible solution for large-scale power systems as centralized control architectures are impractical or hard to implement. Hence, we have developed a method to design the optimal \mathcal{H}_2 decentralized controller for a class of spatially invariant systems. Using Parseval's identity, the optimal \mathcal{H}_2 decentralized control problem is transformed into an infinite number of model matching problems with a specific structure that can be solved efficiently. In addition, the explicit formula of the decentralized controller is derived for the first time. Moreover, a constructive procedure to obtain the state-space representation of the decentralized controller which is more convenient for implementation. An illustrative numerical example is presented.

Most of the new generation resources have limited capability and can contribute to grid stability within a narrow range depending on operating conditions. Therefore, a new approach to design supplementary damping controllers by taking into account the effects of saturation limits is also introduced. The problem of determining the optimal estimation of DA for SMIB power in the presence of saturation on the control signal is considered. To increase the region of stability, state-feedback and output-feedback controllers are designed to enlarge the guaranteed DA. Consequently, the enlargement of the DA of the post-fault

system effectively increases the CCT, which is an important measure of transient stability. Detailed dynamic simulation results demonstrate that the proposed controllers use the available control range to effectively enlarge the DA, improve the damping and enhance the stability in the presence of hard saturation.

This research has also presented a new fault-tolerant WADC such that nominal controller remains operational after faults in the actuator. Geometric measures of controllability and observability were used to select the most effective measurements and control locations for WADC. The design of nominal WADC carried out using multi-objective H_2/H_∞ optimization with pole placement region to achieve high damping performance. The problem of actuator faults is addressed by inserting VAs between the faulty plant and nominal WADC to re-route the control signals to other healthy actuators and recover the performance of fault free system without the need to retune the WADC. The design of the proposed method was analyzed in two detailed case studies. Simulation results demonstrate that the proposed approach provides sufficient damping when the system suffers from actuator failures.

Further, a new approach to designing a fault-tolerant WADC using modal-based control allocation is proposed to coordinate a group of actuators to optimally contribute to damping of inter-area oscillations. In our proposed method when an actuator fails or is unavailable, the supervisory MB-CA distributes the control signals to the remaining healthy actuators based on the effects on modal system, the desired control action and actuator constraints. The MB-CA is designed to manage actuator failures and constraints without redesigning the nominal WADC. The feasibility and performance of the proposed method is analyzed using the WECC system. This approach has also been further developed to sparse MB-CA where supervisory controller only communicates with necessary actuators to achieve the desired performance. The proposed approaches are applied to a modified Western Electricity Coordinating Council (WECC) system with high levels of renewables to verify the feasibility on a complex power system.

In addition, the problem for wide area control of power systems with intermittent information transmission is analyzed using time scale theory. This problem is formulated as the stability of a switched linear system which consists of a set of linear continuous-time and discrete-time systems on a particular time scale. Using the developed stability criteria,

the upper limit on the communication failure time has been computed which guarantees the stability of the system in case of state-feedback and output-feedback controllers. Numerical results show the effectiveness of the proposed scheme. It is also found that the results based on the linear model are reasonably accurate for the nonlinear system.

The previous communication model is not complex enough to truly capture all the effects on the stability of power system, however, it can provide enough information to better understand the effect on stability. Future work will include considering more realistic models for stochastic process of intermittent transmission and random packet loss.

Bibliography

- [1] Arulampalam Atputharajah and Tapan Kumar Saha. Power system blackouts-literature review. In *Industrial and Information Systems (ICIIS), 2009 International Conference on*, pages 460–465. IEEE, 2009. [1](#)
- [2] Antonello Monti, Carlo Muscas, and Ferdinanda Ponci. *Phasor Measurement Units and Wide Area Monitoring Systems*, 2016. [1](#)
- [3] Bassam Bamieh, Fernando Paganini, and Munther Dahleh. Optimal control of distributed arrays with spatial invariance. In *Robustness in identification and control*, pages 329–343. Springer, 1999. [1](#), [4](#), [11](#)
- [4] Prabha Kundur, Neal J Balu, and Mark G Lauby. *Power system stability and control*, volume 7. McGraw-hill New York, 1994. [2](#), [5](#), [61](#), [123](#)
- [5] Arturo Roman Messina. *Inter-area oscillations in power systems: a nonlinear and nonstationary perspective*. Springer Science & Business Media, 2009. [2](#)
- [6] Yang Zhang. *Design of wide-area damping control systems for power system low-frequency inter-area oscillations*. Washington State University, 2007. [3](#)
- [7] Innocent Kamwa, Robert Grondin, and Yves Hébert. Wide-area measurement based stabilizing control of large power systems-a decentralized/hierarchical approach. *IEEE Transactions on Power Systems*, 16(1):136–153, 2001. [3](#), [5](#), [72](#), [95](#)
- [8] John William Simpson-Porco. *Distributed Control of Inverter-Based Power Grids*. University of California, Santa Barbara, 2015. [4](#)
- [9] Zhongjing Ma, Suli Zou, Long Ran, Xingyu Shi, and Ian A Hiskens. Efficient decentralized coordination of large-scale plug-in electric vehicle charging. *Automatica*, 69:35–47, 2016. [4](#)
- [10] J Wolfe, D Chichka, and J Speyer. Decentralized controllers for unmanned aerial vehicle formation flight. In *Guidance, Navigation, and Control Conf.*, page 3833, 1996. [4](#)

- [11] Prabir Barooah, Prashant G Mehta, and Joao P Hespanha. Control of large vehicular platoons: Improving closed loop stability by mistuning. In *American Control Conf. (ACC)*, pages 4666–4671, 2007. [4](#)
- [12] Aditya Mahajan, Nuno C Martins, Michael C Rotkowitz, and Serdar Yüksel. Information structures in optimal decentralized control. In *IEEE Conf. on Decision and Control (CDC)*, pages 1291–1306, 2012. [4](#), [11](#)
- [13] Roy Radner. Team decision problems. *The Annals of Mathematical Statistics*, 33(3):857–881, 1962. [4](#)
- [14] Hans S Witsenhausen. A counterexample in stochastic optimum control. *SIAM Journal on Control*, 6(1):131–147, 1968. [4](#)
- [15] Yu-Chi Ho et al. Team decision theory and information structures in optimal control problems—part i. *IEEE Trans. on Automatic control*, 17(1):15–22, 1972. [5](#)
- [16] Tingshu Hu and Zongli Lin. *Control systems with actuator saturation: analysis and design*. Springer Science & Business Media, 2001. [5](#), [30](#), [34](#)
- [17] Tingshu Hu, Zongli Lin, and Ben M Chen. Analysis and design for discrete-time linear systems subject to actuator saturation. *Systems & Control Letters*, 45(2):97–112, 2002. [5](#), [30](#)
- [18] Yuanlong Li and Zongli Lin. Stability and performance analysis of saturated systems via partitioning of the virtual input space. *Automatica*, 53:85–93, 2015. [5](#), [30](#), [34](#)
- [19] Sophie Tarbouriech, Germain Garcia, João Manoel Gomes da Silva Jr, and Isabelle Queinnec. *Stability and stabilization of linear systems with saturating actuators*. Springer Science & Business Media, 2011. [5](#), [30](#), [34](#), [45](#)
- [20] Reza Yousefian, Amireza Sahami, and Sukumar Kamalasadan. Hybrid transient energy function-based real-time optimal wide-area damping controller. *IEEE Transactions on Industry Applications*, 53(2):1506–1516, 2017. [5](#), [30](#)

- [21] Feifei Bai, Lin Zhu, Yilu Liu, Xiaoru Wang, Kai Sun, Yiwei Ma, Mahendra Patel, Evangelos Farantatos, and Navin Bhatt. Design and implementation of a measurement-based adaptive wide-area damping controller considering time delays. *Electric Power Systems Research*, 130:1–9, 2016. [5](#), [30](#)
- [22] Hesien Liu, Lin Zhu, Zhuohong Pan, Feifei Bai, Yong Liu, Yilu Liu, Mahendra Patel, Evangelos Farantatos, and Navin Bhatt. Armax-based transfer function model identification using wide-area measurement for adaptive and coordinated damping control. *IEEE Transactions on Smart Grid*, 8(3):1105–1115, 2017. [5](#), [30](#)
- [23] Meimanat Mahmoudi, Jin Dong, Kevin Tomsovic, and Seddik Djouadi. Application of distributed control to mitigate disturbance propagations in large power networks. In *North American Power Symposium (NAPS), 2015*, pages 1–6. IEEE, 2015. [5](#), [30](#), [95](#)
- [24] M Ehsan Raoufat, Kevin Tomsovic, and Seddik M Djouadi. Virtual actuators for wide-area damping control of power systems. *IEEE Transactions on Power Systems*, 31(6):4703–4711, 2016. [5](#), [30](#), [50](#), [72](#), [123](#), [124](#)
- [25] Song Zhang and Vijay Vittal. Design of wide-area power system damping controllers resilient to communication failures. *IEEE Transactions on Power Systems*, 28(4):4292–4300, 2013. [5](#), [6](#), [30](#), [51](#), [52](#), [72](#), [95](#)
- [26] Horacio Silva-Saravia, Héctor Pulgar-Painemal, and Juan Manuel Mauricio. Flywheel energy storage model, control and location for improving stability: The chilean case. *IEEE Transactions on Power Systems*, 32(4):3111–3119, 2017. [5](#), [30](#)
- [27] Reza Yousefian, Rojan Bhattarai, and S Kamalasadan. Direct intelligent wide-area damping controller for wind integrated power system. In *Power and Energy Society General Meeting (PESGM), 2016*, pages 1–5. IEEE, 2016. [5](#), [30](#)
- [28] L Jiang, W Yao, QH Wu, JY Wen, and SJ Cheng. Delay-dependent stability for load frequency control with constant and time-varying delays. *IEEE Transactions on Power Systems*, 27(2):932–941, 2012. [6](#), [51](#)

- [29] Wei Zhang, Michael S Branicky, and Stephen M Phillips. Stability of networked control systems. *IEEE Control Systems*, 21(1):84–99, 2001. [6](#), [109](#)
- [30] Jing Wu and Tongwen Chen. Design of networked control systems with packet dropouts. *IEEE Transactions on Automatic control*, 52(7):1314–1319, 2007. [6](#), [109](#)
- [31] Yun-Bo Zhao, Guo-Ping Liu, and David Rees. Design of a packet-based control framework for networked control systems. *IEEE Transactions on Control Systems Technology*, 17(4):859–865, 2009. [6](#), [109](#)
- [32] M Ehsan Raoufat and S. M. Djouadi. Optimal h2 decentralized control of cone causal spatially invariant systems. In *2018 American Control Conference (ACC)*, pages 1–7, 2018. [10](#)
- [33] Aditya Mahajan, Ashutosh Nayyar, and Demosthenis Teneketzis. Identifying tractable decentralized control problems on the basis of information structure. In *Conf. on Comm., Control, and Computing*, pages 1440–1449, 2008. [11](#)
- [34] Aditya Mahajan and Demosthenis Teneketzis. Optimal performance of networked control systems with nonclassical information structures. *SIAM Journal on Control and Optimization*, 48(3):1377–1404, 2009. [11](#)
- [35] Ashutosh Nayyar, Aditya Mahajan, and Demosthenis Teneketzis. Optimal control strategies in delayed sharing information structures. *IEEE Trans. on Automatic Control*, 56(7):1606–1620, 2011. [11](#)
- [36] Bassam Bamieh, Fernando Paganini, and Munther A Dahleh. Distributed control of spatially invariant systems. *IEEE Trans. on Automatic Control*, 47(7):1091–1107, 2002. [11](#)
- [37] Michael C Rotkowitz. Parametrization of all stabilizing controllers subject to any structural constraint. In *IEEE Conf. on Decision and Control (CDC)*, pages 108–113, 2010. [11](#)

- [38] Michael Rotkowitz and Sanjay Lall. A characterization of convex problems in decentralized control. *IEEE Trans. on Automatic Control*, 51(2):274–286, 2006. [11](#)
- [39] Jong-Han Kim and Sanjay Lall. Explicit solutions to separable problems in optimal cooperative control. *IEEE Trans. on Automatic Control*, 60(5):1304–1319, 2015. [11](#)
- [40] Petros G Voulgaris, Gianni Bianchini, and Bassam Bamieh. Optimal h_2 controllers for spatially invariant systems with delayed communication requirements. *Systems & Control Letters*, 50(5):347–361, 2003. [12](#), [13](#), [14](#), [15](#), [18](#), [19](#), [23](#), [26](#)
- [41] Bassam Bamieh and Petros G Voulgaris. A convex characterization of distributed control problems in spatially invariant systems with communication constraints. *Systems & Control Letters*, 54(6):575–583, 2005. [12](#)
- [42] Seddik M Djouadi and Jin Dong. Duality of the optimal distributed control for spatially invariant systems. In *American Control Conf. (ACC)*, pages 2214–2219, 2014. [12](#)
- [43] Seddik M Djouadi and Jin Dong. Operator theoretic approach to the optimal distributed control problem for spatially invariant systems. In *American Control Conf. (ACC)*, pages 2613–2618, 2015. [12](#)
- [44] Seddik M Djouadi and Jin Dong. On the distributed control of spatially invariant systems. In *IEEE Conf. on Decision and Control (CDC)*, pages 549–554, 2015. [12](#), [15](#)
- [45] Jin Dong. *Stochastic and Optimal Distributed Control for Energy Optimization and Spatially Invariant Systems*. PhD thesis, University of Tennessee, 2016. [12](#)
- [46] PL Duren. Theory of h_p spaces. mineola, 2000. [15](#)
- [47] Makan Fardad and Mihailo R Jovanović. Design of optimal controllers for spatially invariant systems with finite communication speed. *Automatica*, 47(5):880–889, 2011. [16](#)
- [48] Kemin Zhou and John Comstock Doyle. *Essentials of robust control*, volume 104. Prentice hall Upper Saddle River, NJ, 1998. [17](#)

- [49] Mathukumalli Vidyasagar. Control system synthesis: a factorization approach, part ii. *Synthesis lectures on control and mechatronics*, 2(1):1–227, 2011. [18](#), [19](#)
- [50] M Ehsan Raoufat, Kevin Tomsovic, and Seddik M Djouadi. Power system supplementary damping controllers in the presence of saturation. In *Power and Energy Conference at Illinois (PECI), 2017 IEEE*, pages 1–6. IEEE, 2017. [29](#), [120](#)
- [51] M Ehsan Raoufat, Alireza Khayatian, and Aslan Mojallal. Performance recovery of voltage source converters with application to grid-connected fuel cell dgs. *IEEE Transactions on Smart Grid*, 9(2):1197–1204, 2016. [30](#)
- [52] M Ehsan Raoufat, B. Asghari, and R. Sharma. Model predictive bess control for demand charge management and pv-utilization improvement. In *Conference on Innovative Smart Grid Technology (ISGT), Washington, DC*, pages 1–5, 2018. [30](#)
- [53] Hiroaki Aotsu, Akira Isono, Masuo Goto, Koichi Kimura, Yasushi Momochi, Takaaki Kai, Satoshi Kitamura, Akihisa Kaihara, Hiroshi Okada, et al. Excitation control apparatus for a generator, January 13 1981. US Patent 4,245,182. [30](#)
- [54] TT Nguyen and R Gianto. Optimal design for control coordination of power system stabilisers and flexible alternating current transmission system devices with controller saturation limits. *IET generation, transmission & distribution*, 4(9):1028–1043, 2010. [30](#)
- [55] M Ehsan Raoufat, Kevin Tomsovic, and Seddik M Djouadi. Control allocation for wide area coordinated damping. *arXiv preprint arXiv:1701.07456*, 2017. [30](#), [94](#), [95](#)
- [56] M Ehsan Raoufat, Kevin Tomsovic, and Seddik M Djouadi. Dynamic control allocation for damping of inter-area oscillations. *IEEE Transactions on Power Systems*, 2017. [30](#), [71](#)
- [57] Debasish Mondal, Abhijit Chakrabarti, and Aparajita Sengupta. *Power system small signal stability analysis and control*. Academic Press, 2014. [33](#)

- [58] Tingshu Hu, Zongli Lin, and Li Qiu. An explicit description of null controllable regions of linear systems with saturating actuators. *Systems & control letters*, 47(1):65–78, 2002. [35](#)
- [59] Brian DO Anderson and John B Moore. *Optimal control: linear quadratic methods*. Courier Corporation, 2007. [36](#)
- [60] Jin Dong, Xiao Ma, Seddik M Djouadi, Husheng Li, and Yilu Liu. Frequency prediction of power systems in fnet based on state-space approach and uncertain basis functions. *IEEE Transactions on Power Systems*, 29(6):2602–2612, 2014. [37](#)
- [61] Shahrokh Akhlaghi, Ning Zhou, and Zhenyu Huang. A multi-step adaptive interpolation approach to mitigating the impact of nonlinearity on dynamic state estimation. *IEEE Transactions on Smart Grid*, 2016. [37](#)
- [62] Shahrokh Akhlaghi, Ning Zhou, and Zhenyu Huang. Exploring adaptive interpolation to mitigate non-linear impact on estimating dynamic states. In *Power & Energy Society General Meeting, 2015 IEEE*, pages 1–5. IEEE, 2015. [37](#)
- [63] Shahrokh Akhlaghi and Ning Zhou. Adaptive multi-step prediction based ekf to power system dynamic state estimation. In *Power and Energy Conference at Illinois (PECI), 2017 IEEE*, pages 1–8. IEEE, 2017. [37](#)
- [64] Thomas Kailath. *Linear systems*, volume 156. Prentice-Hall Englewood Cliffs, NJ, 1980. [37](#)
- [65] Robert TH Alden and Adel A Shaltout. Analysis of damping and synchronizing torques part ia general calculation method. *IEEE Transactions on Power Apparatus and Systems*, (5):1696–1700, 1979. [42](#)
- [66] Yong Li, Christian Rehtanz, Sven Ruberg, Longfu Luo, and Yijia Cao. Wide-area robust coordination approach of hvdc and facts controllers for damping multiple interarea oscillations. *IEEE transactions on power delivery*, 27(3):1096–1105, 2012. [51](#), [72](#), [109](#)

- [67] Nadarajah Mithulananthan, Claudio A Canizares, John Reeve, and Graham J Rogers. Comparison of pss, svc, and statcom controllers for damping power system oscillations. *IEEE transactions on power systems*, 18(2):786–792, 2003. [51](#), [109](#)
- [68] Jingbo He, Chao Lu, Xiaochen Wu, P Li, and J Wu. Design and experiment of wide area hvdc supplementary damping controller considering time delay in china southern power grid. *IET generation, transmission & distribution*, 3(1):17–25, 2009. [51](#), [72](#)
- [69] John Von Neumann. Probabilistic logics and the synthesis of reliable organisms from unreliable components. *Automata studies*, 34:43–98, 1956. [51](#), [72](#)
- [70] Christopher Edwards, Thomas Lombaerts, and Hafid Smaili. Fault tolerant flight control. *Lecture Notes in Control and Information Sciences*, 399:1–560, 2010. [51](#)
- [71] Mogens Blanke, Michel Kinnaert, Jan Lunze, Marcel Staroswiecki, and J Schröder. *Diagnosis and fault-tolerant control*, volume 691. Springer, 2006. [51](#)
- [72] Jan H Richter. *Reconfigurable control of nonlinear dynamical systems: a fault-hiding approach*, volume 408. Springer, 2011. [51](#)
- [73] Jerry Pratt, Ann Torres, Peter Dilworth, and Gill Pratt. Virtual actuator control. In *Intelligent Robots and Systems’ 96, IROS 96, Proceedings of the 1996 IEEE/RSJ International Conference on*, volume 3, pages 1219–1226. IEEE, 1996. [51](#)
- [74] J Lunze and T Steffen. Control reconfiguration by means of a virtual actuator. *IFAC Proceedings Volumes*, 36(5):131–136, 2003. [51](#)
- [75] Yang Zhang and Anjan Bose. Design of wide-area damping controllers for interarea oscillations. *IEEE Transactions on Power Systems*, 23(3):1136–1143, 2008. [52](#), [56](#), [72](#), [73](#), [95](#)
- [76] Wei Yao, Lin Jiang, Jinyu Wen, QH Wu, and Shijie Cheng. Wide-area damping controller of facts devices for inter-area oscillations considering communication time delays. *IEEE Transactions on Power Systems*, 29(1):318–329, 2014. [52](#), [72](#)

- [77] *Transient Security Assessment Tool (TSAT) User Manual* Powertech. Surrey, BC, Canada: Powertech Labs Inc., 2011. [52](#), [54](#), [85](#), [102](#)
- [78] Jan Machowski, Janusz Bialek, and James Richard Bumby. *Power system dynamics and stability*. John Wiley & Sons, 1997. [52](#)
- [79] *IEEE Recommended Practice for Excitation System Models for Power System Stability Studies*. IEEE Std 421.5-2005, 2006. [53](#), [78](#)
- [80] *Dynamic models for turbine-governors in power system studies*. IEEE PES, 2013. [53](#), [78](#)
- [81] Carsten Scherer, Pascal Gahinet, and Mahmoud Chilali. Multiobjective output-feedback control via lmi optimization. *IEEE Transactions on automatic control*, 42(7):896–911, 1997. [54](#), [97](#)
- [82] Keith Glover. All optimal hankel-norm approximations of linear multivariable systems and their l₂-error bounds. *International journal of control*, 39(6):1115–1193, 1984. [55](#), [96](#), [123](#)
- [83] Ajay Chandra V Gummalla and John O Limb. Wireless medium access control protocols. *IEEE Communications Surveys & Tutorials*, 3(2):2–15, 2000. [58](#)
- [84] Xiao He, Zidong Wang, and DH Zhou. Robust fault detection for networked systems with communication delay and data missing. *Automatica*, 45(11):2634–2639, 2009. [58](#)
- [85] Christopher Edwards, Sarah K Spurgeon, and Ron J Patton. Sliding mode observers for fault detection and isolation. *Automatica*, 36(4):541–553, 2000. [58](#)
- [86] Wei Pan, Ye Yuan, Henrik Sandberg, Jorge Gonçalves, and Guy-Bart Stan. Online fault diagnosis for nonlinear power systems. *Automatica*, 55:27–36, 2015. [58](#)
- [87] Qi Zhang, Xiaodong Zhang, Marios M Polycarpou, and Thomas Parisini. Distributed sensor fault detection and isolation for multimachine power systems. *International Journal of Robust and Nonlinear Control*, 24(8-9):1403–1430, 2014. [58](#)

- [88] Guillermo J Silva, Aniruddha Datta, and Shankar P Bhattacharyya. *PID controllers for time-delay systems*. Springer Science & Business Media, 2007. [62](#)
- [89] Anantha Pai. *Energy function analysis for power system stability*. Springer Science & Business Media, 2012. [65](#)
- [90] Yichen Zhang, M Ehsan Raoufat, and Kevin Tomsovic. Remedial action schemes and defense systems. *Smart Grid Handbook*, 2016. [72](#), [110](#), [122](#)
- [91] Florian Dörfler, Mihailo R Jovanović, Michael Chertkov, and Francesco Bullo. Sparsity-promoting optimal wide-area control of power networks. *IEEE Transactions on Power Systems*, 29(5):2281–2291, 2014. [72](#), [73](#)
- [92] Rakibuzzaman Shah, Nadarajah Mithulananthan, Kwang Y Lee, and Ramesh C Bansal. Wide-area measurement signal-based stabiliser for large-scale photovoltaic plants with high variability and uncertainty. *IET Renewable Power Generation*, 7(6):614–622, 2013. [72](#)
- [93] Rakibuzzaman Shah, Nadarajah Mithulananthan, and Kwang Y Lee. Large-scale pv plant with a robust controller considering power oscillation damping. *IEEE Transactions on Energy Conversion*, 28(1):106–116, 2013. [72](#)
- [94] Andres E Leon and Jorge A Solsona. Power oscillation damping improvement by adding multiple wind farms to wide-area coordinating controls. *IEEE Transactions on Power Systems*, 29(3):1356–1364, 2014. [72](#), [73](#), [95](#)
- [95] Maghsoud Mokhtari and Farrokh Aminifar. Toward wide-area oscillation control through doubly-fed induction generator wind farms. *IEEE Transactions on Power Systems*, 29(6):2985–2992, 2014. [72](#), [73](#)
- [96] Lingling Fan, Haiping Yin, and Zhixin Miao. On active/reactive power modulation of dfig-based wind generation for interarea oscillation damping. *IEEE Transactions on Energy Conversion*, 26(2):513–521, 2011. [72](#), [73](#)

- [97] Wang Juanjuan, Fu Chuang, and Zhang Yao. Design of wams-based multiple hvdc damping control system. *IEEE transactions on smart grid*, 2(2):363–374, 2011. [72](#)
- [98] Robin Preece, Jovica V Milanovic, Abddulaziz M Almutairi, and Ognjen Marjanovic. Damping of inter-area oscillations in mixed ac/dc networks using wams based supplementary controller. *IEEE Transactions on Power Systems*, 28(2):1160–1169, 2013. [72](#)
- [99] Jingchao Deng, Can Li, and Xiao-Ping Zhang. Coordinated design of multiple robust facts damping controllers: A bmi-based sequential approach with multi-model systems. *IEEE Transactions on Power Systems*, 30(6):3150–3159, 2015. [72](#)
- [100] Yichen Zhang, Kevin Tomsovic, Seddik M Djouadi, and Hector Pulgar-Painemal. Hybrid controller for wind turbine generators to ensure adequate frequency response in power networks. *IEEE Journal on Emerging and Selected Topics in Circuits and Systems*, 2017. [72](#)
- [101] Yichen Zhang, M Ehsan Raoufat, Kevin Tomsovic, and Seddik M Djouadi. Set theory-based safety supervisory control for wind turbines to ensure adequate frequency response. *Preprint 1803.03694*, 2018. [72](#)
- [102] Ola Harkegard. Efficient active set algorithms for solving constrained least squares problems in aircraft control allocation. In *Decision and Control, 2002, Proceedings of the 41st IEEE Conference on*, volume 2, pages 1295–1300. IEEE, 2002. [73](#), [77](#), [95](#)
- [103] Ola HäRkegåRd and S Torkel Glad. Resolving actuator redundancyoptimal control vs. control allocation. *Automatica*, 41(1):137–144, 2005. [73](#), [95](#), [99](#)
- [104] Halim Alwi and Christopher Edwards. Fault tolerant control using sliding modes with on-line control allocation. *Automatica*, 44(7):1859–1866, 2008. [73](#)
- [105] Pablo A Servidia and Ricardo Sánchez Peña. Spacecraft thruster control allocation problems. *IEEE Transactions on Automatic Control*, 50(2):245–249, 2005. [73](#)

- [106] Jaehyun Jin, Bongkyu Park, Youngwoong Park, and Min-Jea Tahk. Attitude control of a satellite with redundant thrusters. *Aerospace Science and Technology*, 10(7):644–651, 2006. [73](#)
- [107] Qiang Shen, Danwei Wang, Senqiang Zhu, and Eng Kee Poh. Inertia-free fault-tolerant spacecraft attitude tracking using control allocation. *Automatica*, 62:114–121, 2015. [73](#)
- [108] OJ Sørndalen. Optimal thrust allocation for marine vessels. *Control Engineering Practice*, 5(9):1223–1231, 1997. [73](#)
- [109] Thor I Fossen and Tor A Johansen. A survey of control allocation methods for ships and underwater vehicles. In *Control and Automation, 2006. MED'06. 14th Mediterranean Conference on*, pages 1–6. IEEE, 2006. [73](#)
- [110] Åke Björck. *Numerical methods for least squares problems*. SIAM, 1996. [77](#)
- [111] *Test Cases Library of Sustained Power System Oscillations [Online]*. Available: <http://web.eecs.utk.edu/~kaisun/Oscillation/>. [78](#)
- [112] *DSATools User-Defined Model (UDM) User Manual*. Surrey, BC, Canada, Powertech Labs Inc., 2012. [82](#), [85](#)
- [113] Yong Liu, Kai Sun, and Yilu Liu. A measurement-based power system model for dynamic response estimation and instability warning. *Electric Power Systems Research*, 124:1–9, 2015. [83](#)
- [114] *Small Signal Analysis Tool (SSAT) User Manual*. Surrey, BC, Canada, Powertech Labs Inc., 2012. [83](#)
- [115] John B Davidson, Frederick J Lallman, and W Thomas Bundick. Real-time adaptive control allocation applied to a high performance aircraft. 2001. [95](#), [99](#)
- [116] Andres E Leon, Juan Manuel Mauricio, Antonio Gómez-Expósito, and Jorge A Solsona. Hierarchical wide-area control of power systems including wind farms and facts for

- short-term frequency regulation. *IEEE Transactions on Power Systems*, 27(4):2084–2092, 2012. [95](#)
- [117] Song Zhang and Vijay Vittal. Wide-area control resiliency using redundant communication paths. *IEEE Transactions on Power Systems*, 29(5):2189–2199, 2014. [95](#)
- [118] M Ehsan Raoufat, A Taalimi, K Tomsovic, and R Hay. Event analysis of pulse-reclosers in distribution systems through sparse representation. In *Intelligent System Application to Power Systems (ISAP), San Antonio, TX*, pages 1–6, 2017. [97](#)
- [119] WECC Modeling and Validation Work Group. Wecc wind power plant dynamic modeling guide. Technical report, April, 2014. [101](#)
- [120] Willi Christiansen and David T Johnsen. Analysis of requirements in selected grid codes. *Prepared for Orsted-DTU Section of Electric Power Engineering, Technical University of Denmark (DTU)*, 2006. [101](#)
- [121] M Ehsan Raoufat, Fatima Taousser, Kevin Tomsovic, and Seddik M Djouadi. Stability of wide area power system controls with intermittent information transmission. *To be submitted to IEEE Transactions on Power Systems*, 1(1):1–8, 2018. [108](#), [111](#), [112](#), [115](#)
- [122] D Santos, L Fabiano, G Antonova, and M Larsson. The use of synchrophasors for wide area monitoring of electrical power grids. *Actual Trends in Develop. Power Syst. Protect. Autom.*, 2013. [109](#)
- [123] Fatima Zohra Taousser, Michael Defoort, and Mohamed Djemai. Stability analysis of a class of switched linear systems on non-uniform time domains. *Systems & Control Letters*, 74:24–31, 2014. [109](#), [111](#)
- [124] Fatima Zohra Taousser, Michael Defoort, and Mohamed Djemai. Stability analysis of a class of uncertain switched systems on time scale using lyapunov functions. *Nonlinear Analysis: Hybrid Systems*, 16:13–23, 2015. [109](#)

- [125] Martin Bohner and Allan C Peterson. *Advances in dynamic equations on time scales*. Springer Science & Business Media, 2002. [109](#), [111](#)
- [126] T Gard and J Hoffacker. Asymptotic behavior of natural growth on time scales. *Dynamic Systems and Applications*, 12(1/2):131–148, 2003. [109](#), [112](#)
- [127] Zbigniew Bartosiewicz and Ewa Piotrowska. On stabilisability of nonlinear systems on time scales. *International Journal of Control*, 86(1):139–145, 2013. [109](#)
- [128] Thai Son Doan, Anke Kalauch, Stefan Siegmund, and FR Wirth. Stability radii for positive linear time-invariant systems on time scales. *Systems & Control Letters*, 59(3-4):173–179, 2010. [109](#)
- [129] Shaobu Wang, Xiangyu Meng, and Tongwen Chen. Wide-area control of power systems through delayed network communication. *IEEE Transactions on Control Systems Technology*, 20(2):495–503, 2012. [109](#)
- [130] Zhaoyan Liu, Chengzhi Zhu, and Quanyuan Jiang. Stability analysis of time delayed power system based on cluster treatment of characteristic roots method. In *Power and Energy Society General Meeting-Conversion and Delivery of Electrical Energy in the 21st Century, 2008 IEEE*, pages 1–6. IEEE, 2008. [109](#)
- [131] Shaobu Wang, Yonghui Yi, Zhaoyan Liu, Quanyuan Jiang, and Yijia Cao. Wide-area damping control reckoning with feedback signals multiple delays. In *Power and Energy Society General Meeting-Conversion and Delivery of Electrical Energy in the 21st Century, 2008 IEEE*, pages 1–7. IEEE, 2008. [109](#)
- [132] Ravi Agarwal, Martin Bohner, Donal O’Regan, and Allan Peterson. Dynamic equations on time scales: a survey. *Journal of Computational and Applied Mathematics*, 141(1-2):1–26, 2002. [111](#)
- [133] André Teixeira, Iman Shames, Henrik Sandberg, and Karl Henrik Johansson. A secure control framework for resource-limited adversaries. *Automatica*, 51:135–148, 2015. [113](#)

- [134] Christophe Fiter, Laurentiu Hetel, Wilfrid Perruquetti, and Jean-Pierre Richard. A state dependent sampling for linear state feedback. *Automatica*, 48(8):1860–1867, 2012. [114](#)
- [135] Fatima Taousser, Michael Defoort, and Mohamed Djemai. Consensus for linear multi-agent system with intermittent information transmissions using the time-scale theory. *International Journal of Control*, 89(1):210–220, 2016. [114](#)

Appendix

A Controller Parameters

A.1 Controller parameters of case study I:

$$\begin{aligned} A_k &= \begin{bmatrix} -0.114 & 0.151 & -0.015 & -0.017 & 0.015 & 3.736 \\ -0.164 & -0.144 & 0.141 & 0.162 & -0.140 & -35.39 \\ -0.112 & 0.304 & -1.296 & -6.451 & 0.384 & 84.66 \\ 0.387 & -0.999 & 6.298 & -1.574 & 0.974 & 251.2 \\ -0.145 & 0.395 & -0.477 & 0.959 & -0.993 & -159.7 \\ -24.44 & 56.62 & 53.64 & -117.9 & 128.6 & -14690 \end{bmatrix} \\ B_k^T &= \begin{bmatrix} 0 & 0 & -0.388 & 0.605 & -0.509 & 50.710 \\ 0 & 0 & 0.044 & 0.496 & 0.063 & -109.30 \end{bmatrix} \\ C_k &= \begin{bmatrix} 0 & 0 & -0.206 & -0.238 & 0.205 & 51.871 \end{bmatrix} \\ M_2 &= \begin{bmatrix} -36.721 & -24.778 & -9.784 & -67.436 & 1.073 & 24.891 \end{bmatrix} \\ M_3 &= \begin{bmatrix} -0.035 & -8.886 & -9.185 & -1.246 & 56.375 & -9.090 \end{bmatrix} \\ M_4 &= \begin{bmatrix} 0.137 & -0.163 & -0.038 & 0.198 & -1.161 & 1.085 \end{bmatrix} \times 10^6 \end{aligned}$$

A.2 Controller parameters of case study II:

$$\begin{aligned}
A_k &= \begin{bmatrix} -0.229 & -0.180 & 0.045 & 0.023 & 0.021 & -0.035 & 0.058 & -15.30 \\ 0.005 & -2.362 & -0.278 & -0.144 & -0.129 & 0.214 & -0.358 & 94.51 \\ 0.118 & 0.323 & -0.893 & -5.08 & -0.815 & 0.525 & -0.573 & 143.8 \\ -0.001 & 0.031 & 4.942 & -0.904 & -0.326 & 0.758 & -0.407 & 98.28 \\ -0.069 & -0.197 & 0.948 & 0.135 & -0.671 & 4.397 & -0.751 & 185.5 \\ -0.018 & 0.006 & -0.531 & -0.680 & -4.322 & -0.709 & 0.632 & -173.2 \\ -0.136 & -0.390 & 0.564 & 0.013 & -0.358 & 0.302 & -1.158 & 210.0 \\ -20.88 & -79.98 & 142.2 & 65.18 & -165.10 & 175.7 & -163.50 & -35200 \end{bmatrix} \\
B_k^T &= \begin{bmatrix} 0 & 0 & 0.521 & 0.29 & -0.376 & 0.391 & -0.750 & -289.4 \\ 0 & 0 & 0.518 & -0.29 & -0.237 & -0.534 & -0.456 & 99.48 \end{bmatrix} \\
C_k &= \begin{bmatrix} 0 & 0 & -0.553 & -0.286 & -0.258 & 0.427 & -0.715 & 188.5 \end{bmatrix} \\
M_2 &= \begin{bmatrix} 612.755 & -528.161 & 531.363 & 450.957 & 259.774 & -264.1 & -17.325 & -21.36 \end{bmatrix} \\
M_3 &= \begin{bmatrix} -1.936 & 0.228 & -1.402 & -0.142 & -1.107 & 0.149 & -0.039 & 0.203 \end{bmatrix} \times 10^3 \\
M_4 &= \begin{bmatrix} -0.679 & 0.174 & -0.609 & -1.142 & -0.443 & -0.026 & -0.015 & 0.019 \end{bmatrix} \times 10^6
\end{aligned}$$

Vita

M. Ehsan Raoufat is a Ph.D. candidate at the Department of Electrical Engineering and Computer science (EECS) at the University of Tennessee-Knoxville. He is currently a graduate research assistant at CURENT, an NSF-DOE ERC. Prior to his Ph.D., he received M.S degree in from the University of Tennessee-Knoxville in 2014. He also received his B.S. and M.S. degrees in control systems from Shiraz University, Iran, in 2011 and 2013, respectively. His main research interests are in the area of distributed, decentralized and fault-tolerant control with their applications to modern power systems and smart grids. He has interned with Electric Power Board and NEC Laboratories America, in 2016 and 2017, respectively.